1995

Theoretical studies of possible high energy density materials

Nikita Matsunaga
Iowa State University

Theoretical studies of possible high energy density materials

by

Nikita Matsunaga

A Dissertation Submitted to the

Graduate Faculty in Partial Fulfillment of the

Requirements for the Degree of

DOCTOR OF PHILOSOPHY

Department: Chemistry
Major: Physical Chemistry

Approved:

Signature was redacted for privacy.

In Charge of Major Work

Signature was redacted for privacy.

For the Major Department

Signature was redacted for privacy.

For the Graduate College

Iowa State University
Ames, Iowa

1995

Theoretical studies of possible high energy density materials

Nikita Matsunaga

Major Professor: Mark S. Gordon
Iowa State University

Ab initio quantum chemistry methods are applied to possible high energy density materials (HEDM). The candidate molecules are investigated for their structures, energetics, stabilities, nature of bonding, and other properties. The investigation of molecules of interest includes: 1) stabilities and bonding of NH_4^- and PH_4^-, decomposition paths using dynamic reaction coordinates for tetrahedral isomers and their ionization potentials; 2) aromaticity associated with inorganic benzene, $X_3Y_3H_6$ where X and Y are chosen from Zn, B, Al, Ga, C, Si, Ge, N, P, As, O and S such that there are total of six π electrons, by examining their configuration interaction density matrices; 3) stabilities and energetics of inorganic prismanes, $X_3Y_3H_6$ where X and Y are chosen from B, Al, Ga, C, Si, Ge, N, P and As, and the bonding of these molecules examined by total electron density analysis and localized orbitals; 4) potential energy surface of boron-nitrogen prismane and its possible decomposition paths.

Non-adiabatic interaction is examined for XH_2, where X is chosen from C, Si, Ge, Sn and Pb. Spin-orbit coupling using the Breit-Pauli hamiltonian is used to mix the lowest singlet and triplet states.

DEDICATION

In memory of my mother and my brother...

This thesis is also dedicated to my father and Yoshiko Aoki.

TABLE OF CONTENTS

ACKNOWLEDGEMENTS

I would like to express my sincere gratitude to my advisor and a good mentor, Mark S. Gordon. If not for his incredible amount of patience, I would not have come this far. Also, I would like to thank him for supporting my coffee ritual by extended lease of his coffee cup. I would like to acknowledge my good friend Mike Schmidt for giving me insights on just about everything on earth. I can not leave out the fruitful interactions I had with everyone in the Gordon group. Thank you all.

It is certainly not enough space for me to list all the names I would like to acknowledge. Hundreds (or even thousands) of people whom I met, strongly influenced the way I think about and look at the world. I am a product of such influences, and I would like to thank those who gave me their perspecitves.

I would like to acknowledge a number of scientists who helped me a great deal past few years. The names of people whom I am indebted to are: Drs. Mohammad Al-Laham, Riza Bahktire, Kim Baldridge, Tom Cundari, Kenro Hashimoto, Kimihiko Hirao, William Jenks, Shiro Koseki, Takako Kudo, Harvey Michels, John Montgomery, Keiko Takano, Tetsuya Taketsugu and Satoshi Yabushita.

This work was performed at Ames Laboratory under Contract No. W-7405-Eng-82 with the U. S. Department of Energy. The United States government has assigned the DOE Report number IS-T 1759 to this thesis.

Finally, I would like to thank my fiancée Yoko for her TLC.

GENERAL INTRODUCTION

Modern chemistry is a part of an endless endeavor of humans trying to rationalize nature in our own terms and also to recreate what nature has given to us on this planet. We chemists, throughout the years, have created unique knowledge and skills of our own. These knowledge and skills are applied today to make our lives easier. We chemists also have adapted a countless amount of knowledge and skills from our colleagues in other fields of science. One of the most recent could certainly include a field known as quantum chemistry, more specifically *ab initio* quantum chemistry. In recent years *ab initio* quantum chemistry has become undeniably an important area of chemistry. The recent explosive progress in computer technologies, new and efficient algorithm development, and development of accurate and more realistic theoretical foundation, transformed a field that began with a rather specialized field of chemistry into a field native to chemistry. Today the range of predictive power has spread wide into the chemistry fields where one could accurately predict the smallest interaction of helium dimer to large and complicated molecular properties of biomolecules such as metal porphyrin and DNA fragments.

One of the most important aspects of theoretical chemistry is not only to obtain prediction of properties derived from the wave functions, such as energetics, but also to give meaning to the quantity that was calculated for the system under consideration. Explanation of a chemical system under consideration is as important as prediction of properties. Throughout this dissertation, the author has, at least, tried to give explanations to the chemistry under investigation.

In this dissertation quantum chemical methods, more specifically *ab initio* quantum chemistry methods, are applied to a class of molecules called high energy density materials (HEDM)[1]. HEDM are searched for development and understanding of new fuel systems, which may include additives to the existing rocket booster solid fuel systems, such as solid hydrogen and liquid oxygen system. From the beginning of this project, theory played an important role in prediction of possible high energy species.

Figure 1 shows important requirements that a HEDM has to meet, in order to carry out theoretical calculations, especially quantum chemical calculations. A HEDM is a metastable minimum on its potential energy surface (PES), that is connected by means of a minimum energy path to a stable minimum. These two states should be separated by a large energy (ΔH is large) so that a large energy release can be achieved upon chemical transformation. This may be an oxidation process or even isomerization reaction, for the

system under consideration. A HEDM should be kinetically stable; the PES surrounding the metastable minimum should have a high enough barrier so that the molecule is stable enough to be synthesized. Third, the molecular weight of a HEDM candidate is small. One performance measure is obtained through the specific impulse[2] (I_{sp}), which is inversely proportional to the square root of the molecular weight. For the given weight of the material, the energy release achieved by the chemical transformation can be maximized. It is certainly more crucial to the launch of the space shuttle, for example, to maximize the important payload than to carry expendable fuel. The last requirement, but not the least, is that no crossing of states should occur that could lead to dissociation or other transformation to undesired products. For example, the HEDM is typically a singlet state as shown in Figure 1, and if there is a crossing of a low-lying triplet state near the transition state, then the undesired triplet products, which do not release as much energy as the transformation to the lower singlet minimum, could be formed. Depending on how large the spin-orbit coupling at the crossing point is, the molecule could go to the triplet state to obtain undesired products.

Dissertation Organization

A search for molecules that meet the first three HEDM requirements described above is investigated in this dissertation. First four chapters are journal articles that have been published, accepted or in a process to be submitted. In Chapter 1, potential energy surfaces of NH_4^- and PH_4^- are discussed. Also, the stability of tetrahedral isomers of NH_4^- and PH_4^- are discussed in terms of hydride ion dissociation through *ab initio* classical trajectories and of vertical first and second ionization potentials. In Chapter 2, aromaticity of benzene analogs of group IV-group IV benzenes and group III-group V analogs is discussed. Group IV elements are chosen from carbon, silicon and germanium; group III elements are chosen from boron, aluminum and gallium, and group V elements are chosen from nitrogen, phosphorus and arsenic; a total of 15 different benzene isomers were compared. These atoms are arranged in such a way that would keep the analog isoelectronic to benzene. Then, in Chapter 3, the prismane analogs of the same elemental composition as discussed in Chapter 2 are compared for their stabilities and their energetics.

Chapter 4 of this thesis deals with spin-orbit interactions in chemistry. Investigation of group IV XH_2 PES, where X is chosen from carbon, silicon, germanium, tin and lead, and the effect of spin-orbit coupling on the PES is discussed. In this chapter, singlet-triplet

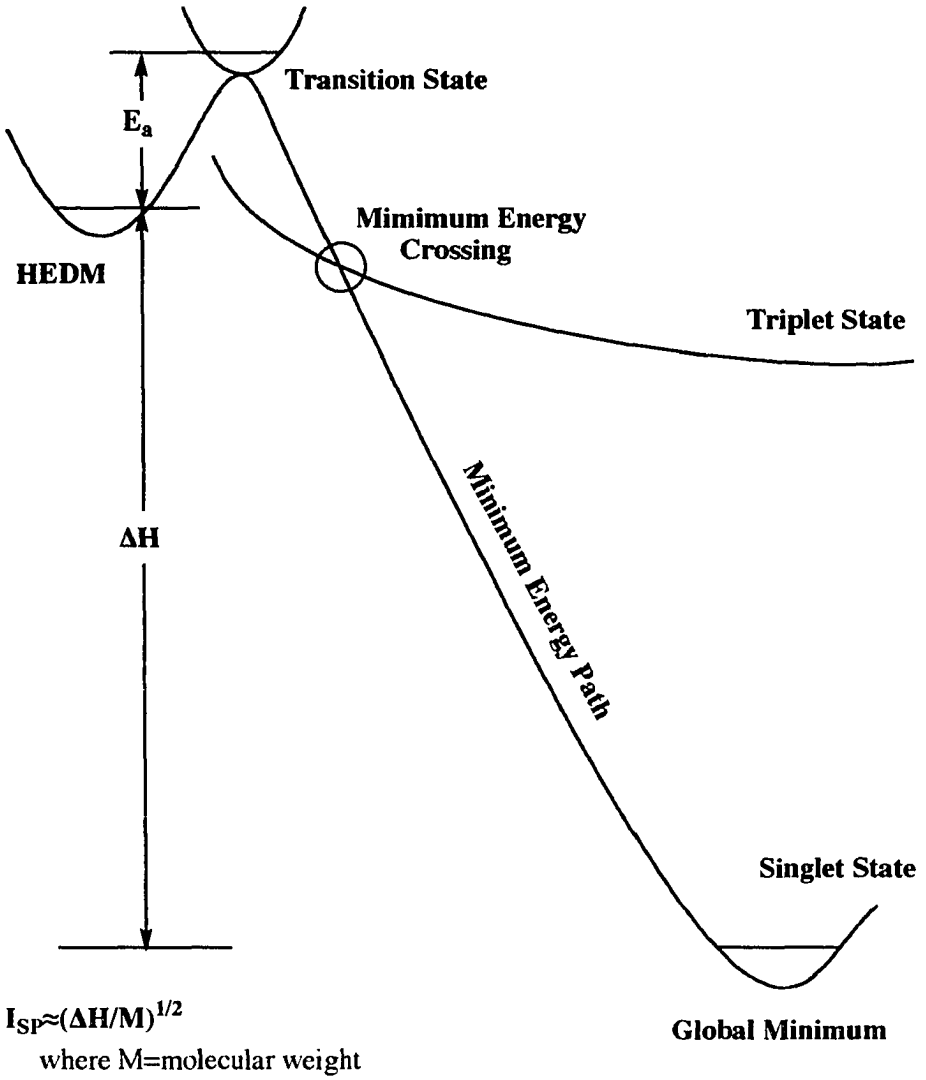

Figure 1. Definition of High Energy Density Material (HEDM).

splittings and minimum energy crossing points are discussed. Simple one dimensional Landau-Zener transition probabilities are calculated at the minimum energy crossing points of the XH_2 molecules to estimate intersystem crossing probabilities.

Chapter 5 discusses preliminary results for the boron-nitrogen prismane potential energy surfaces as an ongoing project and future work. The boron-nitrogen prismane was found to be very high energy (≈160 kcal/mol) when compared with its benzene analog in Chpater 3. The chapter includes geometric and energetic information on the potential energy surfaces of $B_3N_3H_6$ molecules.

Finally, as a summary of this dissertation, general conclusions are drawn from each chapter.

Theoretical Considerations

Hartree-Fock and Perturbation Theory

In this section, the theoretical background of selected materials are discussed. Only the coding projects[3] that the author has done and other important considerations that are of interest to the author are discussed in this section. The following subsection assumes the usual Born-Oppenheimer Hamiltonian is used to solve a form of the Schrödinger equation.

One of the major interests in quantum chemistry is to obtain accurate enough wave functions so that predicted properties such as energetics are reliable. Generally, we start with the Hartree-Fock theory[4] in which the Hamiltonian operator in the Schrödinger equation is approximated by the Fock operator, which has the form

$$F = h + \sum_{a}^{N/2} \left(2J_a - K_a\right)$$

where

$$h = -\tfrac{1}{2}\nabla^2 - \sum_{A} \frac{Z_A}{|r - R_A|} \qquad = \text{one electron operator}$$

$$J_a = \left\langle \phi_a \middle| r_{12}^{-1} \middle| \phi_a \right\rangle \qquad = \text{Coulomb operator}$$

$$K_a \phi_i = \left\langle \phi_a \middle| r_{12}^{-1} \middle| \phi_i \right\rangle \phi_a \qquad = \text{exchange operator}$$

Then the Schrödinger equation becomes

$$F\phi_i = \varepsilon_i \phi_i$$

This differential equation can be converted to a set of algebraic equations and solved by matrix techniques by using a set of known spatial basis functions (namely gaussian functions) to solve the so-called Roothaan equation[5].

$$\boldsymbol{Fc} = \boldsymbol{Sc}\,\varepsilon$$

Successive improvements are made by solving the above equation until the convergence of eigenvalues and eigenvectors is achieved.

In the above formalism, instantaneous electron-electron repulsion, which is called electron correlation, is not considered; only the average electron-electron repulsion is included. In some cases, electron correlation becomes important, and there are a number of ways to treat such a problem. One could expand the wave function to include excited determinants, and then variationally optimize the expansion coefficients. This is called configuration interaction (CI). Another way to treat electron correlation is the perturbation method. One could expand Slater determinants in a cluster expansion, which utilizes an exponential operator, thus giving rise to both linked and unlinked clusters, operating on zeroth order wave function. This method is perhaps the most accurate method available to treat small molecules today. Most popular and less computationally demanding is the Møller-Plesset perturbation method[6].

Møller-Plesset perturbation theory utilizes the results of Rayleigh-Schrödinger perturbation theory. Møller and Plesset partitioned the energy in the following manner

$$H^{(0)} = G - Q$$

where

$$G = \sum_i F_i$$

and

$$F_i = h_i + \sum_j \left(2J_{ij} - K_{ij}\right)$$

F is the Fock operator, and

$$Q = \sum (2J - K)$$

Then, one may express the second-order energy in terms of the two-electron integrals in the

MO basis, J and K, and the differences between the orbital energies of two occupied and two unoccupied (virtual) orbitals. For restricted or unrestricted Hartree-Fock (RHF or UHF) it has the following expression

$$E^{(2)} = -\frac{1}{4}\sum_{ijab}\frac{|\langle ij||ab\rangle|^2}{\varepsilon_a+\varepsilon_b-\varepsilon_i-\varepsilon_j}$$

where ε_m = energy of orbital ϕ_m, and $\langle ij||ab\rangle$ = two-electron integrals in the MO basis, in which the indices i and j run over all occupied MO, and the indices a and b runs over all virtual MO.

One could express this equation in terms of unrestricted Hartree-Fock (UHF) since the UHF has a set of unique orbital energies. However, UHF based MP2 (UMP2) could be spin contaminated due to the contamination in the zeroth order wave function; that is the UHF wave function is not an eigenfunction of spin operator ($\hat{s}^2$). Therefore, it may be advantageous to use the restricted open-shell Hartree-Fock wave function as the zeroth order wave function. The ROHF wave function, however, does not provide a unique set of orbital energies, even though it is not spin contaminated. This dilemma is overcome by a method developed by Handy and co-workers[7a] and simultaneously by Lauderdale *et al*[7b].

After the ROHF energy and density matrix are converged, Fock matrices for α and β electrons are separately constructed. This way Koopman's theorem is obeyed. The α and β Fock matrices can be diagonalized separately in occupied (originally doubly occupied and singly occupied) space and virtual space. Since off-diagonal elements do not contribute to Koopman's theorem, the resulting orbital energies are unique. The resulting α and β Fock matrices after diagonalizations have the form

α Fock Matrix

$$\begin{array}{c} \\ d+s \\ \\ \\ v \end{array}\begin{pmatrix} X_d & 0 & 0 & x_{dv} & x_{dv} \\ 0 & X_d & 0 & x_{dv} & x_{dv} \\ 0 & 0 & X_s & x_{sv} & x_{sv} \\ x_{dv} & x_{dv} & x_{sv} & X_v & 0 \\ x_{dv} & x_{dv} & x_{sv} & 0 & X_v \end{pmatrix}$$

$$\quad d+s \qquad\quad v$$

β Fock Matrix

$$\begin{array}{c} \\ d \\ \\ \\ v \end{array}\begin{pmatrix} X_d & 0 & 0 & x_{dv} & x_{dv} \\ 0 & X_d & 0 & x_{dv} & x_{dv} \\ 0 & 0 & X_v & 0 & 0 \\ x_{dv} & x_{dv} & 0 & X_v & 0 \\ x_{dv} & x_{dv} & 0 & 0 & X_v \end{pmatrix}$$

$$\quad d \qquad\quad v$$

where d and s refer to doubly occupied and singly occupied space in the ROHF wave

function and v refers to the virtual space. Then the second order energy expression can be derived using the unique sets of orbital energies, which now comply with Koopman's theorem.

$$E^{(2)} = -\sum_{ia} \frac{|F_{ia}|^2}{\varepsilon_a - \varepsilon_i} - \frac{1}{4} \sum_{ijab} \frac{|\langle ij||ab\rangle|^2}{\varepsilon_a + \varepsilon_b - \varepsilon_i - \varepsilon_j}$$

The first term arises due to non-zero off diagonal elements of Fock matrices. The second term is the same as the UMP2 energy expression.

The correlation energy calculated by MP2 theory is difficult to interpret in a chemical sense. Pulay *et al.*[8] have suggested the self-consistent electron pair theory (SCEP) to introduce the localized molecular orbitals (LMO)[9] in the MP2 calculation. Their goal of developing the correlated SCEP was two-fold: 1) to eliminate long range interaction and 2) to utilize LMO's to provide interpretation in the calculation.

The latter goal can be achieved by using simple tools[10]. One could use the unitary transformation property of the MP2 energy to obtain LMO based MP2, in which the electron correlation from specific orbitals can be obtained, and therefore the important excitations can be determined.

The canonical MP2 energy can be expressed as a sum of pair energies

$$E^{(2)} = \sum_{ij} e_{ij}^{(2)} = \sum_{ij} \sum_{ab} C_{ij}^{ab} V_{ij}^{ab}$$

where

$$V_{ij}^{ab} = \langle ij||ab\rangle$$

$$C_{ij}^{ab} = \frac{V_{ij}^{ab}}{\varepsilon_i + \varepsilon_j - \varepsilon_a - \varepsilon_b}$$

If a unitary transformation, such as orbital localization $\tilde{\phi} = U\phi$, is applied to C and V, then

$$\tilde{C} = U^{\dagger} C U \quad \text{and} \quad \tilde{V} = U^{\dagger} V U$$

where $\tilde{C}$ and $\tilde{V}$ are the unitary transformed MP2 amplitude and two-electron integral in the MO basis, respectively.

Spin-Orbit Interactions

Up to this section we have dealt with the non-relativistic Born-Oppenheimer

Hamiltonian to describe the systems. However, there are many cases in chemistry where relativistic interactions become important[11], especially for molecules containing heavy elements. Obtaining even a qualitatively correct answer to such molecules is difficult without including some relativistic corrections. For example, one can not possibly calculate a qualitative PES for methyl iodide[12] due to the large spin-orbit coupling of iodine, by using a standard quantum chemical procedure.

There are three main reasons that the relativistic effect is important in chemistry: 1) relativistic contraction of core orbitals, 2) d and f orbital expansion and 3) spin-orbit coupling. The first one arises due to the fact that the mass of an electron around a nucleus changes, because inner s electrons, for example, can be accelerated to a large fraction of the speed of light. This reduces the bohr radius of the electron. The d and f block expansion occurs because of the core contraction; the nucleus is better shielded for the d and f electrons. Spin-orbit coupling arises due to the interaction of the spin magnetic moment and the magnetic field created by its orbital motion.

The first two relativistic effects can be included in a calculation by using effective core potentials (ECP)[13]. The core electrons are projected out in an ECP, the core Hamiltonian is replaced by effective potentials, and the valence electrons are described by nodeless pseudo-orbitals. The potentials are usually obtained by numerical Hartree-Fock[14] for lighter atoms and by the relativistic Dirac-Hartree-Fock[15] for heavy elements. Then, for heavier elements some of the relativistic effects, such as the mass-velocity and Darwin terms, are already included. Therefore the prediction of geometry is generally better than that obtained by all-electron calculations. Also, the ECP is computationally less demanding.

The many-electron wave function used for elucidating spin-orbit coupling is done by a multiconfiguration self-consistent field (MCSCF)[16] calculation. The matrix elements of spin-orbit coupling are calculated by using the microscopic Breit-Pauli Hamiltonian[17] of the form

$$H_{S-O}=\frac{e^2\hbar}{2m^2c^2}\left\{\sum_{i\alpha}\frac{Z_\alpha}{r_{i\alpha}^3}\left(\mathbf{r}_{i\alpha}\times\mathbf{p}_i\right)\cdot\mathbf{s}_i+\sum_{i,j\neq i}\left[\frac{\left(2\mathbf{p}_j-\mathbf{p}_i\right)\times\mathbf{r}_{ij}}{r_{ij}^3}\right]\cdot\mathbf{s}_i\right\}$$

where the first term of the equation above is the one-electron term and I and α in the summation runs over the number of electrons and the number of nuclei, respectively. The $\mathbf{r}\times\mathbf{p}$ term corresponds to the orbital angular momentum and $\mathbf{s}$ is the spin operator. The second term is a two-electron operator, which sums over all electrons. The simplest way to

introduce spin-orbit coupling in a calculation is to use the one-electron term of the operator above, in which the nuclear charge is replaced by the effective nuclear charge, $Z_{i\alpha}^{eff}$

$$H_{S-O}=\frac{e^2\hbar}{2m^2c^2}\left\{\sum_{i\alpha}\frac{Z_{i\alpha}^{eff}}{r_{i\alpha}^3}(\mathbf{r}_{i\alpha}\times\mathbf{p}_i)\cdot\mathbf{s}_i\right\}$$

The effective nuclear charge is obtained by adjusting the nuclear charge to reproduce the experimental spin-orbit coupling constants of the low lying Π states of hydrides (XH species)[18] or the atomic spin-orbit coupling.

Although the form of the Hamiltonian operator above is rather simple, a great deal of chemistry involving heavy elements can be elucidated. Another important aspect of inclusion of the Hamiltonian above is that one can couple two states of different spin. Therefore, one can learn about the PES crossing. If such information can be extracted from the calculations, it is possible to learn about some aspects of dynamics.

References

1 Proceeding of High Energy Density Material Contractors Meeting at Crystal Bay, NV. Air Force Office of Scientific Research, 1994.

2 a) Sutton, G. P. *Rocket Propulsion Elements*, Sixth Ed., John Wiley & Sons Inc., NY, 1992
b) Glassman; Sawyer *The Performance of Chemical Propellants*, Technivision Services, Slough, England, 1970

3 Schmidt, M. W.; Baldridge, K. K.; Boatz, J. A.; Elbert, S. T.; Gordon, M. S.; Jensen, J. H.; Koseki, S.; Matsunaga, N.; Nugyen, K. A.; Su, S.; Windus, T. L.; Dupuis, M.; Montgomery Jr., J. A. *J. Comput. Chem.* **1993**, 14, 1347

4 Szabo, A; Ostland, N. S. *Modern Quantum Chemistry*, 1st. Ed., McGraw-Hill, Inc., 1982

5 Roothaan, C. C. J. *Rev. Mod. Phys.* **1951**, 23, 69

6 Møller, C; Plesset, M. S. *Phys. Rev.* **1934**, 46, 618

7 a) Knowles, P. J.; Andrews, J. S.; Amos, R. D.; Handy, N. C.; Pople, J. A. *Chem. Phys. Lett.* **1991**, 186, 130
b) Lauderdale, W. J.; Stanton, J. F.; Gauss, J.; Watts, J. D.; Bartlett, R. J.; *Chem. Phys. Lett.* **1991**, 187, 21

8 a) Pulay, P.; Saebo, S. *Theoret. Chim. Acta* **1986**, 69, 357
b) Saebo, S.; Pulay, P. *Annu. Rev. Phys. Chem.* **1993**, 44, 213

9 a) Edmiston, C.; Ruedenberg, K. *Rev. Mod. Phys.* 1963, 35, 457
b) Boys, S. F. in *Quantum Science of Atoms, Molecules, and Solides*, Lowdin, P. O. Ed., Academic Press, NY, **1966**, 253
c) Pipek, J.; Mezey, P. Z. *J. Chem. Phys.* **1989**, 90, 4916

10 Petersson, G. A.; Al-Laham, M. A. *J. Chem. Phys.* **1991**, 94, 6081

11 a) Pyykko, P.; Desclaux, J. P. *Acc. Chem. Res.* **1979**, 12, 276
b) Krauss, M.; Stevens, W. J. *Ann. Rev. Chem.* **1984**, 35, 357
c) Christiansen, P. A.; Ermler, W. C.; Pitzer, K. S. *Ann. Rev. Phys. Chem.* **1985**, 36, 407
d) Ermler, W. C.; Ross, R. B.; Christiansen, P. A. *Advances in Quantum Chemistry*, Sabin, J. R.; Zerner, M. C. Eds., Academic Press, San Diego, 1988, p. 139
e) Sadlej, A. J. in *Lecture Notes in Quantum Chemistry II, European Summer School in Quantum Chemistry*, Roos, B. O. Ed. vol. 64, Springer-Verlag, Germany, 1994, p. 203

12 a) Yabushita, S.; Morokuma, K. *Chem. Phys. Lett.* **1988**, 153, 517
b) Amatatsu, Y.; Morokuma, K.; Yabushita, S. *J. Chem. Phys.* **1991**, 94, 4858

13 Many applicatioins are done with: a) Stevens, W. J.; Basch, H.; Krauss, M. *J. Chem. Phys.* **1984**, 81, 6026
b) Stevens, W. J.; Basch H.; Krauss, M.; Jasien, P. *Can. J. Chem.* **1992**, 70, 612

14 Hurley, A. C. "Introduction to the Electron Theory of Small Molecules", Academic Press Inc., NY, 1976, p. 264

15 a) Desclaux, J. P.; Mayers, D. F.; O'Brien, F. *J. Phys. B: Atom. Molec. Phys.* **1971**, 4, 631
b) Desclaux, J. P. *Comput. Phys. Commun.* **1975**, 9, 31

16 a) Werner, H. -J. *Adv. in Chem. Phys.* **1987**, 69, 1
b) Shepard, R. *ibid.*, 63
c) Roos, B. O. *ibid.*, 399

17 a) Richards, W. G.; Trivedi, H. P.; Cooper, D. L. *Spin-Orbit Coupling in Molecules*, Oxford Science Publications, NY, 1981
b) Langhoff, S.; Kern, C. W. in *Modern Theoretical Chemistry*, Vol. 4, Schaefer, H. F. Ed., Plenum Press, NY, 1977, p. 381

18 a) Koseki, S.; Schmidt, M. W.; Gordon, M. S. *J. Phys. Chem.* **1992**, 96, 10768
b) Koseki, S.; Schmidt, M. W.; Gordon, M. S.; Matsunaga, N. *J. Phys. Chem.*, in press, 1995

CHAPTER 1. A THEORETICAL STUDY OF NH_4^- AND PH_4^-

A paper to be published in *Journal of Physical Chemistry*

Nikita Matsunaga and Mark S. Gordon*

Abstract

The potential energy surfaces of NH_4^- and PH_4^- were investigated using *ab initio* electronic structure calculations. Additivity of correlation and basis set effects was used to estimate relative energies. The tetrahedral structures of NH_4^- and PH_4^- are predicted to be minima on the respective potential energy surfaces. *Ab initio* classical trajectory calculations were carried out in order to elucidate possible dissociation paths of tetrahedral ions. The dissociation barrier was estimated to be 32.5 kcal/mol for NH_4^- and 5.5 kcal/mol for PH_4^-. Ionization potentials for the tetrahedral structures of NH_4^- and PH_4^- were calculated to be 0.39 and 0.32 eV, respectively.

Introduction

Structures in which a central atom is surrounded by more than the usual octet of electrons, is sometimes referred to hypervalency, and there are many synthetic examples of hypervalent compounds in the literature[1]. Such species are most common when the central atom is in the third or lower periods, such as five-coordinate silicon species[1b,c]. Several studies of hypervalent silicon and aluminum have been performed in this laboratory[2].

There have been a number of explanations for how the expanded octet is achieved to obtain hypervalency. One of the oldest explanations, due to Pauling[3], describes hypervalency in penta coordinated species by invoking d-orbitals to construct sp^3d hybrid orbitals. However, the existence and the structures of these compounds are readily explained by molecular orbital theory without d-orbital participation. For an excellent discussion of this topic, the reader is referred to the paper by Reed and Schleyer[4]. This issue was placed in an interesting perspective by Cooper *et al.*[5] who suggest that it is the democratic right of every valence electron to take part in chemical bonding if it so desires. In other words, valence electrons can participate in bonding if there is sufficient energy incentive.

The hypervalent NH_4^- anion has been observed via Fourier-transform mass spectrometry[6] using a deuterium labeling study. The authors have concluded that the

observed ion is best described as a hydride ion solvated by an ammonia molecule. Other experimental evidence, from photoelectron spectroscopy[7], suggests that tetrahedral NH_4^- exists on the potential energy surfaces (PES).

Several theoretical calculations have been done to date[8-16]. The complex between NH_3 and H^-, in which the hydride ion is almost collinear with one of the N-H bonds, has been speculated to be a global minimum on the potential energy surface. Also, the tetrahedral structure was predicted[8,14-16] to be a minimum. Vibrational frequencies of the tetrahedral isomer was also reported[11,15,16].

The phosphorus analog, PH_4^-, has been paid much less attention theoretically and experimentally to date. Trinquier *et al.*[17] have used a pseudopotential method to investigate two structures, C_{2v} and C_{4v}, and proposed the possibility that a pseudorotation motion connects the two structures. Ortiz[15] has reported structures, virbrational frequencies, and ionization potentials of tetrahedral and trigonal bipyramidal C_{2v} isomers. Moc and Morokuma[18] have studied T_d, D_{4h}, C_{4v}, and C_{2v} isomers of XH_4^- and XF_4^- (where X=P, As, Sb and Bi) using a pseudopotential method as well as all-electron *ab initio* calculations.

We report here the results of *ab initio* calculations on the NH_4^- and PH_4^- ions. First, the structures and the potential energy surfaces (PES) of NH_4^- and PH_4^- are explored. Then, the stability of the T_d isomers are examined.

Computational Approach

The energetic calculations were performed using locally modified versions of Gaussian 86[19] and Gaussian 88[20]. The methods for calculating the energetics of the NH_4^- and PH_4^- isomers is similar in spirit to the additivity of basis set and correlation effects described by Ignacio and Schlegel[21].

The structures were optimized using second-order Møller-Plesset perturbation theory (MP2)[22] with 6-31++G(d,p)[23] and 6-311++G(d,p)[24] basis sets, denoted as MP2/6-31++G(d,p) and MP2/6-311++G(d,p), respectively. Due to the diffuse nature of the orbitals in anions, all basis sets are augmented with diffuse p-functions for both nitrogen and phosphorus and diffuse s-function for hydrogen to provide more flexibility[25]. The matrices of the energy second derivatives (hessians) were calculated in order to verify the given geometry is a minimum (all eigenvalues of hessian are positive) or a transition state (the hessian has one and only one negative eigenvalue). The energy was further refined by fourth-order Møller-Plesset perturbation theory (MP4) with 6-311++G(2d,2p) and

6-311++G(2df,2pd), denoted as MP4/6-311++G(2d,2p) and MP4/6-311++G(2df,2pd). Also, quadratic configuration interaction(QCI) singles, doubles and perturbative triples (SD(T))[26] calculations were performed with the 6-311++G(2d,2p) basis set (QCI/6-311++G(2d,2p)).

The next step is to calculate the contributions of successive improvements in one- and many-electron basis sets to obtain the QCI/6-311++G(2df,2pd) energies by the following additivity scheme:[21] First, we define four levels of theory

$$A = \text{MP4/6-311++G(2d,2p)}$$
$$B = \text{MP4/6-311++G(2df,2pd)}$$
$$C = \text{QCI/6-311++G(2d,2p)}$$
$$D = \text{QCI/6-311++G(2df,2pd)}$$

At the MP4 level, the improvement due to basis set is

$$\Delta E(B) = E(B) - E(A)$$

and with the 6-311++G(2d,2p) basis set, the MP4 to QCI improvement is

$$\Delta E(C) = E(C) - E(A)$$

Assuming additivity of these two improvements, we can estimate E(D) as

$$E(D) = E(A) + \Delta E(B) + \Delta E(C)$$

The MP2/6-31++G(d,p) intrinsic reaction coordinates (IRC: minimum energy paths connecting reactants with products through transition states) are calculated with either 4th order Runge-Katta[27] or the second-order method of Gonzalez and Schlegel[28] to check the connectivity of two minima on the PES.

Classical trajectory calculations were performed using the *ab initio* force method[29], sometimes called a dynamic reaction coordinate (DRC) calculation, recently implemented in the GAMESS quantum chemistry package[30]. The RHF/6-31++G(d,p) level of theory was used to calculate the trajectories. At the starting point, the equilibrium tetrahedral geometry, an initial kinetic energy of $\leq$ 35 kcal/mol was given to one of the hydrogens chosen to be on the C_3 axis. The symmetry was turned off during the trajectory calculations, except for the generation of initial tetrahedral geometry, to ensure that there is no artificial constraint in all degrees of freedom.

Nuclear motions obtained from the DRC runs were analyzed by a method developed by Taketsugu and Hirano[31], in which the appropriately mass-weighted projection of the DRCs onto each normal mode of tetrahedral NH_4^- and PH_4^- was calculated. In other words, the mass-weighted dot product between the displacement of atoms from the equilibrium

structure and a particular normal mode was calculated. Only the totally symmetric normal modes possess non-zero projections.

Localized orbitals described by Boys[32] were constructed from several geometries obtained by a trajectory calculation to elucidate the nature of bonding during the dissociation of the tetrahedral isomer of PH_4^- into PH_3 and H^-.

Results and Discussions

Structures.

Figure 1 shows the MP2 optimized geometries of NH_4^- and PH_4^-. As can be seen from the figure, there are some structurally similar isomers on the PES of NH_4^- and PH_4^-; both possess C_{2v}(**1b** and **2b**), T_d(**1d** and **2d**), and C_s (**1c** and **2c**) structures.

The structures **1a** and **2a** are rather different. **1a** is the complex, noted earlier, between a hydride ion and ammonia, whereas **2a** can be characterized as a hydrogen molecule complexed with a PH_2^-. The difference in the structures **1a** and **2a** reflect by the thermodynamic stabilities of the two dissociation asymptotes, *i.e.* $NH_3 + H^-$ and $NH_2^- + H_2$ verses $PH_3 + H^-$ and $PH_2^- + H_2$. There has been some speculation that **1a** might be the global minimum on the NH_4^- PES[15]. Indeed, **1a** is the lowest minimum found in this study, and **2a** is found to be the lowest energy isomer on the PH_4^- surface.

The bifurcated structure **1c** is a transition state leading in both directions to **1a**. On the other hand, **2c** is a transition state at the MP2/6-31++G(d,p) level of theory, but at the MP2/6-311++G(d,p) it is a minimum.

Structure **1e** is unique to NH_4^-; it is a transition state leading in one direction to the **1a** structure and in the other to **1b**. The latter is also a transition state that leads to **1a**. Structure **2b** is a transition state, however it is very close to the dissociation limit, $PH_2^- + H_2$.

Structures **2e**, **2f**, and **2g** are related through the inversion motion of four hydrogens in the molecule, and they are unique to PH_4^-. The following scheme shows the normal

modes associated with **2e** and **2f**.

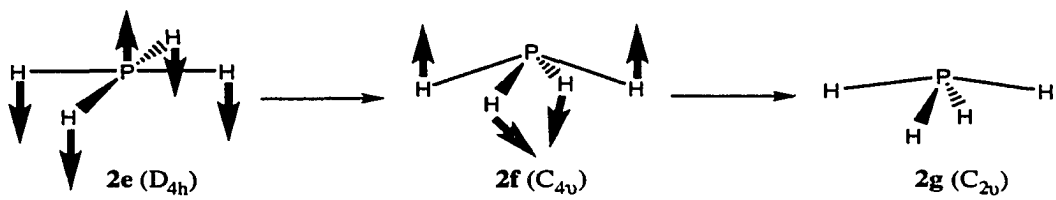

This scheme shows that the motions of the atoms in this process are related to Berry pseudorotation[33] in agreement with the suggestion of Trinquier *et al*[17]. First the hydrogens in **2e** move in a downward direction (A_{2u} representation) to attain the C_{4v} transition state **2f**. The motions of the hydrogens in the imaginary mode in **2f** have B_1 symmetry such that exchange of the "axial" and "equatorial" hydrogens occurs, leading to the minimum **2g**.

The isomer with D_{4h} symmetry in NH_4^- possesses three imaginary frequencies (one is B_{1g} and other two are E_u), at the MP2/6-31++G(d,p) level of theory. However, at the MP2/6-311++G(d,p) level it becomes a transition state with one B_{1g} imaginary normal mode.

Other structures have been found for NH_4^-; however, such species are second- or higher order saddle points. The trifurcated structure shown below is a doubly degenerate second-order saddle point. Moving the attacking hydrogen in the direction of the normal mode vector and reoptimizing the structure leads to structure **1a**.

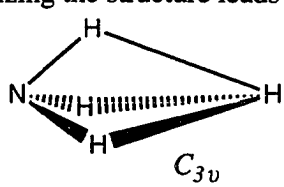

The complex between NH_2^- and H_2 in C_{2v} symmetry, see below, has a repulsive potential energy. Therefore, the distance between the nitrogen atom and the hydrogen molecule continues to elongate during geometry optimization.

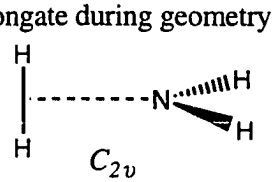

The C_{3v} structure shown below leads to the T_d isomer when optimized.

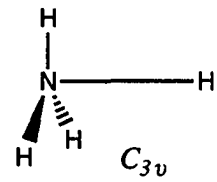

C_{3v}

Cremer and Kraka[10] have calculated the geometries of NH_4^- ions with the MP2/6-31++G(d,p). Their results are essentially identical with the corresponding level of the present work, except for **1a** and **1c**, in which their bond lengths between hydride ion and a hydrogen on ammonia in **1a** and between hydride ion and two hydrogens on ammonia in **1c** are off by 0.05Å. Ortiz[13] has calculated the geometry of **1a** with the MP2/6-311++G(d,p), and his bond lengths are within 0.024Å apart from our results, however, the bond length between hydride ion and ammonia is off by 0.15Å. For **1d**, Cremer and Kraka[10]and Ortiz[15] gave similar results as we have obtained here. Simon and Gutowski[16] have used CASSCF[35] and obtained similar results for **1d**.

In the case of PH_4^-, Ortiz[15] has calculated the geometries of **2d** and **2g**, in which the latter species agrees well with the present work. The bond length of **2d** is off by 0.07Å. Trinquier *et al.*[17] have calculated the geometries of **2g** by limited configuration interaction using pseudopotential with DZP basis sets. Their results agree with our results except for the axial bond length; it is longer by 0.04Å. Moc and Morokuma[18] have calculated **2d**, **2g** and **2f** isomers by MP2 using effective core potentials with DZP basis augmented with diffuse functions, and their values are essentially identical with the preset study.

Energetics.

The total energies of the reference atoms and molecules in this study are shown in Table 1. Table 2 shows the enthalpy differences for NH_4^- with respect to $NH_3 + H^-$, and Table 3 shows the analogous enthalpy differences for PH_4^-. As can be seen from the tables, electron correlation is very important calculating the energetics. The RHF level of theory in the tables are irrelevant in terms of determining energetics, since the geometries are optimized at the MP2 level of theory; the RHF values in the tables are shown as reference. The essential trends are given correctly by MP2. Higher-order perturbation theory, such as MP4 or QCI is necessary only to determine quantitative energy differences. The differences in the

predicted energetics between the MP4/6-311++G(2d,2p) and the QCI/6-311++G(2d,2p) level of theory are quite small.

One-electron bases are well converged at 6-311++G(2df,2pd). The energetics obtained by MP4 with the 6-311++G(2df,2pd) and 6-311++G(2d,2p) basis sets agree to less than 1 kcal/mol, except for **2e** and **2f**. The latter differ by more than 2 kcal/mol. These differences reappear when the QCI/6-311++G(2df,2pd) energies are deduced by the additivity scheme discussed in the previous section. The QCI/6-311++G(2df,2pd) values, except for two mentioned above, are very similar to the values obtained using the QCI/6-311++G(2d,2p) level of theory.

The G1 theory of Pople *et al.*[34] has successfully predicted the heats of formation for many small molecules. Their expected deviation from the experimental heats of formation is about 2 kcal/mol. The energetics calculated in the present work do not include empirical parameter ("high level correction"), however, the number of bound paired valence electrons are the same for most cases, and one larger than the reference $XH_3 + H^-$ or $XH_2^- + H_2$. So, the expected deviation from experiment is ≤ 4 kcal/mol.

A few attempts have been made to form an ion complex of PH_4^- in a flowing afterglow apparatus, however, they have been unsuccessful thus far[35]. The difficulty, as shown in Table 3, is due to the fact that, unlike the NH_4^- PES, the lowest energy complex **2a** is only 1 kcal/mol below the $PH_2^- + H_2$ asymptote, and thus this complex is not very stable. The PES in this region is quite flat, and the structures **2a** and **2b** have essentially the same energy.

The relative energies for $NH_3 + H^-$ verses $NH_2^- + H_2$ were previously[8] calculated to be 13 kcal/mol at the HF level, in good agreement with the result obtained here at a similar level of theory. Cremer and Kraka[10] have calculated **1a** to be ≈ 9 kcal/mol more stable relative to $NH_3 + H^-$ at the MP2/6-31++G(d,p) level of theory, in agreement with our most accurate calculation. However, their relative energy for tetrahedral NH_4^- (**1d**) is 1.3 kcal/mol. This is underestimated by over 10 kcal/mol in comparison to the present work. Cardy *et al.*[11] have calculated the relative energies of **1a** and **1d** using the CISDQ/4-31++G(d,p) level of theory, and have obtained -6.3 and 6.1 kcal/mol relative to $NH_3 + H^-$, respectively. The relative energy of **1d** is underestimated by ≈ 6 kcal/mol in comparison to the present work.

Trinquier *et al.*[17] has calculated the relative energy of **2g** with respect to $PH_3 + H^-$ using HF/DZP+ and CI/DZP+, to be 4.8 and 1.4 kcal/mol, respectively. Their CI result (1.4

kcal/mol) is underestimated by 6 kcal/mol using the QCI/6-311++G(2df,2pd) levels of the present work. They have also reported that the structure **2f** is higher in energy than **2g** by 9 kcal/mol at the HF level of theory. The result of the present work estimates the energy difference between **2f** and **2g** to be ≈ 5 kcal/mol. More recently, the relative energies calculated for **2e**, **2f** and **2g** by Moc and Morokuma[18] are in good agreement with our best, QCI/6-311++G(2df,2pd), results.

Stability of Tetrahedral Isomers.

The tetrahedral isomers of NH_4^- and PH_4^- are not connected to any other isomers through the IRCs studied here. It is important to understand the origin of the stability and the nature of bonding of these tetrahedral isomers. Two tools that are useful for this endeavor are the dynamic reaction coordinate (DRC) analysis and the ionization potentials.

Cardy *et al.*[11] have investigated the reaction profile of tetrahedral NH_4^-, in which one of the hydrogens is pulled outward in the direction along the C_{3v} dissociation pathway, by fixing the dissociating bond distance at successively larger values and optimizing the remaining geometric parameters. Their CISD/DZ+P barrier to dissociation along the C_{3v} path is 18.6 kcal/mol relative to the tetrahedral structure.

It is indeed possible that there is no transition state associated with the T_d structures due to their high symmetry. On the H-C≡P potential energy surface, for example, there is no transition state[36]. Instead, there is a second order saddle point, possessing doubly degenerate imaginary vibration modes, to convert H-C≡P to C=P-H. This is indicative of having high ($C_{\infty v}$) symmetry. The tetrahedral structures of NH_4^- and PH_4^- might fall into such a category, and there may not be a transition state that connects the T_d structures to other isomers. To investigate this possibility in a qualitative manner, we turn to a dynamic reaction coordinate analysis.

a) DRC analysis.

A trajectory calculation initiated by giving an initial kinetic energy to a hydrogen in a C_s plane was carried out. However, this resulted only in molecular rotation, therefore no further C_s trajectory was calculated. Other trajectories (using scissoring motions, Q4 and Q5 in Figure 2) were considered; however, this C_{2v} process must occur at very high energy,

since two bond breakings must occur in order to have a reaction in the C_{2v} path, to preserve symmetry. Therefore such a reaction is less likely to occur, and therefore no trajectory was calculated.

Trajectories with C_{3v} symmetry were calculated for up to 300 fs with an initial kinetic energy ≤ 35 kcal/mol. No dissociation was observed until 32.5 kcal/mol of kinetic energy was introduced. Figure 2 shows the normal modes of tetrahedral NH_4^- in C_{3v} symmetry. Since a DRC preserves the symmetry of the reaction coordinate[31], one expects those normal mode vibrations that are symmetric with respect to C_{3v} symmetry (A_1 modes Q3, Q6 and Q7 of Figure 4) to be the ones that participate in the bond breaking process to obtain ammonia and a hydride ion.

The energy changes during the trajectory calculations (initial kinetic energy = 32.0 and 32.5 kcal/mol), giving energy to one of the hydrogens chosen as the C_{3v} axis in NH_4^-, are shown in Figure 3. The total energy is, of course, conserved in these calculations, and kinetic and potential energies oscillate in opposite directions. The molecule undergoes large amplitude motions during the trajectory with an initial kinetic energy of 32.0 kcal/mol, which is the threshold of the bond breaking process at the RHF/6-31++G(d,p) level of theory. The nuclear motions can be described by mapping the DRC onto the normal modes of vibration[31]. Figure 4 shows the plots of these projected coordinates. As expected, the only normal modes that can contribute in the C_{3v} dissociation path are Q3, Q6 and Q7. Q6 and Q7 are in resonance with each other, while Q3 contributes in the opposite direction during the large amplitude motions shown in Figure 4a. The axis bond compresses and stretches from 0.83Å to 1.60Å, corresponding to about 80% to 156% of the equilibrium bond length.

Dissociation would occur for an initial kinetic energy of 32.5 kcal/mol given to the axial hydrogen. Since this energy is rather high, the dissociation occurs during the first energy oscillation. The amplitudes of oscillation after dissociation take place, correspond roughly to the inversion barrier of ammonia, and the kinetic energy of the dissociated hydride ion is about 0.06 hartree (1.6 eV), as shown in Figure 3b.

The threshold of dissociation in PH_4^- is only 5.0 kcal/mol, quite different from NH_4^-. The nuclear motion is still oscillatory at 5.0 kcal/mol, but it is much smaller than that of NH_4^-. Figure 5 shows the energy change during the trajectory calculations for PH_4^-. Dissociation (Figure 5) does not take place until the seventh energy oscillation. The energetic profiles are similar to those found for NH_4^- except for the smaller amplitudes. Figure 6 shows the plots of the vibrational mapping of the DRC. The oscillations of the mapped

coordinates are rather different from the NH_4^-. In both cases, above and below the threshold, the oscillatory period of Q3 is about twice as large as those for Q6 and Q9. In fact, the dissociation occurs after completing one period of Q3 vibrational motion. Below threshold the axial bond compresses and stretches from about 1.23Å to 1.665Å, which is about 90% to 112% of the equilibrium bond length. This is due to the fact that only a small amount of energy is given to the bond of interest. As a consequence, the phosphine has a small amount of vibrational energy. The dissociated hydride ion in PH_4^- has a larger kinetic energy (0.075 hartree or 2.0 eV) than that of NH_4^-, despite the smaller amount of initial energy. Referring to Table 3, note that the sum of the initial kinetic energy plus the energy released by breaking the XH_3-H^- bond ($T_d \rightarrow XH_3 + H^-$) is about the same for X = N, P. It is sensible therefore that the H^- receding from the heavier PH_3 will have greater kinetic energy.

Figure 7 shows the localized orbitals of PH_4^- constructed at several geometries during a trajectory calculation to show how orbitals are rearranged during dissociation. The left-hand side of Figure7a is a σ bonding orbital, and as the time progresses in the dissociation process, the orbital becomes the s^2 orbital of H^-. On the other hand, the diffuse s-type orbital, double-Rydberg orbital[37], on the right-hand side of Figure 7 becomes a lone pair of PH_3 as the time progresses. Figure 7b, taken at the highest energy geometry, is at the threshold of bond dissociation which occurs at 58.5 fs. As the bond stretches further the orbital become more diffuse in nature.

b) Ionization Potentials.

There is only one experimental ionization potential dealt with the tetrahedral isomer of NH_4^- in the literature[7b]. The first ionization potential for NH_4^- is 0.472 eV obtained by photoelectron spectroscopy, and *the structure of this isomer is suspected to be tetrahedral.* The ionization potential has the same value as the electron affinity of neutral NH_4, indicating that the structure of NH_4^- is similar to the neutral.

First and second vertical ionization potentials (Table 4) of the tetrahedral isomers were calculated with several levels of theory by taking differences between the energies calculated at the respective levels of theories between anion and neutral for the first IP and between neutral and cation for the second IP. The first ionization potential of NH_4^- is -0.6 and -0.04 eV at the Hartree-Fock and MP2 levels of theory, respectively, using the

6-31++G(d,p) basis set. This means that the electron in the highest occupied orbital is unstable, and would therefore autoionize. A full valence CASSCF[38] calculation does not correct the sign of the ionization potential. Dynamical electron correlation is very important, based on the RHF-MP2 difference, and at least MP4 is needed to obtain the correct sign. Furthermore, the effect of basis set is also crucial for calculating the IP of the anion. Inclusion of two diffuse functions at each center is needed to obtain an IP close to the experimental value. A similar conclusion was indicated earlier by Ortiz[13]. The IP obtained with the QCI/6-311(2+,2+)G(2df,2pd) (not by additivity, but with the frozen core approximation) is essentially the same as the one obtained with the UMP4/6-31(2+,2+)G(d,p) level of theory. The second ionization potential is large and positive, indicating that the neutral radical species is stable toward autoionization.

A similar trend occurs for PH_4^-. As the level of theory is improved, the first ionization potential goes from negative to slightly positive. The second ionization potential is large and positive, indicating that the neutral radical is stable toward autoionization. The first IP for tetrahedral PH_4^- is slightly less than that obtained for NH_4^-. By starting from NH_4^+ and PH_4^+, the electron attachment process to make the neutral radical species should not be difficult. By using these neutral radicals, trying to attach an electron is perhaps more difficult. Because of the apparently small dissociation barrier calculated by the DRC, even though the first IP is similar to the NH_4^-, observation of the tetrahedral isomer of PH_4^- is expected to be more difficult.

Conclusions

We have examined the PES of NH_4^- and PH_4^-, and the energy differences are deduced by additivity rules to obtain the QCI/6-311++G(2df,2pd) energies. The most stable structure is a complex between an ammonia molecule and a hydride ion, and a complex between H_2 and PH_2^-. The highest energy isomers in both cases are tetrahedral structures.

DRC calculations show that these tetrahedral structures could dissociate into a hydride ion and XH_3. In the case of NH_4^-, it was shown that the energy needed to break an N-H bond in C_{3v} dissociation path is 32.5 kcal/mol. For PH_4^-, the dissociation occurs when 5.5 kcal/mol is given to the P-H bond. These values are likely to be reduced by several kcal/mol upon the introduction of electron correlation and improvement of the basis set.

The first ionization potential predicted for tetrahedral NH_4^- is close to the experimental value, and therefore this anion is stable. Similarly, the first IP for the tetrahedral PH_4^- is

somewhat smaller than that for the NH_4^-, but is predicted to be positive (0.32 eV). The neutral radicals, on the other hand, are stable; both second IP's are about 4 eV.

Since the dissociation of the tetrahedral NH_4^- ion appears to require considerably more energy than ionization to the neutral, it is likely that the molecule will autoionize before it has a chance to dissociate. This is less likely to be the case for tetrahedral PH_4^-.

Acknowledgment.

This work was supported in part by a grant from the Air Force Office of Scientific Research (F49620-95-1-0077). The calculations were performed in part on the North Dakota State University IBM ES9000 computer under a joint study agreement with IBM and in part on an IBM RS6000/530 obtained via a grant to M.S.G. from AFOSR. Some calculations were performed on IBM RS6000/350 computers made available by the Iowa State University. We would like to acknowledge helpful discussions with Dr. Tetsuya Taketsugu on normal mode mapping analysis.

References

1 a) Tandura, S. N.; Voronkov, M. G.; Alekseev, N. V. *Top. Curr. Chem.* **1986**, 131, 99.
b) Curriu, R. J. P. *J. Organomet.* **1990**, 400, 81.
c) Chuit, C.; Corriu, R. J. P.; Reye, C.; Young, J. C. *Chem. Rev.* **1993**, 93, 1371.

2 Windus, T. L.; Gordon, M. S.; Davis, L. P.; Burgraf, L. W. *J. Am. Chem. Soc.* **1990**, 112, 7167.

3 Pauling, L. *The Nature of the Chemical Bond*, 3rd ed.; Cornell University Press: Ithaca, NY, 1960; p 145.

4 Reed, A. E.; Schleyer, P. v. R. *J. Am. Chem. Soc.* **1990**, 112, 1434.

5 Cooper, D. L.; Cunningham, T. P.; Gerratt, J.; Karadakov, P. B.; Rimondi, M. *J. Am. Chem. Soc.* **1994**, 116, 4414.

6 Kleingeld, J. C.; Ingemann, S.; Jalonen, J. E.; Nibbering, N. M. M. *J. Am. Chem. Soc.* **1983**, 105, 2474.

7 a) Coe, J. V.; Snodgrass, J. T.; Freidhoff, C. B.; McHugh, K. M.; Bowen, K. H. *J. Chem. Phys.* **1985**, 83, 3169.
b) Snodgrass, J. T. ; Coe, J. V.; Freidhoff, C. B.; McHugh, K. M.; Bowen, K. H. *Faraday Discuss. Chem. Soc.* **1988**, 86, 241.

8 Ritchie, C. D.; King, H. *J. Am. Chem. Soc.* **1968**, 90, 838.

9 Kalcher, J.; Rosmus, P.; Quack, M. *Can. J. Phys.* **1984**, 62, 1323.

10 Cremer, D.; Kraka, E. *J. Ame. Chem. Soc.* **1986**, 90, 33.

11 Cardy, H.; Larrieu, C.; Dargelos, A. *Chem. Phys. Lett.* **1986**, 131, 507.

12 Hirao, K.; Kawai, E. *J. Molec. Struct. THEOCHEM* **1987**, 149, 391.

13 Ortiz, J. V. *J. Chem. Phys.* **1987**, 87, 3557.

14 Gutowski, M.; Simon, J.; Hernandez, R.; Taylor, H. L. *J. Phys. Chem.*, **1988**, 92, 6179.

15 Ortiz, J. V. *J. Phys. Chem.* **1990**, 94, 4762.

16 Simon, J; Gutowski, M. *Chem. Rev.* **1991**, 91, 669.

17 Trinquier, G.; Daudey, J. P.; Caruana, G.; Madaule, Y. *J. Am. Chem. Soc.* **1984**, 106, 4794.

18 Moc, J.; Morokuma, K. *Inorg. Chem.* **1994**, 33, 551.

19 Frisch, M. J.; Binkley, J. S.; Schlegel, H. B.; Raghavachari, K.; Melius, C. F.; Martin, R. L.; Stewart, J. J. P.; Borowicz, F. W.; Rohlfing, C. M.; Kahn, L. R., DeFree, D. J.; Seeger, R.; Whiteside, R. A.; Fox, D. J.; Fleuder, E. M.; Pople, J. A. Carnegie-Mellon Quantum Chem. Publishing Unit, Pittsburgh, PA 15213.

20 Frisch, M. J.; Head-Gordon, M.; Schlegel, H. B.; Raghavachari, K.; Binkley, J. S.; Gonzalez, C.; Defrees, D. J.; Fox, D. J.; Whiteside, R. A.; Seeger, R.; Melius, C. F.; Baker, J.; Martin, R. L.; Kahn, L. R.; Stewart, J. J. P.; Fluder, E. M.; Topiol, S.; Pople, J. A. Gaussian 88 (Gaussian Inc., Pittsburgh, PA, 1988).

21 Ignacio, E. W.; Schlegel, H. B. *J. Comput. Chem.* **1991**, 12, 751.

22 Møller, C; Plesset, M. S. *Phys. Rev.* **1934**, 46, 618.

23 a) Hehre, W. J.; Ditchfield, R.; Pople, J. A. *J. Chem. Phys.* **1971**, 54, 724.
b) Francl, M. M.; Pietro, W. J.; Hehre, W. J.; Binkley, J. S.; Gordon, M. S.; DeFrees, D. J.; Pople, J. A. *J. Chem. Phys.* **1982**, 77, 3654.

24 a) Raghavachari, K.; Binkley, J. S.; Seeger, R.; Pople, J. A. *J. Chem. Phys.* **1980**, 72, 650.
b) McLean, A. D.; Chandler, G. S. *J. Chem. Phys.* **1980**, 72, 5639

25 We have used the following diffuse gaussian exponents: N; 0.0639, P; 0.0348, H; 0.0360.

26 Pople, J. A.; Head-Gordon, M.; Raghavachari, K. *J. Chem. Phys.* **1987**, 87, 5968.

27 Baldridge, K. K.; Gordon, M. S.; Steckler, R.; Truhler, D. G. *J. Phys. Chem.* **1989**, 93, 5107.

28 a) Gonzales, C.; Schlegel, H. B. *J. Phys. Chem.* **1990**, 94, 5523.
b) Gonzales, C.; Schlegel, H. B. *J. Chem. Phys.* **1991**, 95, 5853.

29 a) Stewart, J. J. P.; Davis, L. P.; Burgraff, L. W. *J. Comput. Chem.* **1987**, 8, 1117.
b) Maluendes, S. A.; Dupuis, M. *J. Chem. Phys.* **1990**, 93, 5902.

30 a) Schmidt, M. W.; Baldridge, K. K.; Boatz, J. A.; Elbert, S. T.; Gordon, M. S.; Jensen, J. H.; Koseki, S.; Matsunaga, N.; Nguyen, K. A.; Su, S.; Windus, T. L.; Dupuis, M.; Montgomery, J. A. *J. Comput. Chem.* **1993**, 14, 1347.
b) Contact Mike Schmidt at mike@si.fi.ameslab.gov concerning this program.

31 a) Taketsugu, T.; Hirano, T., submitted to *J. Phys. Chem.* **1995.**
b) For application, see Taketsugu, T.; Gordon, M. S., *J. Phys. Chem.* submitted **1995.**

32 Boys, S. F. in Quantum Science of Atoms, Molecules, and Solids; Lowdin, P. O., Ed.; Academic Press, New York, 1966; p 253.

33 a) Berry, R. S. *J. Chem. Phys.* **1960**, 32, 933.
b) Mislow, K. *Acc. Chem. Res.* **1970**, 3, 321.

34 Pople, J. A.; Head-Gordon, M.; Fox, D. J.; Raghavachari, K.; Curtiss, L. *J. Chem. Phys.* **1989**, 90, 5622

35 Bierbaum, V., private communication, 1990.

36 Dykema, K. A.; Gordon, M. S. *J. Am. Chem. Soc.* **1985**, 107, 4535.

37 A double-Rydberg ion is described as two electrons in a diffuse Rydberg type orbital interacting with the cationic core providing an electrostatic potential. See Ref. 14, 15 and 16 for explanation.

38 CASSCF; Complete Active Space Self-Consistent Field or FORS-MCSCF Ruedenberg, K.; Schmidt, M. W.; Gilbert, M. M.; Elbert, S. T. *Chem. Phys.* **1982**, 71, 41, 51 and 65.

Table 1. Total energies and zero point energies of the reference atom and molecules. (Energies in hartree)

	Theory	6-31++G(d,p)[a]	6-311++G(d,p)[b]	6-311++G(2d,2p)[b]	6-311++G(2df,2pd)[b]
NH_3					
	RHF	-56.20085	-56.21436	-56.21768	-56.21874
	MP2	-56.39633	-56.43468	-56.45440	-56.47582
	MP4	-56.41420	-56.45425	-56.47442	-56.49678
	QCI			-56.45289	
	ZPE[c]	0.03534	0.03489		
NH_2^-					
	RHF	-55.52742	-55.54122	-55.54448	-55.83614
	MP2	-55.73552	-55.77458	-55.79780	-55.81819
	MP4	-55.75051	-55.79132	-55.81495	-55.83614
	QCI			-55.79213	
	ZPE[c]	0.01899	0.01886		
PH_3					
	RHF	-342.45503	-342.47896	-342.48251	-342.48475
	MP2	-342.59289	-342.66045	-342.68686	-342.71155
	MP4	-342.62008	-342.69042	-342.71910	-342.74530
	QCI			-342.66392	
	ZPE[c]	0.02523	0.02498		
PH_2^-					
	RHF	-341.85779	-341.88105	-341.88328	-341.88510
	MP2	-341.99299	-342.05891	-342.09164	-342.11489
	MP4	-342.01718	-342.08528	-342.12036	-342.14583
	QCI			-342.06484	
	ZPE[c]	0.01358	0.01345		
H_2					
	RHF	-1.13140	-1.13250	-1.13301	-1.13301
	MP2	-1.15777	-1.16030	-1.16280	-1.16466
	MP4	-1.16469	-1.16776	-1.17026	-1.17174
	QCI			-1.17085	
	ZPE[c]	0.01047	0.01033		
H^-					
	RHF	-0.48707	-0.48693	-0.48696	-0.48696
	MP2	-0.50363	-0.50561	-0.50958	-0.51049
	MP4	-0.51039	-0.51285	-0.51820	-0.51859
	QCI			-0.51973	

[a]Geometries optimized at MP2/6-31++G(d,p)

[b]Geometries optimized at MP2/6-311++G(d,p)

[c]ZPE, zero-point energies are calculated at the MP2 level of theory for corresponding basis set.

Table 2. The Enthalpy Difference of NH_4^- with respect to $NH_3 + H^-$ (kcal/mol) and Zero-Point Energies(hartree)

	Theory	6-31++G(d,p)[a]	6-311++G(d,p)[b]	6-311++G(2d,2p)[b]	6-311++G(2df,2pd)[b]
1a(C_s)	RHF	-4.4	-4.1	-3.9	-3.9
	MP2	-7.8	-8.5	-8.8	-9.0
	MP4	-7.5	-8.4	-8.7	-9.0
	QCI[c]			-8.5	-8.8
	ZPE[d]	0.03736	0.03681		
1b(C_{2v}[ts])	RHF	13.2	12.3	12.6	12.6
	MP2	2.5	-2.6	-3.7	-3.8
	MP4	0.1	-1.0	-1.3	-1.4
	QCI[c]			0.1	0.1
	ZPE[d]	0.03335	0.03287		
1c(C_s)	RHF	-4.3	-4.1	-3.9	-3.8
	MP2	-2.0	-6.7	-6.7	-6.9
	MP4	-6.1	-6.6	-6.9	-7.0
	QCI[c]			-7.0	-7.1
	ZPE[d]	0.03650	0.03606		
1d(T_d)	RHF	16.7	17.0	17.5	17.4
	MP2	11.5	8.3	11.9	11.8
	MP4	6.0	7.5	12.1	11.5
	QCI[c]			12.7	12.2
	ZPE[d]	0.04489	0.04428		
1e(C_s[ts])	RHF	17.0	16.5	16.8	16.8
	MP2	4.6	-1.2	-2.0	-2.5
	MP4	2.4	0.3	0.1	-0.4
	QCI[c]			1.5	1.0
	ZPE[d]	0.03736	0.03203		
$NH_2^-+H_2$	RHF	14.6	13.8	13.5	13.5
	MP2	0.5	-0.2	-1.5	-1.4
	MP4	2.2	1.4	1.1	1.1
	QCI[a]			2.5	2.5

[a]Geometries are optimized at MP2/6-31++G(d,p).

[b]Geometries are optimized at MP2/6-311++G(d,p).

[c]QCI/6-311++G(2d,2p) results are of actual calculations and QCI/6-311++G(2df,2pd) values are deduced by assuming additivity (see text).

[d]ZPE, zero-point energies are calculated at MP2 level of theory for corresponding basis set.

Table 3. The Enthalpy Difference of PH_4^- with respect to $PH_3 + H^-$(kcal/mol) and Zero-Point Energies(hartree)

	Theory	6-31++G(d,p)[a]	6-311++G(d,p)[b]	6-311++G(2d,2p)[b]	6-311++G(2df,2pd)[b]
2a(C_s)	RHF	-29.2	-29.4	-28.9	-28.6
	MP2	-34.6	-34.0	-37.0	-36.7
	MP4	-32.8	-32.0	-34.1	-34.4
	QCI[c]			-33.0	-33.5
	ZPE[d]	0.02689	0.02679		
2b(C_{2v}[ts])	RHF	-29.6	-30.0	-29.5	-29.2
	MP2	-34.8	-34.2	-37.2	-37.0
	MP4	-33.0	-32.2	-34.4	-34.7
	QCI[c]			-33.2	-33.8
	ZPE[d]	0.02644	0.02612		
2c(C_s)	RHF	-2.0	-1.4	-1.8	-1.9
	MP2	-2.8	-3.1	-4.1	-4.2
	MP4	-2.6	-3.0	-4.1	-4.2
	QCI[c]			-4.3	-4.1
	ZPE[d]	0.02574	0.02605		
2d(T_d)	RHF	43.6	42.2	42.0	41.4
	MP2	32.8	31.7	35.9	35.9
	MP4	32.6	31.4	36.8	36.4
	QCI[c]			37.4	37.0
	ZPE[d]	0.02555	0.02384		
2e(D_{4h})	RHF	22.8	22.1	21.3	20.7
	MP2	10.5	8.3	5.0	1.8
	MP4	12.0	9.7	7.5	4.3
	QCI[c]			8.8	5.3
	ZPE[d]	0.03073	0.03049		
2f(C_{4v})	RHF	14.0	13.2	12.5	11.5
	MP2	4.0	1.4	-1.0	-3.3
	MP4	5.4	2.4	0.6	-1.6
	QCI[c]			1.8	-0.6
	ZPE[d]	0.02930	0.02898		
2g(C_{2v})	RHF	6.7	6.2	5.1	3.4
	MP2	-0.9	-3.4	-6.7	-8.2
	MP4	0.4	-2.6	-5.6	-6.9
	QCI[c]			-4.4	-5.2
	ZPE[d]	0.02799	0.02778		

Table 3. continued.

$PH_2^-+H_2$	RHF	-31.0	-30.6	-30.1	-28.6
	MP2	-36.4	-34.1	-37.2	-36.8
	MP4	-34.6	-32.0	-34.2	-34.4
	QCI[c]			-32.4	-32.3

[a]Geometries are optimized at MP2/6-31++G(d,p).
[b]Geometries are optimized at MP2/6-311++G(d,p).
[c]QCI/6-311++G(2d,2p) results are of actual calculations and QCI/6-311++G(2df,2pd) values are deduced by assuming additivity (see text).
[d]ZPE, zero-point energies are calculated at the MP2 level of theory for corresponding basis set.

Table 4. Calculted vertical ionization potentials (IP) of the tetrahedral isomers of NH_4^- and PH_4^- (in eV)[a]

	First IP	Second IP
NH_4^-		
UHF/6-31++G(d,p)	-0.58	4.06
(10,8)CASSCF/6-31++G(d,p)	-0.61	3.11
UMP2/6-31++G(d,p)	-0.05	4.42
UMP4/6-31++G(d,p)	0.12	4.44
QCISD(T)/6-31++G(d,p)	0.12	4.44
UHF/6-31(2+,2+)G(d,p)	-0.18	4.07
UMP2/6-31(2+,2+)G(d,p)	0.22	4.42
UMP4/6-31(2+,2+)G(d,p)	0.39	4.44
UHF/6-311++G(d,p)	-0.58	4.06
QCISD(T)/6-311++G(2df,2pd)	0.16	4.53
UHF/6-311(2+,2+)G(d,p)	-0.18	4.07
UMP2/6-311(2+,2+)G(d,p)	0.24	4.45
UMP4/6-311(2+,2+)G(d,p)	0.40	4.47
QCISD(T)/6-311(2+,2+)G(d,p)	0.40	4.48
QCISD(T)/6-311(2+,2+)G(2df,2pd)	0.39	4.53
Experiment[b]	0.472	
PH_4^-		
UHF/6-31++G(d,p)	-0.64	3.58
QCISD(T)/6-31++G(d,p)	0.01	4.05
UHF/6-311++G(d,p)	-0.64	3.58
UMP2/6-311++G(d,p)	-0.08	4.05
UMP4/6-311++G(d,p)	0.04	4.10
QCISD(T)/6-311++G(2df,2pd)	0.06	4.18
QCISD(T)/6-311(2+,2+)G(d,p)	0.30	4.12
QCISD(T)/6-311(2+,2+)G(2df,2pd)	0.33	4.19

[a]Ionization potentials are calculated from the geometries of the anion optimized at the MP2 level of theory with either 6-31++G(d,p) or 6-311++G(d,p). The frozen core approximation is used to obtain the QCI values, others are done with the inclusion of core excitations. 6-31(2+,2+)G indicates that two diffuse functions are used at each center with the 6-31G basis.

[b]See reference 7b.

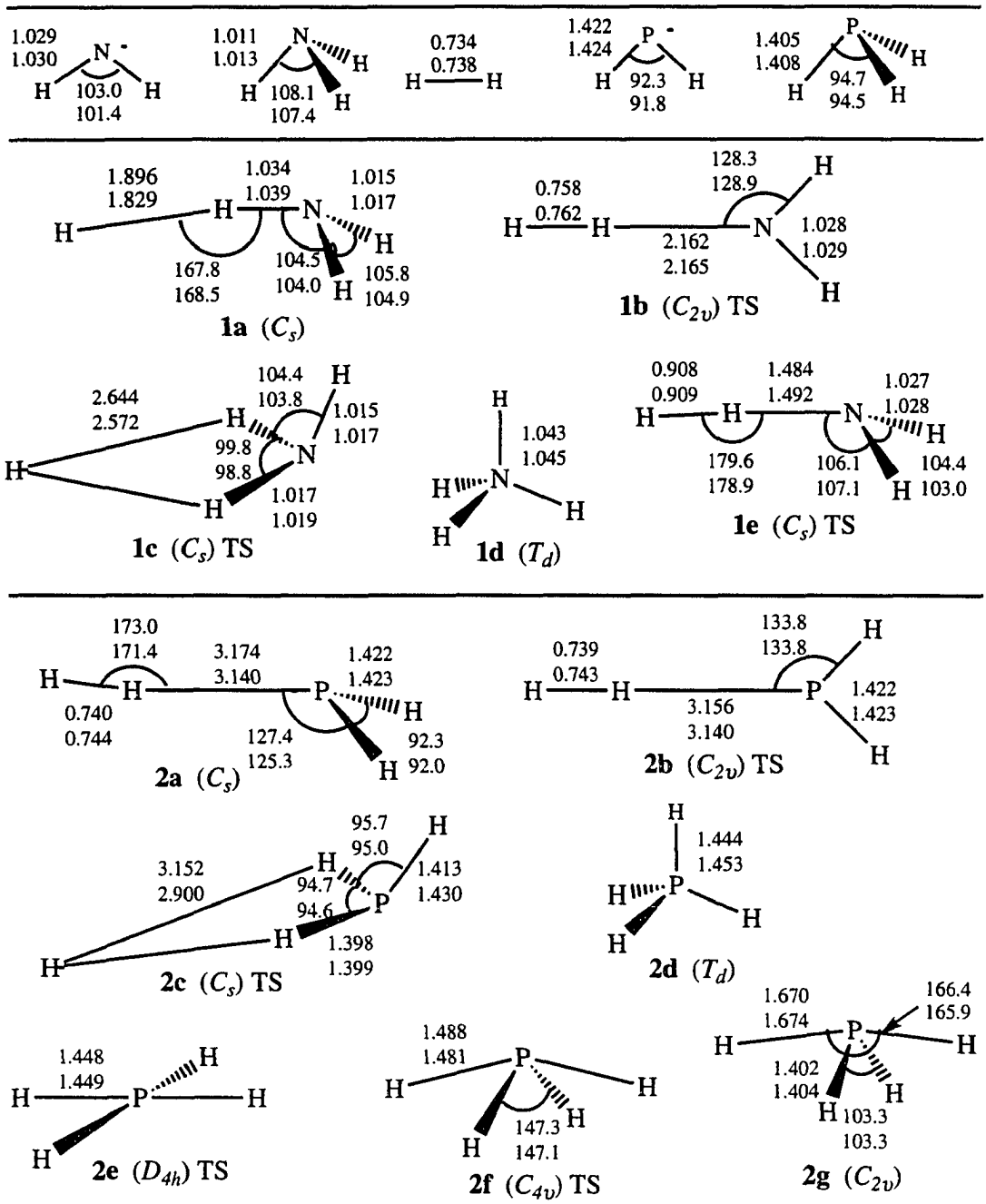

Figure 1. MP2 optimized structures of NH_4^- and PH_4^- and related molecules. The geometries are optimized with MP2/6-31++G(d,p)(the values at the top) and MP2/6-311++G(d,p) (the values on the bottom) levels of theory. TS indicates that the isomer is a transition state.

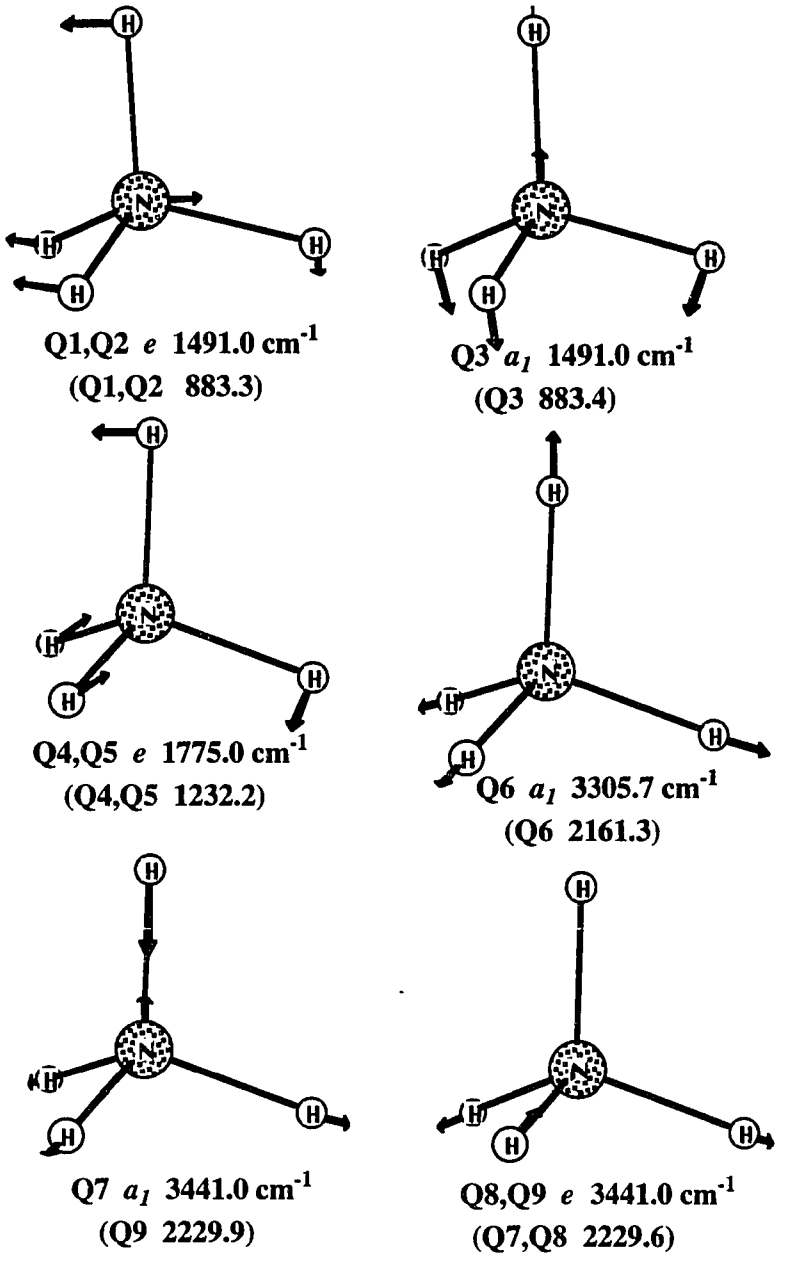

Figure 2. Normal modes of tetrahedral NH_4^- and PH_4^-. Normal mode vectors and thier frequecies are shown in terms of C_{3v} symmetry. The values in parentheses are for PH_4^-.

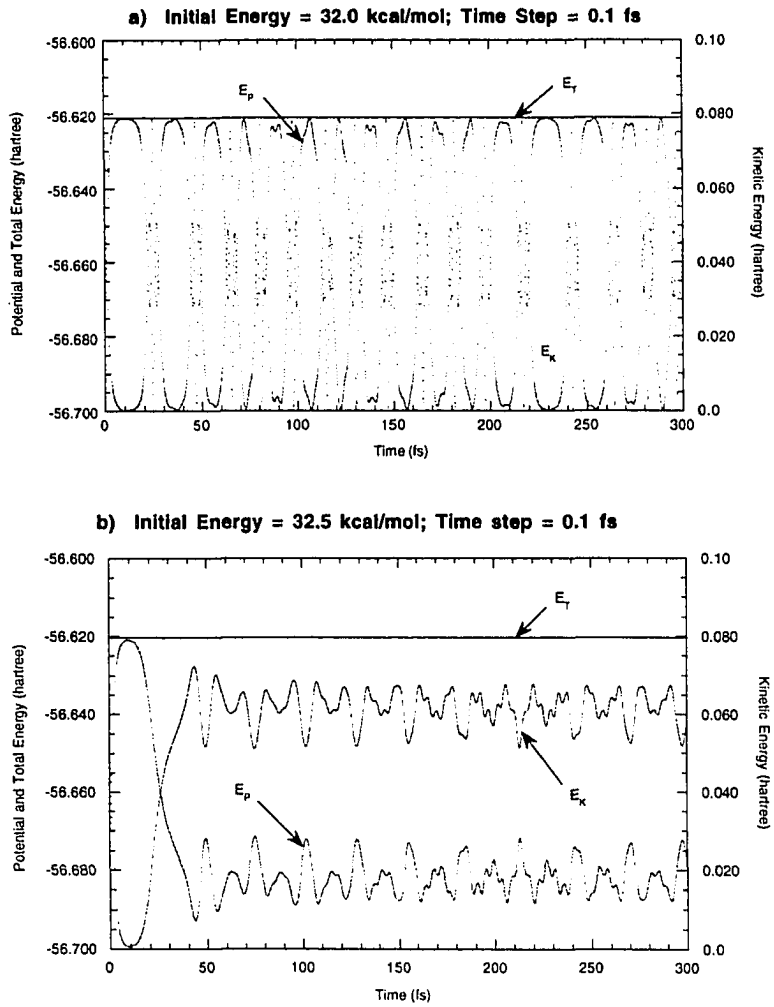

Figure 3. Energy change during trajectory calculations of NH_4^-. Total energy (E_T), potential energy (E_P) and kinetic energy (E_K) are plotted with respect to time (in femtosecond). a) Initial kinetic energy (32.0 kcal/mol) is given to a hydrogen atom in the C_3 axis direction. b) Initial kinetic energy is 32.5 kcal/mol.

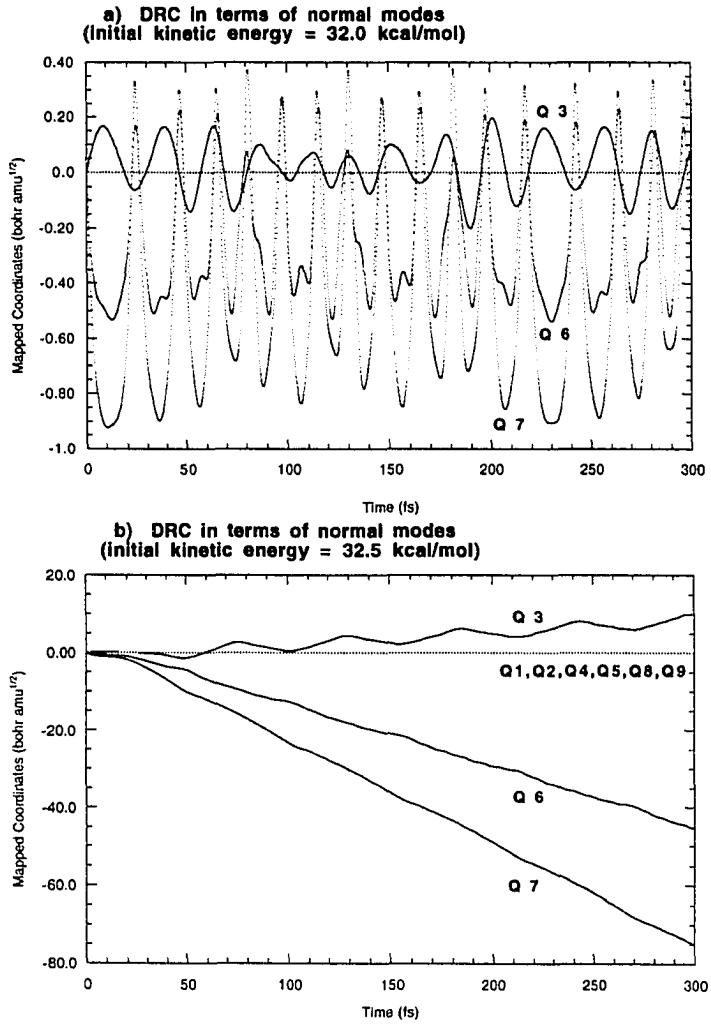

Figure 4. DRC of NH_4^- in terms of normal modes of vibration. The trajectory coordinates are mapped in terms of normal modes of tetrahedral NH_4^- in C_{3v} symmetry. a) shows the normal mode contributions to the trajectory calculated with an initial kinetic energy of 32.0 kcal/mol given to a hydrogen atom on the C_3 axis. b) 32.5 kcal/mol.

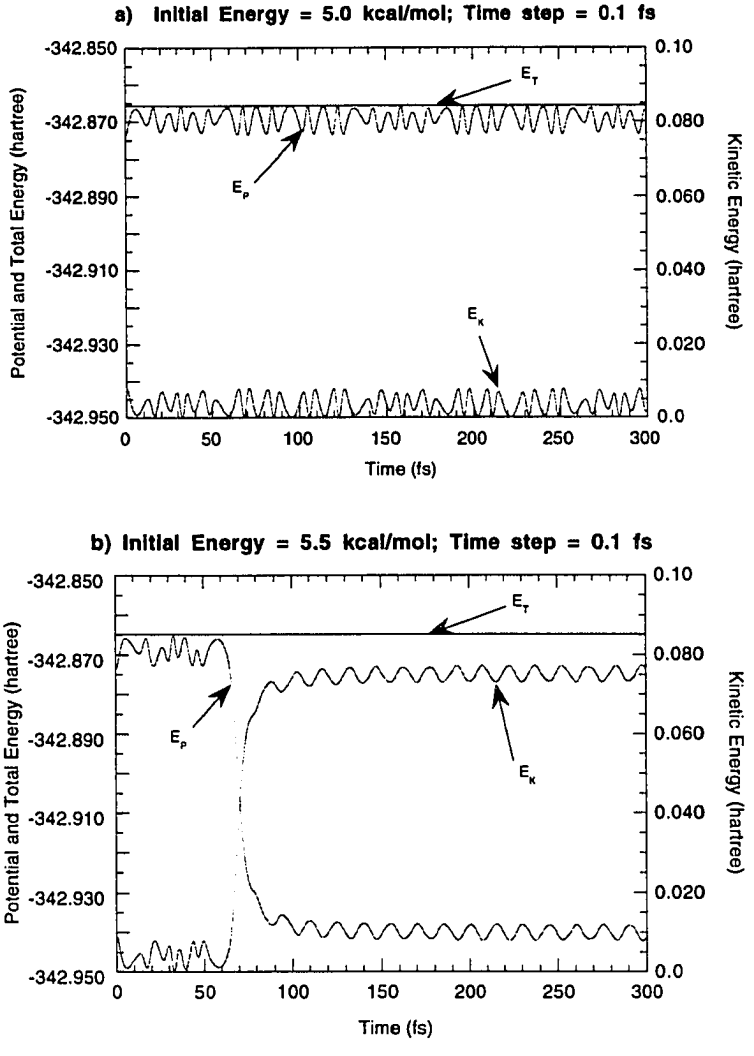

Figure 5. Energy change during trajectory calculations of $PH_4^{\cdot}$. Total energy (E_T), potential energy (E_P) and kinetic energy (E_K) are plotted with respect to time (in femtosecond). a) Initial kinetic energy (5.0 kcal/mol) is given to a hydrogen atom in the C_3 axis direction. b) Initial kinetic energy is 5.5 kcal/mol.

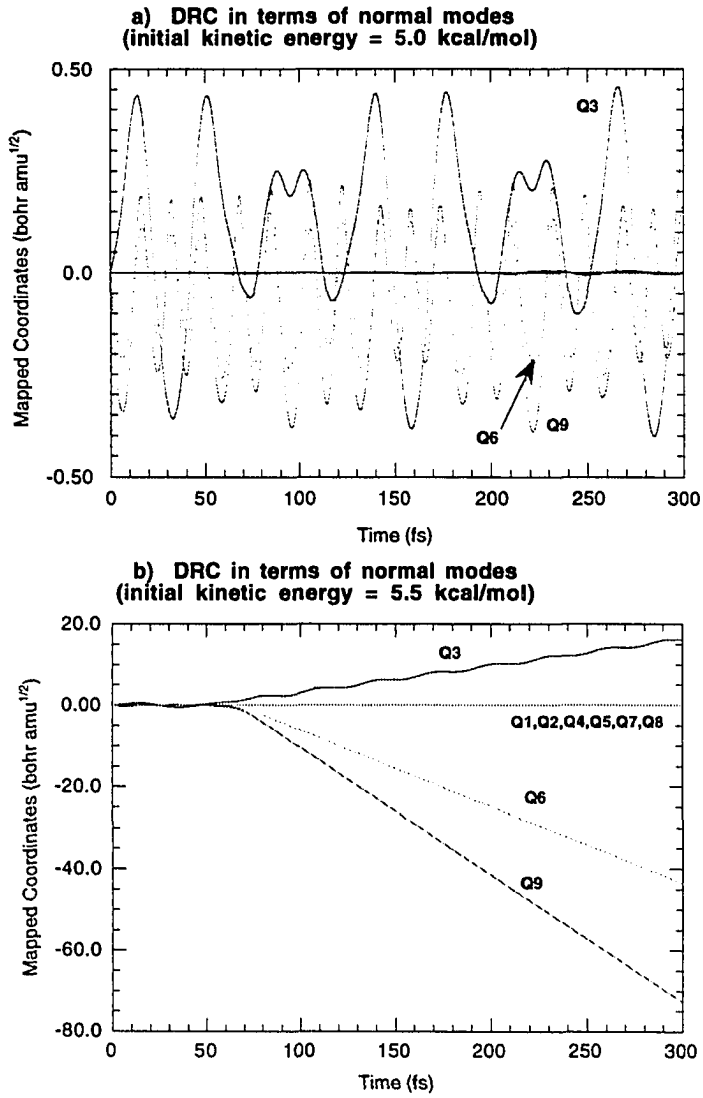

Figure 6. DRC of PH_4^- in terms of normal modes of vibration. The trajectory coordinates are mapped in terms of normal modes of tetrahedral PH_4^- in C_{3v} symmetry. a) shows the normal mode contributions to the trajectory calculated with an initial kinetic energy of 5.0 kcal/mol given to a hydrogen atom on the C_3 axis. b) is of 5.5 kcal/mol.

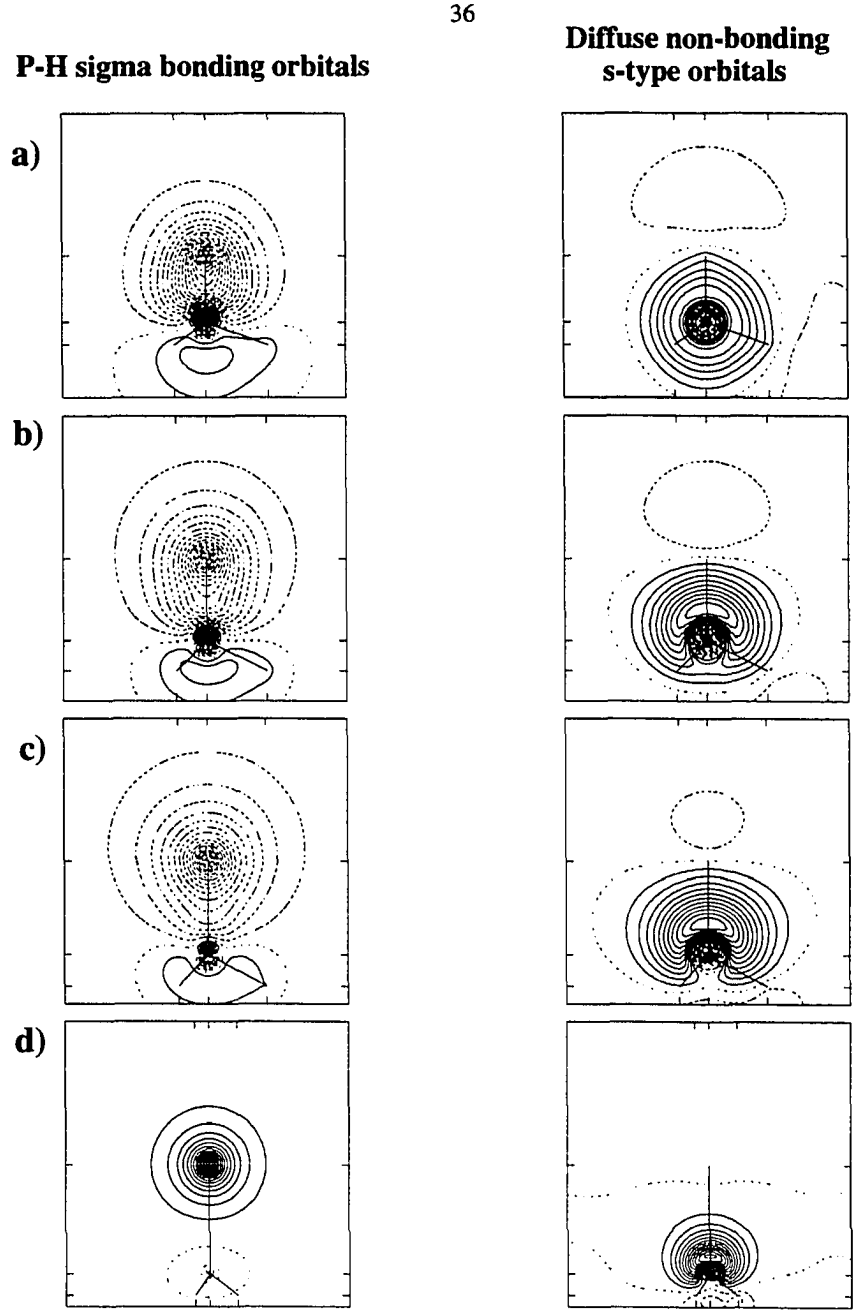

Figure 7. Localized orbitals of PH_4^- for the geometries taken during trajectory run. Each contour is drawn at 0.02 $bohr^{-3/2}$. The geometries at which the localized orbitals are constructed are a) at equilibrium tetrahedral structure (bond length=1.419Å), b) at 58.5 fs, the highest energy point (1.720Å), c) at 65.0 fs (1.960Å), and d) at 80.0 fs (4.206Å).

CHAPTER 2. A COMPARATIVE STUDY OF BONDING IN HETEROATOM ANALOGS OF BENZENE*

A paper published in *Theoretica Chemica Acta*, **1992**, 83, 57

Nikita Matsunaga, Thomas R. Cundari**,
Michael W. Schmidt, and Mark S. Gordon

Abstract

Inorganic benzenes $X_3Y_3H_6$ are investigated, with X and Y chosen from Zn, B, Al, Ga, C, Si, Ge, N, P, As, O, and S such that there are a total of 6 π electrons. Geometries and bond orders are used to qualitatively assess the degree of aromatic π bonding in these species. Bond orders are extracted from the CI density matrix over localized molecular orbitals, using methods pioneered by Ruedenberg. Second row elements C, N, O are found to be more effective at this bonding. The aromatic bonding is poorest when X and Y have a large electronegativity difference.

Introduction

Much attention has been focused on the bonding in the main group analogues of benzene such as borazine ($B_3N_3H_6$). Power has reviewed the examples which exist[1]. Many of these compounds have properties which make them similar to benzene. For example, analogous benzene and borazine transition metal complexes have been synthesized[2]. However, the main-group analogues differ in many respects from benzene, most notably in their kinetic instability. We consider here compounds of the general formula $X_3Y_3H_6$, where X and Y are chosen from Group IIB (Zn) with Group VI (O, S), Group III (B, Al, Ga) with Group V (N, P, As), or Group IV (C, Si, Ge). Throughout this paper X will refer to the more electropositive of the two elements.

Benzene itself is the only such Group IV $X_3Y_3H_6$ molecule extant, although singly substituted silatoluene has been known for some time[3]. Silabenzene[4], disilabenzene[5], and

---

*Dedicated to Prof. Klaus Ruedenberg

**Current Address:* Elvis Presley Professor of Chemistry, Memphis State University, Memphis, TN 38152, USA

germabenzene[4], along with similar species have been considered previously by this group, as well as others[6,7]. The literature of these molecules is well developed, with several reviews available[8,9,10]. Of course, a good deal of attention has been paid to the nature of the π bonding in benzene. We mention here only two studies, both using localized orbitals at the SCF level. Edmiston and Ruedenberg have proven that if only the π orbitals are localized, there are in fact an infinite number of equivalent localized orbitals[11]. Pictures of these were later published[12], showing how the two equivalent Kekule structures can be evolved into each other. Interestingly, when England and Gordon also included the σ orbitals in the localization[13], the resulting orbitals were 3 alternating CC σ bonds, and 3 pairs of banana bonds between the other CC pairs.

In addition to borazine[14], the Group III-Group V analogues of benzene synthesized thus far are the B-P, Al-N, and Ga-P systems. The trimeric B-P compound $[MesBPPh]_3$ was first synthesized by Power and co-workers[15]. Its main structural features include a coplanar ring with equal B-P bond lengths, which are significantly shorter than typical B-P single bond values. Delocalization of the π electrons is suggested by ^{31}P and ^{11}B NMR chemical shifts in which the phosphorus peaks appeared 70 ppm further downfield and the boron peaks 40-50 ppm upfield in comparison with the corresponding dimer. Power and co-workers[16] have also synthesized and structurally characterized an alumazene, $[MeAlN(2,6\text{-}i\text{-}Pr_2C_6H_3)]_3$, in which the ring is also planar. As for the boraphosphazene, a slight upfield shift of the Group III metal (^{27}Al NMR), relative to polyiminoalane was observed. Although the ring is not planar (slightly twisted boat conformation), the Ga-P system, $[(2,4,6\text{-}Ph_3)C_6H_2)GaP(cyclo\text{-}C_6H_{11})]_3$, has been isolated by Power and co-workers[17]. Fink and Richards[18] used homodesmic reactions to calculate the resonance energies of some of these species. Their results, in kcal/mol, are

C-C(22.1) > B-P(12.7) > B-N(11.1) > Al-N(1.9)

Not surprisingly, benzene is found to be more aromatic than the other three inorganic benzenes, with aluminum found to be particularly poor. It isinteresting that there is little apparent difference between N and its heavier congener P.

Known Group IIB-Group VI species include Zn-S trimers[19] $(R'ZnSR'')_3$, with $R'=Me_3SiCH_2$ and $R''=2,4,6\text{-}i\text{-}Pr_3C_6H_2$ or $2,4,6\text{-}t\text{-}Bu_3C_6H_2$. Both of these species

are approximately planar. Solution phase trimeric Zn-O compounds were reported some years ago[20], but otherwise Zn-O trimers have proven elusive[19]. A six membered ring with tetra-coordinate Zn atoms was reported recently[21], but since this molecule cannot be aromatic, it has alternating Zn-O bond lengths. Group IIB-VI compounds (e.g. ZnO, ZnS) have received attention in connection with their use as electronics materials[22].

The interest in the bonding in the main-group benzene analogues has of course focused on the bonding in the π orbitals, in particular the existence or lack of aromaticity. It is the purpose of this paper to use *ab initio* wavefunctions in an attempt to analyze the electronic structure of main group inorganic benzenes.

Calculational Methods

All calculations described herein were performed with the GAMESS *ab initio* quantum chemistry program package[23]. The calculations were performed using the Stevens-Basch-Krauss (SBK) effective core potentials and basis sets[24] for all heavy atoms, and the 3-21G basis [25] for hydrogen. These bases were augmented with a single d polarization function[26] for all elements except hydrogen and zinc. The SBK basis for Zn includes a triple zeta valence d basis, as well as a double zeta valence s and p set. All geometry optimizations were carried out at the restricted Hartree-Fock (RHF) level of theory, within the constraints of D_{3h} or D_{6h} symmetry for heteronuclear and homonuclear analogues, respectively. The energy hessian was calculated numerically at the resulting planar geometries, in order to verify them as minima (all real frequencies), transition states (one imaginary frequency), or higher order saddle points (more than one imaginary frequency).

Our study of the bonding combines ideas from Ruedenberg's Full Optimized Reaction Space MCSCF model[27] with his orbital self-energy localization method[28]. In order to perform the analysis, the LOCL program from the ALIS program system[29] has been incorporated within GAMESS. As shown by Ruedenberg[30], the first order density matrix for a CI wavefunction, expressed in terms of localized orbitals, reveals atomic populations and information about bond orders in a directly interpretable way.

The CI calculation requires 6 localized orbitals, since the rings possess 6 atoms. The simplest way to obtain the necessary 6 π orbitals is a high spin calculation, placing one electron in each of them. These heptet state calculations are carried out at the ground state RHF/SBK(d) geometries. The resulting ROHF canonical π orbitals are then localized so as to maximize their self repulsion energy sum. The localization yields 6 atom-like p orbitals,

referred to as "AO-like" MOs, one located on each atom within the ring. It is important to note that these orbitals, although similar to atomic orbitals, are in fact orthonormal MOs, not valence bond hybrids[30]. A full π CI calculation, including excitations up to 6 electrons, is then performed based on these 6 localized ROHF orbitals, *for the singlet ground state.* The first order density matrix of this localized orbital CI (LMO/CI) has the following two interpretations: (a) The diagonal elements are the electron populations of the atom, and in the present case these necessarily sum to 6; and (b) the off diagonal elements of the density matrix correspond to bond orders, with a large positive number meaning strong bonding, and a negative value indicative of an antibonding interaction. For this reason, Ruedenberg usually refers to such a density matrix constructed over localized MOs as the charge/bond order matrix.

An alternative to the foregoing procedure is to obtain the necessaryorbitals from FORS-MCSCF calculations on the ground state. These include 6 active electrons within an active space consisting of the 6 π and π^* orbitals. Optimizing the orbitals for the singlet gound state of course yields a lower energy than a CI using orbitals optimized for a heptet excited state, but we encountered two difficulties. The first is that in a number of instances, it is not possible to carry out the desired MCSCF calculation. Some of the π orbitals are so polarized that the best correlating orbitals for them are not π^* orbitals. Instead they are (n+1)p orbitals providing in-out correlation on the electronegative element Y. This difficulty is encountered for the Al-N, Al-P, Ga-N, Zn-O, and Zn-S cases. Secondly, even when the calculation does converge to π^* orbitals which are left-right correlating, the bond order matrix for the corresponding localized orbitals is less easily interpreted.

Because our prime interest here is a comparison of benzene analogues with the reference compound benzene itself, only the planar rings are considered. A later work will examine all possible isomeric structures.

Results and Discussion

A. Geometries and Frequencies. The $X_3Y_3H_6$ species considered here possess only alternating electropositive X, and electronegative Y atoms. Choosing X,Y=C,Si,Ge; or X from B,Al,Ga with Y from N,P,As; or X=Zn with Y=O,S ensures that the rings are valence isoelectronic with benzene. Thus, each is potentially aromatic in its planar geometry.

The calculated planar geometries for the species of interest are in excellent

agreement with the available experimental values (Table 1). Apart from Zn-S, errors in bond lengths are less than 0.03A. The deviations of the inner-ring angle from 120-, where experimentally available, are also quite well reproduced by the calculations. The distortion from a hexagon is small in the main group analogues (≈5°), but much larger for the zinc containing rings (≈20°).

The three lowest vibrational frequencies of all species discussed here belong to the a_2" and e" representations of D_{3h}. The a_2" modes lead to chair conformations, while the doubly degenerate e" modes lead to two equivalent boat conformations. The calculated harmonic frequencies at the RHF/SBK(d) level are presented in Table 2. Note that apart from benzene and borazine, all of the rings are rather easily made nonplanar, as the largest frequency calculated for these motions is barely larger than 300 cm^{-1}. In fact, many of the species are not minima on the potential energy surface, as they possess imaginary frequencies for the a_2" or e" modes, indicating their aromaticity is insufficient to maintain planarity. Replacing any second row atom with a third row atom decreases the a_2" and e" frequencies. There is a similar but smaller decline when a third row atom is replaced by a fourth row atom. These are indicative of the decreasing rigidity of the planar rings.

Table 2 shows that all rings containing the second row elements C, N, or O are minimum energy structures. This is consistent with results for isolated π bonds obtained previously in this group[32]: the ability to form a π bond was found to be in the order O ≈ N > C >> S > P > Si. Note however that the presence of the second row atom B is not sufficient to ensure a planar minimum.

Although many of these species are first or third order transition states, the frequencies are small enough that they remain of chemical interest. Steric or electronic effects caused by substituents can perhaps stabilize the planar structures. For example, the B-P system has three small imaginary frequencies when the substituents are hydrogen, but nonetheless a planar B-P ring has been reported with bulky groups[15]. Similarly, the Zn-S trimeric ring which has been reported[19] is close to planarity.

As previously noted by Nagase[7], hexasilabenzene is a transition state leading to a chair conformation, provided the basis is of double zeta plus polarization quality. The Si-Ge analogue is the only other true transition state, with an imaginary frequency of 126cm^{-1}. The remaining species all have three imaginary frequencies, and are thus unstable to both boat and chair distortions. Note that in all cases if the planar geometry is not stable, the vibrational distortion is always with respect to out of plane motions, rather than towards

unequal bond lengths. Thus, each of the molecules seems to have at least some ability to participate in aromatic binding in its planar arrangement.

The most revealing feature of Table 1 is that each species possesses six equal bond lengths in the planar geometry. The group IV X-Y bond lengths are intermediate to the corresponding single and double bond lengths, shown in Table 3. A similar comparison for the other inorganic benzenes is complicated due to the paucity of experimental data and ambiguities in defining a typical single bond. For the group III-V case, it is not clear whether this should be H_3B-NH_3 (which has a weak dative bond) or H_2B-NH_2 (which has a partial dative π bond).

B. Bond Separation Reactions. A quantitative measure of aromatic stabilization, relative to isolated single and double bonds, is the energy of a bond separation reaction[40]. For these isodesmic reactions, one conserves bond type (identical numbers of XH, YH, X-Y and X=Y bonds), but compares the conjugated π system in the ring to separated molecules. The bond separation reactions, along with their energetics are shown in Table 4. For reasons noted above, these are examined only for the Group IV compounds.

The Group IV species show a trend that is consistent with the frequency results presented above. Benzene is the most aromatic species by this measure, and the molecules containing 3 carbon atoms are the next most aromatic. Those rings which do not contain carbon are slightly less aromatic. While there is a considerable drop in the calculated MP2 bond separation energy upon replacing carbons in benzene, there is little variation among the benzene analogues themselves. Even so, those with no carbons are not minima on the potential energy surfaces.

C. Electronic Structure. The degree of covalency in the inorganic benzenes can be assessed from the charge, or electron population in the localized orbital located on each of the 6 atoms. These π atomic populations n_X and n_Y are given in Table 5. When the atoms X and Y are identical, or very similar in electronegativity (e.g., Si-Ge), the 6 π electrons are equally shared. Si-C and Ge-C are also close to full delocalization ($n_Y \approx 1.15$ electrons). The group III-V rings are noticeably more ionic, with $n_Y \approx 1.3$ for B rings, and 1.5 for Al or Ga rings. The orbitals for the two Zn compounds are from approximately converged ROHF calculations (due to orbital symmetry breaking problems), but indicate an

even higher degree of ionicity, $n_Y \approx 1.8$.

The *ortho*, two different *meta*, and *para* bonding interactions are also given in Table 5. The nearest neighbor *ortho* interaction is always the largest, and represents partial bonding. It is largest for benzene itself (0.614) and is only slightly smaller (≈ 0.59) for the remainder of the Group IV rings and for the boron containing rings. This bonding interaction drops off slightly for the aluminum or gallium containing rings, to 0.55, and dramatically for the very ionic zinc rings, to 0.40.

In order to calibrate these bond orders, consider the analogous quantities for the ethylenes $H_2X{=}YH_2$, presented in Table 6. The bond order for a full π bond in C=C is 0.897, and there is a small decrease in bond order, in the range 0.83-0.85, for the other Group IV compounds. The bond order index is therefore not very sensitive to the π bond energy, which is 65 kcal/mol for C=C, and is much smaller for Si=C and Si=Si, 37 and 23 kcal/mole, respectively[32]. Note that the bond orders for all of the rings are somewhat less than these full π bonds, indicative of the delocalization. The majority of the nearest neighbor bond orders in Table 5 fall in the range 0.55-0.61, so that the nearest neighbor interaction in the rings is a significant percentage of the 0.83-0.90 value typical of group IV π bonds.

The large density matrix elements for the non-nearest neighbor π interactions are also indicative of the delocalized interactions in these molecules. There is a fairly substantial bonding interaction (up to 0.11) between the electropositive XX atoms, which is canceled by an approximately equal antibonding interaction between the electronegative and hence electron rich YY pairs (up to -0.11). When X and Y are the same element, or have similar electronegativities, the values for the XX and YY bond orders are much smaller. In all cases, the net *meta* interactions are essentially zero.

The XY *para* interaction is quite substantially antibonding, ranging up to about -0.25. Thus, the density matrix tells us that while all nearest neighbor XY pairs have a bond order that is a substantial fraction of a full π bond, there is a smaller antibonding interaction across the ring. It is this additional antibonding contribution that yields the chemist's perception that benzene's π bond order is 0.5, as the nearest neighbor interactions themselves are stronger than a half bond. We can define an overall π bond order by summing the *ortho*, *meta*, and *para* interactions

$$(6\rho_o(XY) + 3\rho_m(XX) + 3\rho_m(YY) + 3\rho_p(XY))/6$$

In all cases except the two Zn compounds, this average bond order lies in the range 0.46-0.48. The poorly delocalized Zn compounds have values of 0.41 for Zn-O, and 0.37 for Zn-S.

Many other chemists have tried to assign a bond order in benzene. Coulson's simple consideration[41] of the two Kekule structures of benzene leads to a bond order of 0.5; inclusion of Dewar benzene and other valence bond structures leads to a lower value. Pauling[42] used valence bond calculations and bond length-bond order considerations to obtain a π bond order of 0.5. Streitweiser[43] used simple Huckel MO theory to assign a bond order of 2/3 for benzene.

The *para* element of the LMO/CI bond order matrix is just one way of presenting the partial antibonding inherent in a 6 π electron aromatic system. Two possibly more familiar ways involve the ground state SCF orbitals. The canonical MOs of benzene consist of a completely bonding a_{2u} orbital, and a degenerate e_{1g} pair. Each of these e_{1g} orbitals has one node, and this antibonding reduces their formal bond order to just 2/6 of that in the a_{2u} orbital. A pictorial way to display the same antibonding is with the localized closed shell SCF orbitals. In the present $X_3Y_3H_6$ compounds, the localized π orbitals center themselves on Y, with equivalent delocalization towards each neighboring X. As may be seen in Figure 1, there is always an antibonding tail on the Y atom in the *para* position!

The orbitals for the LMO/CI calculation can be obtained directly from MCSCF calculations on the ground state in a number of cases. Where available these values are also included in Table 5. The same trends in ionic character are observed for n_X and n_Y. The bond orders are even closer to each other than when obtained from a CI based on the high spin ROHF orbitals. This close correspondence between the MCSCF and ROHF orbital optimization approaches is encouraging, in the light of their intrinisic N^5 versus N^4 computational expense.

Conclusions

The present calculations consider a number of existing and hypothetical inorganic benzenes. The ionic character increases in the order group IV-IV < group III-V < group IIB-VI, in line with chemical intuition and basic electronegativity arguments. A number of

these compounds possess one or three small imaginary frequencies, but each must still be regarded as a potential synthetic target, as planar B-P and approximately planar Zn-S compounds already exist. Inclusion of the second period atoms C, N, or O is a way to stabilize the rings, as all such rings are minimum energy structures, even with H substituents. This is true even for the Zn-O ring, which has so far proven elusive in the laboratory[19].

The bond orders presented here are very similar for many of the compounds, and are the same as those previously obtained from valence bond or bond length-bond order calculations. They probably do not closely track the bond energies (or "aromaticity"), as AB bonds of the same order n always have different bond strengths (compare H_3C-CH_3) with F-F). Since the bond orders for all rings not containing Zn are actually very similar, it is possible that one day all of them will be isolated in the laboratory.

In closing, we call attention to the beautiful work on localized orbitals for benzene (and many polycyclic aromatic hydrocarbons) by Professor Ruedenberg and his students[12]. That paper shows how the SCF localized orbitals for benzene can be evolved from set of Kekule-like orbitals, to orbitals like that shown here for borazine, to the other equivalent set of Kekule-orbitals. Figure 12 of that paper deserves to be included in every introductory organic chemistry text.

Acknowledgements

This work was supported by a grant from the National Science Foundation (CHE 8911911). The calculations were performed on DECstation 3100 and IBM RS/6000-530 workstations, obtained with the aid of grants from the National Science Foundation, and on an IBM 3090-200E/VF, obtained in part by a Joint Study Agreement with IBM.

References

1. Power, P. P. *J. Organomet. Chem.* **1990**, 400, 49
2. Lagowski, J. J. *Coord. Chem. Rev.* **1977**, 22, 185
3. a) Barton, T.J.; Banasiak,D. *J. Am. Chem. Soc.* **1977**, 99, 5199
   b) Barton, T.J.; Burns, G. T. *J. Am. Chem. Soc.* **1978**, 100, 5246
4. Baldridge, K.K.; Gordon, M. S. *J. Am. Chem. Soc.* **1988**, 110, 4024

5. Baldridge, K. K.; Gordon, M. S. *J. Organomet. Chem.* **1984**, 271, 369

6. Clabo, D. A.; Schaefer, H. F.*J. Chem. Phys.* **1986**, 84, 1664

7. a) Nagase, S.; Teramae, H.; Kudo, T. *J. Chem. Phys.* **1987**, 86, 4513
b) Nagase, S.; Kudo, T; Aoki, M. *J. Chem. Soc., Chem. Commun.* **1985**, 1121

8. Baldridge, K. K.; Boatz, J. A.; Koseki, S.; Gordon, M. S. *Theoretical Studies of Silicon Chemistry.* In: Strauss, H. L.; Babcock, G. T.; Moore, C. B. (ed) *Ann. Rev. Phys. Chem.*, volume 38. Annual Reviews, Inc, Palo Alto, CA, 1987, pp 211-252

9. Gordon, M.S. *Theoretical Studies of Multiple Bonding to Silicon.* In: Liebman JF, Greenberg A (ed) *Molecular Structure and Energetics*, volume 1. VCH Publishers, Weinheim, 1986, pp 101-122

10. Raabe, G.; Michl, J. *Chem. Rev.* **1985**, 85, 419

11. Edmiston, C.; Ruedenberg, K. *Localized Atomic and Molecular Orbitals.* In: Lowdin, P. O. (ed) *Quantum Theory of Atoms, Molecules, and the Solid State.* Academic Press, New York, 1966, pp 263-279

12. England, W.; Salmon, L. S.; Ruedenberg, K. *Localized Molecular Orbitals: A Bridge between Chemical Intuition and Molecular Quantum Mechanics.* In: *Fortschritte der Chemischen Forschung*, volume 23. Springer-Verlag, New York, 1971, pp 31-123

13. England, W.; Gordon, M. S. *J. Am. Chem. Soc.* **1969**, 91, 6864

14. Boyd, R. J.; Choi, S. C.; Hale, C. C. *Chem. Phys. Lett.* **1984**, 112, 136

15. a) Dias, H. V. R.; Power, P. P. *Angew. Chem., Int. Ed. Engl.* **1987**, 99, 1320
b) Dias, H. V. R.; Power, P. P. *J. Am. Chem. Soc.* **1989**, 111, 144
c) Power, P. *Angew. Chem., Int. Ed. Engl.* **1990**, 29, 449

16. a) Waggoner, K. M.; Hope, H.; Power, P. P. *Angew. Chem., Int. Ed. Engl .* **1988**, 27, 1699
b) Waggoner, K. M.; Power, P. P. *J. Am. Chem. Soc.* **1991**, 113, 3385

17. Hope, H.; Pestana, D. C.; Power, P. P. *Angew. Chem., Int. Ed. Engl.* **1991**, 30, 691

18. Fink, W. H.; Richards, J. C. *J. Am. Chem. Soc.* **1991**, 113, 3393

19. Olmstead, M. M.; Power, P.P.; Shoner, S. C.*J. Am. Chem. Soc.* **1991**, 113, 3379

20. a) Noltes, J. G.; Boersma, J. *J. Organomet. Chem.* (1968)12:425
b) Coates, G. E.; Ridley, D. *J. Chem. Soc.* **1966**, *A* 1064

21. Gorrell, I. B.; Looney, A.; Parkin, G.; Rheingold, A. L.
J. Am. Chem. Soc. **1990**, 112, 4068

22. Spanhel, L.; Anderson, M. A. *J. Am. Chem. Soc.* **1991**, 113, 2826

23. a) Schmidt, M. W.; Baldridge, K. K.; Boatz, J. A.; Jensen, J. H.; Koseki, S.; Gordon, M. S.; Nguyen, K. A.; Windus, T. L.; Elbert, S. T.
QCPE Bulletin **1990**, 10, 52
b) Contact mike@si.fi.ameslab.gov concerning this program.

24. a) B-O, Al-S: Stevens, W. J.; Basch, H.; Krauss, M.
J. Chem. Phys. **1984**, 81, 6026
b) Zn-Ge: Stevens, W. J.; Basch, H.; Krauss, M.; Jasien, P. G.
submitted to *Can. J. Chem.*

25. Ditchfield, R.; Hehre, W. J.; Pople, J. A. *J. Chem. Phys.* **1971**, 54, 724

26. a) standard d polarization exponents were used: B=0.6, C=N=O=0.8, Al=0.325, Si=0.395, P=0.55, S=0.65, Ga=0.207, Ge=0.246, As=0.293.
b) B: Binkley, J. S.; Pople, J. A. x*J.Chem.Phys.* **1971**, 68, 879
c) C,N,O: Hariharan, P. C.; Pople, J. A.*Theoret. Chim. Acta* **1973**, 28, 213
d) Al,P,S: Francl, M. M.; Pietro, W.J.; Hehre, W. J.; Binkley, J. S.; Gordon, M. S.; DeFrees D. J.; Pople, J. A. *J.Chem.Phys.* **1982**, 77, 3654
e) Si: Gordon, M. S. *Chem. Phys. Lett.* **1980**, 76, 163
c) Ga,Ge,As: Huzinaga, S. *Gaussian Basis Sets for Molecular Calculations* Elsevier, Amsterdam, 1984

27. Ruedenberg, K.; Schmidt, M. W.; Gilbert, M. M.; Elbert, S. T.
Chem. Phys. **1982**, 71, 41, 51, 65

28. Edmiston, C.; Ruedenberg, K. *Rev. Mod. Phys.* **1963**, 35, 457

29. Elbert, S. T.; Cheung, L. M.; Ruedenberg, K. *National Resource for Computations in Chemistry Software Catalog*, program QG01, 1980

30. Feller, D. F.; Schmidt, M. W.; Ruedenberg, K. *J. Am. Chem. Soc.* **1982**, 104, 960

31. Harmony, M. D.; Laurie, V. W.; Kuczkowski, R. L.; Schwendeman, R. H.; Ramsay, D. A.; Lovas, F. J.; Lafferty, W. J.; Maki, A. G. *J. Phys. Chem. Ref. Data* **1979**, 8, 630

32. Schmidt, M. W.; Truong, P. N.; Gordon, M. S.*J. Am. Chem. Soc.* **1987**, 109, 5217

33. Bartell, L. S.; Higgenbotham, H. K. *J. Chem. Phys.* **1965**, 42, 851

34. Wiberg, N.; Wagner, G.; Muller, G.*Angew. Chem., Int. Ed. Engl.* **1985**, 24, 229

35. Lazroq, M.; Escudie, J.; Couret ,C.; Satgé, J.; Dräger, M.; Dammel, R. *Angew. Chem., Int. Ed. Engl.* **1988**, 27, 828

36. Mayer, H.; Baum ,G.; Massa, W.; Berndt, A. *Angew. Chem., Int. Ed. Engl.* **1988**, 99, 790

37. West, R. *Angew. Chem., Int. Ed. Engl.* **1987**, 26, 1201

38. Snow, J. T.; Murakami, S.; Masamune, S.; Williams, D. J.*Tetrahedron Lett.* **1984**, 25, 4191

39. Goldberg, D.; Hitchcock, P.B.; Lappert, M. F.; Thomas, K. N.; Thorne, A. J.; Haaland, A.; Schilling, B. E. R. *Chem. Soc., Dalton Trans.* **1986**, 2387

40. Hehre, W. J.; Ditchfield, R.; Radom, L.; Pople, J. A. *J. Am. Chem. Soc.* **1970**, 92, 4796

41. Coulson, C. A. *Valence.* Oxford University Press, London, 1961, p. 267

42. Pauling, L. *Nature of the Chemical Bond*, 2nd Ed. Cornell University Press, Ithaca NY, 1948, p. 174

43. Streitweiser, A. J. *MO Theory for Organic Chemists.* Wiley and Sons, New York, 1961, p. 168

Table 1. RHF/SBK(d) geometries of inorganic benzenes[a]

$X_3Y_3H_6$	R_{X-Y}	R_{X-H}	R_{Y-H}	θ_X	θ_Y
C_6H_6[b]	1.406 (1.396)	1.091 (1.083)		120.0 (120.0)	
$Si_3C_3H_6$	1.766	1.483	1.094	118.7(Si)	121.3(C)
$Ge_3C_3H_6$	1.828	1.527	1.080	121.4(Ge)	118.6(C)
Si_6H_6	2.223	1.483		120.0	
$Si_3Ge_3H_6$	2.262	1.475	1.523	119.2(Si)	120.8(Ge)
Ge_6H_6	2.306	1.521		120.0	
$B_3N_3H_6$[c]	1.434 (1.44)	1.209 (1.20)	1.008 (1.00)	117.5 (118.)	112.5 (112.)
$B_3P_3H_6$[d]	1.868 (1.84)	1.198	1.397	116.6 (115.)	123.4 (124.)
$B_3As_3H_6$	1.956	1.186	1.482	116.0	124.0
$Al_3N_3H_6$[c]	1.787 (1.78)	1.584	1.016	114.2 (115.)	125.8 (125.)
$Al_3P_3H_6$	2.275	1.578	1.405	112.8	127.1
$Al_3As_3H_6$	2.359	1.573	1.489	112.4	127.6
$Ga_3N_3H_6$	1.814	1.564	1.006	114.0	126.0
$Ga_3P_3H_6$	2.264	1.556	1.393	113.4	126.6
$Ga_3As_3H_6$	2.345	1.554	1.489	112.8	127.2

Table 1. continued.

$Zn_3O_3H_6$	1.956	1.567	0.952	102.4	137.6
$Zn_3S_3H_6$[f]	2.394 (2.31~2.32)	1.560	1.327	99.1 (≈100.)	140.9 (≈140.)

[a]X refers to the more electropositive elements. θ_X and θ_Y are internal ring angles. Bond lengths are in Å and angles are in degrees. The values in parenthesis are experimental geometries.

[b]see Reference 31 (p.717)

[c]see Reference 14 (reference therein)

[d]see Reference 15

[e]see Reference 15

[f]see Reference 19

Table 2. Three lowest calculated frequencies[a]

species	a_2''	e''
C_6H_6	637	441
$Si_3C_3H_6$	313	230
$Ge_3C_3H_6$	208	197
Si_6H_6	70 (i)	101
$Si_3Ge_3H_6$	126 (i)	59
Ge_6H_6	145 (i)	57 (i)
$B_3N_3H_6$	395	294
$B_3P_3H_6$	225 (i)	183 (i)
$B_3As_3H_6$	267 (i)	247 (i)
$Al_3N_3H_6$	219	148
$Al_3P_3H_6$	145 (i)	155 (i)
$Al_3As_3H_6$	173 (i)	219 (i)
$Ga_3N_3H_6$	187	132
$Ga_3P_3H_6$	178 (i)	218 (i)
$Ga_3As_3H_6$	175 (i)	259 (i)
$Zn_3O_3H_6$	68	34
$Zn_3S_3H_6$	78 (i)	66 (i)

[a]The harmonic frequencies are calculated at the RHF/SBK(d) level of theory. The values are in cm^{-1}. The (i) indicates an imaginary frequency.

Table 3. Comparison of X-Y bond lengths.

X-Y	exp. single[a]	---------this work-------- aromatic[b]	double[b]	exp. double[a]	
C-C	1.534[c]	1.406	1.350	1.339	
Si-C	1.869	1.766	1.703	1.702[d]	
Ge-C	1.945	1.828	1.759	1.803[e]	1.827[f]
Si-Si	2.327	2.223	2.134	2.140[g]	
Si-Ge	2.357	2.262	2.175		
Ge-Ge	2.403	2.306	2.224	2.213[h]	2.347[i]

[a]experimental values, taken from reference 31 unless specified.

[b]calculated

[c]see Reference 33

[d]see Reference 34

[e]see Reference 35

[f]see Reference 36

[g]see Reference 37

[h]see Reference 38

[i]see Reference 39

Table 4. Energy differences ($\Delta H_{reaction}$) of bond separation reactions(kcal/mol)

reaction	RHF[a]	MP2[b]
$C_6H_6 + 6\,CH_4 \rightarrow 3\,H_2C{=}CH_2 + 3\,H_3C\text{-}CH_3$	61.4	74.7
$Si_3C_3H_6 + 3\,SiH4 + 3\,CH_4 \rightarrow 3\,H_3Si{=}CH_2 + 3\,H_3Si\text{-}CH_3$	60.2	62.0
$Ge_3C_3H_6 + 3\,GeH4 + 3\,CH_4$ ä $3\,H_3Ge{=}CH_2 + 3\,H_3Ge\text{-}CH_3$	58.7	65.3
$Si_6H_6 + 6\,SiH_4 \rightarrow 3\,H_2Si{=}SiH_2 + 3\,H_3Si\text{-}SiH_3$	42.3	57.8
$Si_3Ge_3H_6 + 3\,SiH4 + 3\,GeH_4 \rightarrow 3\,H_3Si{=}GeH_2 + 3\,H_3Si\text{-}GeH_3$	41.0	60.2
$Ge_6H_6 + 6\,GeH_4 \rightarrow 3\,H_2Ge{=}GeH_2 + 3\,H_3Ge\text{-}GeH_3$	40.3	59.9

[a]The corrected zero-point energies (multiplied by 0.89) are used.
[b]Second order Møller-Plesset energies at the RHF/SBK(d) geometries, using the corrected RHF zero-point energies.

Table 5. LMO/CI populations and bond orders for the π orbitals[a]

$X_3Y_3H_6$	n_X	n_Y	$\rho_o(XY)$	$\rho_m(XX)$	$\rho_m(YY)$	$\rho_p(XY)$
using ROHF orbitals						
C_6H_6	1.000		0.614	-0.001		-0.271
$Si_3C_3H_6$	0.835	1.165	0.599	0.071	-0.067	-0.250
$Ge_3C_3H_6$	0.869	1.131	0.590	0.061	-0.056	-0.245
Si_6H_6	1.000		0.590	0.061		-0.249
$Si_3Ge_3H_6$	0.992	1.008	0.593	0.004	-0.007	-0.247
Ge_6H_6	1.000		0.590	-0.001		-0.244
$B_3N_3H_6$	0.614	1.386	0.589	0.116	-0.110	-0.220
$B_3P_3H_6$	0.681	1.319	0.596	0.051	-0.053	-0.247
$B_3As_3H_6$	0.714	1.286	0.595	0.038	-0.041	-0.251
$Al_3N_3H_6$	0.507	1.493	0.552	0.139	-0.125	-0.170
$Al_3P_3H_6$	0.452	1.548	0.544	0.104	-0.103	-0.168
$Al_3As_3H_6$	0.471	1.529	0.549	0.098	-0.098	-0.178
$Ga_3N_3H_6$	0.567	1.433	0.562	0.128	-0.112	-0.193
$Ga_3P_3H_6$	0.489	1.511	0.555	0.100	-0.098	-0.184
$Ga_3As_3H_6$	0.508	1.492	0.559	0.092	-0.092	-0.193
$Zn_3O_3H_6$	0.235	1.765	0.434	0.098	-0.095	-0.060
$Zn_3S_3H_6$	0.171	1.829	0.384	0.077	-0.077	-0.034

Table 5. continued.

using MCSCF orbitals						
C_6H_6	1.000		0.620	-0.001		-0.279
$Si_3C_3H_6$	0.891	1.109	0.620	0.114	-0.109	-0.286
$Ge_3C_3H_6$	0.905	1.095	0.614	0.103	-0.097	-0.282
Si_6H_6	1.000		0.603	-0.001		-0.259
$Si_3Ge_3H_6$	0.991	1.009	0.601	0.006	-0.009	-0.257
Ge_6H_6	1.000		0.598	-0.001		-0.254
$B_3N_3H_6$	0.862	1.138	0.640	0.105	-0.099	-0.306
$B_3P_3H_6$	0.643	1.356	0.600	0.086	-0.087	-0.241
$B_3As_3H_6$	0.667	1.333	0.600	0.071	-0.073	-0.246
$Al_3As_3H_6$	0.689	1.311	0.624	0.106	-0.103	-0.269
$Ga_3P_3H_6$	0.721	1.279	0.630	0.098	-0.095	-0.280
$Ga_3As_3H_6$	0.656	1.343	0.616	0.113	-0.111	-0.255

[a]The orbital populations (n) and *ortho*, *meta*, and *para* bond orders (p) are calculated using two orbital sets (see text).

Table 6. Populations and bond orders in ethylenes $H_2X{=}YH_2$

X-Y	n_X	n_Y	$\rho(XY)$
C-C	1.000		0.897
Si-C	0.875	1.125	0.849
Ge-C	0.870	1.130	0.833
Si-Si	1.000		0.852
Si-Ge	0.977	1.023	0.847
Ge-Ge	1.000		0.841

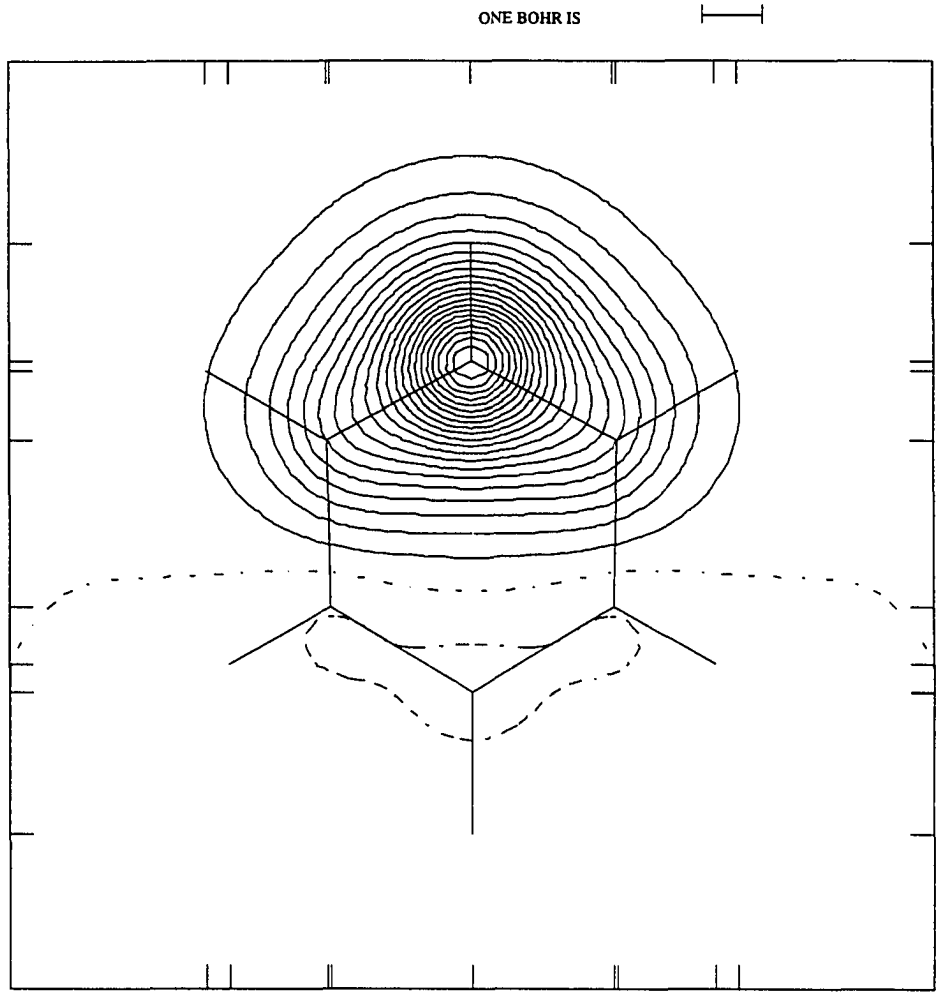

Figure 1. One of three equivalent localized SCF orbitals for borazine, drawn 0.75Å above the plane with a contour increment of 0.010 $bohr^{-3/2}$. Note bonding from nitrogen to each *ortho* boron, and antibonding to the *para* boron.

CHAPTER 3. STABILITIES AND ENERGETICS OF INORGANIC BENZENE ISOMERS: PRISMANES

A paper published in *Journal of American Chemical Society*, **1994**, 116, 11407

Nikita Matsunaga and Mark S. Gordon

Abstract

Ab initio calculations of inorganic prismanes, with the formula $(XH\text{-}YH)_3$, where X = B, Al and Ga and Y = N, P and As, as well as X or Y = C, Si and Ge, were carried out. Energetics of these species are compared with those of the planar benzene analog and chair/boat conformers. The prismane and planar structures containing first period elements (B, C and N) are all stable (*i.e.* minima on the potential energy surfaces). Chair and boat conformers are potential energy minima only in compounds containing second or fourth period elements. For those species with a first period element in the 1, 3, 5 positions, the planar, benzene-like structure is the global minimum; otherwise, the planar structure is not a minimum. The lowest minimum found is the prismane arrangement for Si_6H_6 and Ge_6H_6 and the chair structure for $Si_3Ge_3H_6$. Other molecules have distorted minima.

Introduction

More than 20 years ago, Woodward and Hoffman[1] observed that, "*...the excess energy of the prismane molecule must have the aspect of an angry tiger unable to break out of a paper cage.*" Subsequently, these authors analyzed the nature of the bonding in prismane, and demonstrated that the above is not at all true: Upon breaking three of the σ bonds in prismane the resulting π orbital is an anti-bonding orbital of benzene, thus the isomerization is a symmetry forbidden reaction. This results in a high energy transition state, and hence prismane is kinetically stable.

There are a number of valence isomers of benzene, including Dewar benzene, prismane and benzvalene, that can be synthesized[2]. In particular, the photochemical conversion of benzene into these isomers has been known for some time. For example,

when substituted benzene is irradiated with UV light (λ=254nm), it is converted into prismane and Dewar benzene[2f]. Other photochemical paths have been established to convert Dewar benzene to prismane and benzene, and to convert prismane to Dewar benzene and benzene[2k].

The first heavier group IV containing organometallic benzene analog, silatoluene, was isolated by Barton and co-workers[3]. Silabenzene and 1,4-disilabenzene were isolated later in a low temperature argon matrix[4]. These studies have spawned several theoretical investigations on compounds that are potentially aromatic. Singly substituted silabenzenes[5b], disilabenzene[5a], and germabenzene[5b] have been studied by this group. The only other species investigated theoretically was hexasilabenzene[6]. Though the structure of 1,3,5-trisilabenzene is yet to be determined, there is recent experimental evidence that a gas-phase dehydrogenation reaction of 1,3,5-trisilacyclohexane with a Cp-transition metal (Fe, Co or Ni) cationic complex forms a [Cp-M]$^+$-1,3,5-trisilabenzene complex[7].

Borazine had been the only inorganic isomer of benzene known for quite some time[8]. With increasing attention paid to exotic species, three group III-group V benzene analogs have recently been synthesized by Power, *et al.*[9,10]. These are B-P ([MesBPPh]$_3$), Al-N ([MeAlN(2,6-*i*-Pr$_2$C$_6$H$_3$)]$_3$) and Ga-P ([(2,4,6-Ph$_3$C$_6$H$_2$)GaP(*cyclo*-C$_6$H$_{11}$)]$_3$) systems containing alternating group III and group V elements. They have been isolated with large substituents to stabilize the ring. NMR evidence together with X-ray crystallographic data suggest that the B-P and the Al-N species are planar, and that there is some delocalization of the lone pair from the group V elements into the empty p-orbitals of neighboring group III elements[9c,d]. In the case of the Ga-P system the ring is not planar; it assumes a slightly twisted boat conformation[10]. Fink and Richards[11] have calculated the "resonance energies" of the planar B-N, B-P, and Al-N systems by using homodesmic reactions[12], and have concluded that the resonance energy of the B-P system is about the same as that of borazine.

In our previous paper[13] on this subject we explored the possible existence of inorganic benzenes and the extent to which the π-electrons are delocalized. The species investigated included 1,3,5/2,4,6 combinations of the group III(B, Al, Ga)-group V(N, P, As) elements, and group IV E_6H_6 (E= C, Si and Ge). In that paper only planar species were considered, and it was found that only those compounds with carbon or nitrogen in alternating positions correspond to minima on their potential energy surfaces (PES). The

remaining species have at least one imaginary frequency corresponding to an out-of-plane motion. Those that are not minima are either transition states or higher-order saddle points that lead to boat and/or chair conformations.

There are only a handful of studies on the subject of geometrical isomers of inorganic benzenes. Even fewer studies are available in the literature on the subject of prismane analogs[14,15,6]. Hexagermaprismane with six bis(trimethylsilyl)methyl substituents was the first inorganic analog of prismane reported by Sakurai *et. al.*[14]. Recently the same group has reported the synthesis of 2,6-diisopropylphenyl substituted hexasilaprismane, as well as hexagermaprismane[15]. Although they belong to the same group, the behavior of silicon is markedly different from that of carbon. For example, C_6H_6 in a prismane framework is stable (a minimum on the PES), but it is one of the highest energy isomers. However, theoretical calculations predict that the silicon analog of benzene is easily distorted to become a chair conformation[6c], and the prismane analog appears to be the global minimum. The prismane Si_6H_6 structure is estimated to be about 10 kcal/mol[6a,b] *more* stable than the planar geometry with an RHF wavefunction using an effective core potential basis set.

In this paper, we focus our attention on the structures and the energetics of prismane analogs(**4**) relative to the benzene-like planar structure(**1**) and "chair"(**2**) and "boat"(**3**) conformers. The species considered here have the general formula $X_3Y_3H_6$ (with X and Y alternating in a ring), where X and Y are chosen from Group III(B, Al, and Ga), Group IV (C, Si, Ge), and group V (N, P, and As), such that each compound is valence isoelectronic with prismane. Also, the nature of the bonding in **4** is analyzed in order to determine a correlation between bonding characteristics and the stabilities as a function of X and Y.

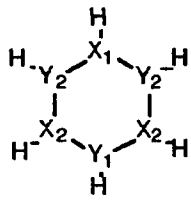

1

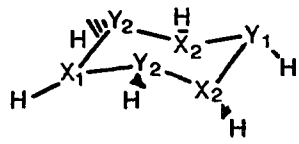

2

X = B, Al or Ga
Y = N, P or As

for heteroatom Group IV,
X = more electropositive elements
Y = more electronegative elements

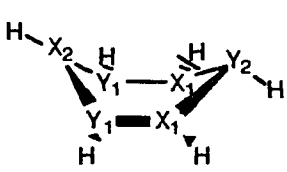

3

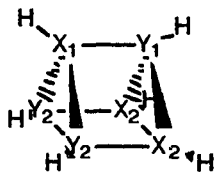

4

Computational Approach

All calculations described here were performed with the GAMESS *ab initio* quantum chemistry program package[16]. These extensive calculations were facilitated by the recent implementation of a parallel version of the code for use on a CM5 and an iPSC/860. The initial calculations were carried out at the restricted Hartree-Fock (RHF) level of theory using the Stevens-Basch-Krauss-Jasien (SBKJ) effective core potentials (ECP) and basis sets[17] for all heavy atoms, and the -31G basis[18a] for hydrogen. The full core potential, that projects out all 3d electrons, and the corresponding basis set, was used for gallium atom. These bases are augmented with d-polarization functions[19] for all heavy atoms.

Geometries of **4** were optimized in C_s symmetry for the heteronuclear prismanes (X ≠ Y) and in D_{3h} symmetry for the homonuclear prismanes. Geometries of **2** and **3** were optimized in C_{3v} and C_s symmetries, respectively, for the heteronuclear species, and in D_{3d} and C_{2v} for the homonuclear species. Geometries predicted using the SBKJ effective core potentials and associated basis sets (these bases are referred to below as basis-A) have been found to be in good agreement with experimental results for both main group[13,20] and transition metal[21] compounds. The matrices of energy second derivatives (hessians) were calculated numerically from analytically determined gradients, in order to verify the given

geometry is a minimum (all eigenvalues of hessian are positive) or a transition state (the hessian has one and only one negative eigenvalue).

Structures **1** and **4** of three species (Ge-C, Ge-Ge and B-N) were optimized with the MP2/basis-A level of theory using Gaussian 92[22] in order to examine the effect of correlated wavefunctions on geometries and relative energies. These three species were chosen because the largest differences between the RHF and MP2 energies were observed for them using geometries obtained with the RHF/basis-A level of theory.

At each stationary point found with the RHF/basis-A level of theory, RHF and MP2 energies were recalculated with two all electron basis sets: basis-B consists of 6-31G(d)[18b-e] for the first and second period elements and the (14s12p6d) primitive gaussian set contracted to [6s5p2d][24] for the third period elements. Basis-C consists of 6-311G(d,p)[23] for the first and second period elements and the [9s7p3d] contraction[24] using the (14s12p6d) primitive set for the third period elements. The correlation energy was calculated by means of second-order Møller-Plesset perturbation theory (MP2)[25] for both the ECP and all-electron bases.

Bonding in prismanes was analyzed by using localized molecular orbitals (LMO), constructed with the method of Mezey and Pipek[26]. The AIMPAC system of programs[27] was also used to elucidate the nature of the bonding. The density analysis has been discussed in detail elsewhere, and only a few key points will be repeated here. Bond and ring critical points will be of interest in the following discussion. A bond critical point exists between two atoms if there is a "saddle point" in the electron density ρ_c between the two atoms. At such a point the gradient of the electron density is zero and the hessian of the electron density has one positive eigenvalue along the bond axis. The existence of a bond critical point implies the existence of a bond path (path of maximum electron density passing through the bond critical point), and the two atoms are said to be bonded. The hessian of the electron density at a ring critical point has two positive and one negative eigenvalues, with the density ρ_r at the ring critical point being smaller than that of all the surrounding bond critical points. The wavefunctions used for this analysis were obtained with the all electron basis set (basis-C).

Results and Discussions

A. Chair and Boat Conformers

As has been mentioned previously[6,11,13], many of the planar structures **1** are not minima on the corresponding PES. For the group III-group V analogs only the planar structures containing alternating nitrogen atoms are minima. For the Group IV analogs, only those species containing alternating carbon atoms are minima. The only true transition states (with one imaginary frequency) are the planar geometries of Si_6H_6 and $Si_3Ge_3H_6$. The remaining planar compounds studied here are third-order saddle points, with three imaginary frequencies. The geometries of conformers **2** (chair) and **3** (boat) are shown in Tables 1 and 2, respectively (the supplemental material gives complete cartesian coordinates for each species). The geometries of the benzene-like planar structures are included in Table 3, adopted from our previous paper[13]. The energy hessian information, indicating whether the compound is a minimum, transition state or higher-order saddle point, is also included in Table 1, 2 and 3.

The normal mode corresponding to the negative eigenvalue of the energy hessian for each of the true transition states (see Table 3), *i.e.* Si_6H_6 and $Si_3Ge_3H_6$ of structure **1**, is distortion to the chair conformation **2**, and belongs to the a_2" representation of D_{3h} symmetry. The remaining planar structures, namely hexagermabenzene and the ones containing phosphorus and arsenic, are third-order saddle points (Table 3). One of the normal modes, a_2", is a distortion to **2** as noted for Si_6H_6 and $Si_3Ge_3H_6$. The other two imaginary modes belong to the e" representation of D_{3h}, and are doubly degenerate distortions to **3**. Therefore, while our main interest in this work is in the structure, stability and bonding of prismane, we begin with a brief discussion of the chair (**2**) and boat (**3**) conformations.

The gross features of the Group III-Group V chair structures **2** consist of three nearly coplanar X atoms (Group III) bonded to Y atoms (Group V) in which the bond angles around the Y atoms are somewhat larger than their YH_3 counterparts (as shown in Table 4) to compensate for the cyclization. The sum of the angles around the X atoms is close to 360° in both the group III-group V and the hexasila-structure (Table 1). In the case of the boat conformer **3** (Table 2) the X atoms are nearly planar, except for the hexagerma-analog, and the angles around the Y atoms deviate considerably from the equilibrium angle of YH_3. The X-Y bond lengths in **2** and **3** are, in general, longer than those of the corresponding structure **1**.

It is apparent that the phosphorus and arsenic containing compounds do not have good overlap among their π orbitals, and the deformation of **1** is therefore inevitable[5,32]. These distortions can be understood by examining the inversion barriers of YH_3 where Y is either N, P or As. The calculated barriers are 6.5, 34.9 and 42.6 kcal/mol, respectively, at the MP2/basis-A//RHF/basis-A level of theory, as shown in Table 4. These barriers are in good agreement with previous *ab initio* calculations[28]. The ammonia inversion barrier is substantially smaller than those for phosphine and arsine, and the H-N-H angle is much larger than H-P-H and H-As-H. This, combined with the weak π overlap, means that the compounds containing phosphorus and arsenic are expected to have a greater tendency to bend away from planarity. The force constants associated with the "umbrella motion" (a_2" symmetry) of XH_3, where X is either B, Al or Ga, are nearly the same for all three cases. The fact that these force constants, shown in Table 4, are similar, and the barriers of inversion are substantially higher in PH_3 and AsH_3 than in NH_3, suggest that distortions away from planarity will occur upon cyclization.

Similar arguments can be used for the group IV benzenes. Methyl radical is a planar molecule, however, SiH_3 and GeH_3 radicals are both pyramidal[29]. Furthermore, the inversion barriers of SiH_3 and GeH_3 are relatively low[30](5.9 and 5.2 kcal/mol). Also, the π bond strengths, or the rotational barriers, for the group IV ethylene analogs (XH_2=YH_2) for C-C, Si-C, Ge-C, Si-Si, Si-Ge and Ge-Ge systems are 65.4, 35.6, 32.2, 25.1, 25.7 and 25.4, respectively[31,32]. It can be seen that the ability of carbon to form strong π bonds and the low inversion barriers of SiH_3 and GeH_3 contribute to the stability of planar carbon containing benzenes.

Attempts were made to determine if chair or boat conformers exist for the species containing carbon and nitrogen. The geometries were distorted from **1** to either the chair or boat conformations by moving the atoms in the direction of the corresponding normal mode vectors. Subsequent re-optimization returned the structure back to the planar geometry. Similarly, those compounds whose planar structures are transition states were distorted to a boat conformation. Again, they return to the previously determined stationary points on the PES.

The energetics of these conformers with respect to structures **1** are compared in Table 5 for **2** and Table 6 for **3**. Although the B-P benzene analog has three imaginary frequencies, this species with large substituents ($[MeBPPh]_3$) was synthesized[9a-c,f]. All basis sets used here predict the B-P chair conformation to be lower than the benzene

structure at the RHF level of theory, but there is essentially no difference between these two isomeric forms at the MP2 level of theory. This is also true for hexasilabenzene, as has been reported earlier[6c,d].

For the chair conformer of hexagermabenzene, there is considerable disagreement in energetics obtained with the three different basis sets used here; at both the RHF and MP2 levels of theory basis-A predicts **2** to be ≈15 kcal/mol lower relative to **1** than does basis-B. The values obtained with basis-C are in between the values obtained with basis-A and B. The two basis sets are in better agreement with each other for the Al-P and Ga-As chair structures, both favor the chair conformer by ≥10 kcal/mol. The B-As chair structure exhibits a large correlation effect and basis set effect, with MP2 preferentially favoring the planar structure. The Ga-P and Al-As species are also predicted to strongly favor the chair over the planar structure at all levels of theory. Each of these exhibit a 5-10 kcal/mol basis set effect, but little effect of correlation. In all cases for which both structures are predicted to be minima, **3** is found to be higher in energy than **2** by a few kcal/mol.

The hexagerma-analog of **2** is a transition state. The normal mode corresponding to the imaginary vibration (64.3*i* cm^{-1}) is shown in Figure 1, along with the product structure, obtained by following the intrinsic reaction coordinate (IRC) using the second-order method of Gonzalez and Schlegel[33]. This structure is a minimum on the PES, and lies only 1.7 kcal/mol below **2** at the RHF/basis-A level of theory. However, this structure is calculated to be 8.0 kcal/mol higher in energy than **2** at the MP2/basis-A//RHF/basis-A level of theory. The subsequent MP2/basis-A geometry optimization and the subsequent hessian calculation reveal that the all-germanium chair conformer is in fact a minimum on the PES, and the compound on the right in Figure 1 does not exist. The relative energy of the chair conformer with respect to the planar analog is -18.5 kcal/mol. This is in agreement with the value obtained at the MP2/basis-A//RHF/basis-A level of theory (Table 5).

The boat conformer **3** of the hexagerma-analog is a second-order saddle point, even when the double difference technique for obtaining a numerical hessian is used. Figure 2 shows the normal modes associated with the two imaginary frequencies (117.1*i* cm^{-1} and 9.5*i* cm^{-1}). The first mode corresponds to the direction leading to the chair conformer **2**. The second mode assumes a "twisted-boat" conformation. Although it is isoenergetic with **3** (at the MP2 and RHF/basis-A//RHF/basis-A levels of theory), the optimized configuration of the twisted-boat is a transition state, having an imaginary frequency of 57.3*i* cm^{-1}. Both forward and reverse directions along the IRC lead to the chair conformer,

which is about 16 kcal/mol below **3** at the RHF/basis-A level of theory.

For those chair structures which are minima on the respective potential energy surfaces, the following qualitative trend of stabilities is apparent in Table 5, using MP2/basis-C energies:

$$Ga\text{-}As > [Ga\text{-}P \approx Al\text{-}As] > Al\text{-}P > [Si\text{-}Si \approx Si\text{-}Ge] > [B\text{-}P \approx B\text{-}As]$$

So, as the participating elements become heavier, distortions from planarity become more favorable, as noted above.

B. Prismanes

Structures and Energetics.

As shown in **Scheme 1**, the relationship between structures **1** and **4** can be thought of as an intramolecular isomerization. One possible mechanism is an initial cleavage of the X_1-Y_1 bond, followed by breaking the two bonds X_2-X_2 and Y_2-Y_2 and forming three π bonds to obtain **1**.

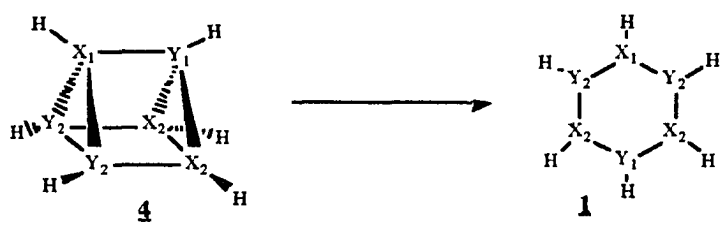

Scheme 1

Table 7 shows the bond lengths and the bond angles for prismane analogs (the supplemental material gives complete cartesian coordinates for each species **4**). The bonds between X and Y are substantially longer in **4** than those in the corresponding structures **1**. The differences in the bond distances for hydrogens are small, the largest difference being 0.009Å. The MP2/basis-A optimized structures for X = Ge, Y = C; X = Y = Ge; and X = B, Y = N give bond lengths that are up to 0.02Å longer than the SCF structures, since correlation generally introduces some antibonding character. An exception is that the X_2Y_2 bond in the B-N system has been shortened slightly by 0.005Å. This means that the correlation might favor the stabilization of the two three-membered ring units in the B-N prismane. However, there are no dramatic structural effects due to correlation.

The only experimentally known geometries of prismane isomers either have an all-

carbon backbone (hexamethylprismane) obtained by electron diffraction[34], an all-silicon frame with six 2,6-diisopropylphenyl groups[15] or an all-germanium backbone with six $(Me_3Si)_2CH$ groups[14] and six 2,6-diisopropylphenyl groups[15] obtained by X-ray crystallography. The experimental X_1-Y_1 bond lengths in the C-C and Si-Si systems are 1.551 and 2.373Å, respectively, and the X_1-Y_2 bond lengths are 1.540 and 2.380Å. These geometries are in good agreement with the calculated values shown in Table 7. The experimental bond lengths for the Ge-Ge prismane with the $(Me_3Si)_2CH$ groups are 2.52Å for X_1-Y_1 and 2.58Å for X_1-Y_2. In the case of 2,6-diisopropylphenyl substituted Ge-Ge prismane the X_1-Y_1 and X_1-Y_2 bond lengths are 2.468Å and 2.503Å respectively, so there is considerable variation as a function of substituents. The RHF/basis-A bond lengths for the bonds are both 2.49Å, much closer to the latter experimental values. Geometry optimization with MP2 has no effect on X_1-Y_1, but lengthens X_1-Y_2 by 0.03Å. The deviation from the MP2 calculated bond lengths are much smaller for the 2,6-diisopropylphenyl substituted Ge-Ge prismane than that in the $(Me_3Si)_2CH$ substituted compound.

The angle formed by two planes, $Y_1X_2X_2$ and $X_2X_2Y_2Y_2$ or by $X_1Y_2Y_2$ and $X_2X_2Y_2Y_2$ in **4**, is distorted from the ideal angle 90° for the group III-group V prismanes. These angles are summarized in Table 8. The structures for the X = Y structures (C, Si, Ge) have, of course, the ideal (undistorted) angle. The most important trend for the mixed compounds is that the distortions in the group III-group V prismanes clearly increase most as the group V elements get heavier. The other distortions are not nearly as large. All of the P and As containing prismanes possess angles about 10° different from the ideal angle. It appears that the large difference in the atomic size *alone* does not explain these distortions. These distortions are closely related to the inversion barriers of YH_3, where Y is N, P or As. As shown in Table 4, the inversion barrier of AsH_3 is the largest among YH_3 species. Note also that tetravalency is easily achieved for the XH_3 (X = B, Al or Ga) moiety upon accepting an electron-pair into its empty p-orbital. Then, it follows that the group III elements are easily distorted and that the arsenic would prefer to assume an angle close to its minimum energy angle, 93.7°, of AsH_3. It is consistent among the arsenic containing species (see angle 2 in Table 8) that they possess large distortions. Phosphorus analogs are also strongly distorted. On the other hand, nitrogen containing species prefer to remain close to the ideal angle due to the relatively low inversion barrier. In the case of the group IV species, the angles are all nearly 90.0°. Again the atomic size difference does not play an

important role in this distortion. Even for the C-Ge analog that has the largest difference in atomic size, the deviation is only a few degrees.

The relative energies of prismanes are compared with the corresponding structures 1 in Table 9. If nitrogen or carbon is present in a molecule, the relative energy becomes high. The B-N prismane is the highest energy species of all, lying 163 kcal/mol above borazine at the MP2/basis-C level of theory. The C-C prismane is also quite energetic (114 kcal/mol above benzene), but as heavier Group IV elements are substituted the prismane structure is increasingly stabilized relative to the planar structure. The same trend is observed for the Group III-Group V species. Indeed, the all Ge prismane is a low-lying minimum on the Ge_6H_6 surface. These thermodynamic stabilities in hexagerma- and hexasilaprismane have contributed to the recent syntheses of these compounds[14,15].

There are significant basis set and correlation effects on the relative stabilities of the prismane structures. With the exception of the Ga-N compound, the general trend is that improvement of the basis set and introduction of correlation correction both preferentially stabilize the prismane. However, note that for several compounds the ECP basis set-A is in much better agreement with the largest basis-C than either is with the intermediate basis-B. This suggests that in those cases in Tables 5 and 6 for which there are serious disagreements between basis sets A and B, the basis-A results are more reliable.

It is difficult to quantify the seemingly unusual stabilities of all-silicon and all-germanium prismanes. The three-membered ring species (*cyclo*-propyl units) of group IV elements, in fact, becomes more strained as the carbon is replaced by silicon or germanium[6e]. Hence it is counter intuitive for the prismanes to have such stabilities. One can, however, speculate about the relative stabilities of π bonds and the impact on the structures of prismanes. The three π bonds of all-silicon benzene destabilize the planar conformation relative to benzene itself. As mentioned above, the π bond strength of ethylene analogs decreases as carbon is replaced with silicon and germanium, and so these species become more stable as trans-bent species. It is perhaps more advantageous thermodynamically to have only σ bonds in these heavy group IV molecules.

To assess the effect of correlation on predictions of structures and energetics, the geometries of the Ge-C, Ge-Ge and B-N prismanes were re-calculated at the MP2/basis-A level of theory. In each case, the trend in ΔE from RHF/basis-A to MP2/basis-A//RHF/basis-A continues when the geometry is re-optimized with correlation included.

The relative energies (including ZPE) of the Ge-C, Ge-Ge and B-N prismanes(**4**) with respect to the planar(**1**) structure, optimized at the MP2/basis-A level of theory, are 18.7, -22.4 and 160.0 kcal/mol, respectively.

As was the case for **1**, not all the prismane analogs are minima on the PES (see the last column of Table 7). The B-P, Al-As and Ga-P systems are transition states, and the B-As and Ga-As systems are second-order saddle points. The normal mode corresponding to the imaginary vibration of the B-P prismane and its bicyclic product structure determined by following the IRC are shown in Figure 3. A heterolytic cleavage of one of the Y_1X_2 bonds has occurred. This bond is the weakest bond in this prismane, as shown from the value of electron density at the bond critical point in Table 10 (*vide infra*). Another heterolytic cleavage has occurred at the X_2Y_2 bond, the second weakest bond, to form the product. The product is calculated to be 38.2 kcal/mol more stable than the prismane structure at the MP2/basis-A level of theory. The IRC was not followed for the Al-As and Ga-P systems since they have similar normal modes, however the product structures were optimized. The relative energies of these species with respect to the corresponding prismanes are -15.3 and -9.2 kcal/mol, respectively, at the same level of theory.

The B-As and Ga-As structures were distorted along the respective normal modes, and the geometries were optimized. As normal modes in both species are similar, only the normal modes for Ga-As prismane are shown in Figure 4. Distortion along either of the two modes shown in Figure 4 and subsequent geometry optimization leads to the structure shown below or to an equivalent enantiomer. The result is an unusual boat-like six-membered ring, and is a minimum on the PES. The relative energy of the final structure is -13.5 kcal/mol at the MP2/basis-A//RHF/basis-A level of theory. Similarly, the relative energy of the distorted Ga-As prismane is calculated to be -12.8 kcal/mol, relative to the planar structure at the MP2/basis-A//RHF/basis-A level of theory.

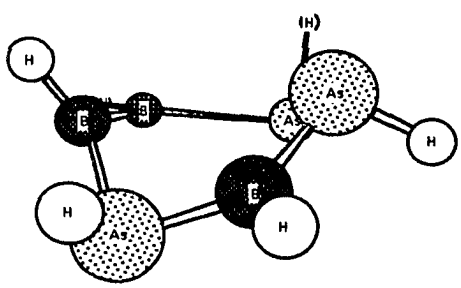

Bonding

The bonding of the prismane structures was analyzed with the atoms-in-molecules method of Bader[27]. Table 10 shows the values of RHF/basis-C electron densities at the critical points[35]. In general, aluminum containing prismanes have smaller electron densities at the bond critical points than do their boron or gallium analogs, and there is a general decrease in p_c upon going from N to P to As for a given group III element.

The positions of the bond critical points illustrate how the electron density is polarized in the bond. This is, then, ostensibly related to the electronegativity of an atom. Figure 5 shows the positions of critical points in heteronuclear analogs of **4**. Since electronegative atoms draw the electron density from the neighboring atoms to become electron-rich atoms, the position of the electron density maximum, the bond critical point, is shifted toward the less electronegative of the two atoms. The positions of the bond critical points, denoted by smaller circles, between group III and group V elements lay closer to the group III elements, since these are less electronegative. An exception is the B-As prismane. This is consistent with the equal electronegativities assigned to B and As by Pauling[36]. Although not shown in Figure 5, the homonuclear group IV prismanes have bond critical points equidistant from the two nuclei, and ring critical points are found at the center of the surrounding nuclei (The only ring critical points searched for in this study were within the two rings formed by $X_1Y_2Y_2$ and $Y_1X_2X_2$). The bond critical points of the bonds X_1Y_2, Y_1X_2, Y_2Y_2 and X_2X_2 for the group IV analogs can be found outside the ring or close to the conventionally drawn bonds. However, all of the bond critical points except for the bond X_2X_2 are found on the ring or inside the ring for the group III-group V analogs.

Bond critical points were not found for all apparent bonds, especially if the *effective* atomic sizes are quite different. The effective atomic size can be defined as the relative size of the electron density of an atom in a molecule[27] (see Figure 6, where it may be seen that phosphorus is much larger than aluminum). For example, no bond critical points were found between X_1Y_2, Y_1X_2 or X_2X_2 in Al-P prismane (Table 10). However, a substantial amount of electron density exists in the bond region, as shown in Figure 6, even in cases for which a bond critical point was not found (see below).

The localized orbitals plotted in the $X_1Y_2Y_2$ and $Y_2X_1X_1$ plane in the B-N prismane, are shown in Figure 7a. The valence electrons are all involved in bonding, and all of the X-Y bonds are somewhat polarized toward the nitrogen. The electron-pair donor and acceptor can be readily identified due to the polarization of the localized orbitals, especially those for

which the electronegativity difference is large. The localized orbitals show that all bonds are strained, since the contour lines bend outside the ring, even though the bond critical point is found close to the center of the ring. There is no apparent anomaly found in the localized orbital corresponding to the Al-Al bond in Figure 7b for Al-P prismane, even though no critical point was found for this bond. As discussed in earlier papers[20], this illustrates the presence of significant bonding interaction even when there is no bond critical point. Again the electron-pair donor and acceptor are easily identified.

The bond between two As atoms in the B-As analog, Figure 7c, is an electron-deficient multicenter type (the figure in the lower right-hand corner). A substantial amount of boron p-orbital is mixed into this σ orbital. This is the only compound in this study possessing such bonding. Note that B and As were assigned the same value of the electronegativity by Pauling[36]. The experimental As-As single bond length of 2.372Å, obtained by X-ray diffraction[37] of $As_3Co(CO)_3$, is substantially shorter than the one found here. The total electron density map in the plane of interest is shown in Figure 8. This illustrates that there is a continuous smooth decrease in electron density from the boron center to the midpoint of the two arsenic atoms, in contrast to the saddle point shown in Figure 6.

There seems to be some correlation between the bond strength of a given bond type X-Y and the value of electron density at the bond critical point ρ_c(X-Y). The ρ_c values are plotted in Figure 9 against the elongation of X_1-Y_1, chosen to be the reference bond for the group III-group V prismanes. A similar plot for the heteronuclear group IV species is shown in Figure 10. For a given group III element in the molecule, the slope of the curves are similar. Note also that the bond that possesses the smallest value of ρ_c was cleaved in B-P prismane to form the product, shown in Figure 3. The observed trend is consistent with the structures obtained by distorting the B-As prismane along its imaginary normal modes, in which two bonds with the smallest ρ_c are cleaved. In general, either the bond X_2Y_2 or Y_1X_2 has the smallest ρ_c among X-Y bonds. It is interesting to note that the highest ρ_c values are assigned to the bonds Y_2Y_2 and X_1Y_1, except for the B-P and B-As analogs. This could imply that the reaction shown in **Scheme 1**, initiating the reaction by breaking the X_1Y_1 bond, is less likely to occur than by breaking other bonds with smaller ρ_c

values.

Summary

In this study we have examined the structures and the stabilities of inorganic prismane analogs, as well as chair and boat conformers of inorganic benzenes. Table 11 summarizes the lowest and highest energy minima in this study. It is interesting to note that, even though theory predicts that the chair conformer of Ga-P benzene is 6 kcal/mol more stable than the boat conformer, the synthesis[10] has yielded a boat structure. This is likely to be due to the more complex substituents in the experimentally studied compounds.

The nitrogen and carbon containing prismanes are stable on the PES, but they are very high in energy, the lowest energy structures being planar when these atoms are present. The B-N system is the highest energy isomer, being 163 kcal/mol above borazine. The hexasila- and hexagermaprismane are the lowest energy prismane isomers found in this study. This thermodynamic stability contributed to the recent syntheses[15,16] of these compounds. Phosphorus and arsenic prismanes are unstable, except for the Al-P system; they are either transition states or second-order saddle points.

The total electron density analysis together with the localized molecular orbitals give greater insight into stabilities of these molecules. The stability of these molecules can be correlated with the value of electron density of the given bond type at the bond critical points and the shapes of localized orbitals. The localized orbitals show that all of the valence electrons are involved in bonding. The bonds are polarized where electronegativity difference exists for a given bond, and the donor and acceptor are readily identified. The bond X_1Y_1 possesses the highest ρ_c values and are the shortest bonds in heteronuclear prismanes, except for the Si-Ge analog. For homonuclear prismanes the ρ_c values are nearly the same for all bonds between heavy atoms, and in turn the bond lengths are also similar.

Acknowledgements

This work was supported in part by grants from the Air Force Office of Scientific Research (92-0226) and the National Science Foundation (CHE-93-13717). The calculations were performed in part on the North Dakota State University IBM ES9000 computer under a joint study agreement with IBM, and in part on IBM RS6000/530 obtained via a grant to MSG

from AFOSR. Some calculations were performed on IBM RS6000/350 computers made available by Iowa State University. Parallel GAMESS was used for some calculations on the CM5 at the Army High Performance Computer Center at the University of Minnesota and on the Intel iPSC/860 at Kirtland Air Force Base. The generous allocation of computer time for calculations of direct MP2 energies on Cray Y-MP and Cray Y-MP C-90 at the Waterway Experimental Station in Vicksburg, MS, and Cray Y-MP C-90 at the San Diego Supercomputer Center are also acknowledged.

Supplementary Material Available: Cartesian coordinates of optimized geometries of chair, boat and prismanes (11 pages).

References

1 Woodward, R. B.; Hoffmann R. *The Conservation of Orbital Symmetry*, Verlag Chemie GmbH, Weinheim/Bergstr, 1970; p107-112

2 a) van Tamelen, E. E.; Pappas, S. P. *J. Ame. Chem. Soc.* **1962**, 84, 3789
b) van Tamelen, E. E.; Pappas, S. P. *J. Ame. Chem. Soc.* **1963**, 85, 3297
c) Viehe, H. G.; Merenyi, D. R.; Oth, J. F. M.; Senders, J. R.; Vahange, P. *Angew. Chem. Int. Ed. Engl.* **1964**, 3, 755
d) van Tamelen, E. E. *Angew. Chem. Int. Ed., Engl.* **1965**, 4, 738
e) Viehe, H. G. *Ang. Chem. Int. Ed.Engl.* **1965**, 4, 746
f) Wilzbach, K. E.; Kaplan, L. *J. Ame. Chem. Soc.* **1965**, 87, 4004
g) Bryce-Smith, D.; Gilbert, A.; Robinson, D. A. *Angew. Chem. Int. Ed., Engl* **1971**, 10, 745
h) van Tamelen, E. E.; Pappas, S. P.; Kirk, K. L. *J. Ame. Chem. Soc.* **1971**, 93, 6092
i) Breslow, R.; Napierski, J.; Schmidt, A. H. *J. Ame. Chem. Soc.* **1972**, 94, 5906
j) Katz, T. J.; Acton, N. *J. Ame. Chem. Soc.* **1973**, 95, 2738
k) Turro, N. J.; Ramamurthy, V.; Katz, T. J. *Nouv. J. Chim.* **1977**, 1, 363
l) Potgieter, J. H. *J. Chem. Educ.* **1991**, 68, 280

3 a) Barton, T. J.; Banasiak, D. *J. Ame. Chem. Soc.* **1977**, 99, 5199
b) Barton, T. J.; Burns, G. T. *J. Ame. Chem. Soc.* **1978**, 100, 5246
c) Barton, T. J.; Vuper, M. *J. Ame. Chem. Soc.* **1981**, 103, 6788

4 Maier, G.; Mihm, G.; Reisenauer, H. P. *Angew. Chem. Int. Ed., Engl.* **1980**, 19, 52

5 a) Baldridge, K. K.; Gordon, M. S. *J. Organomet Chem.* **1984**, 271, 369
b) Baldridge, K. K.; Gordon, M. S. *J. Ame. Chem. Soc.* **1988**, 110, 4204

6 a) Nagase, S.; Kudo, T.; Aoki, M. *J. Chem. Soc., Chem. Commun.* **1985**, 1121
b) Sax, A.; Janoschek, R. *Angew. Chem. Int. Ed. Engl.* **1986**, 25, 651
c) Clabo Jr., D. A.; Schaefer, H. F. *J. Chem. Phys.* **1986**, 84, 1664
d) Nagase, S.; Teramae, H.; Kudo, T. *J. Chem. Phys.* **1987**, 86, 4513
e) Nagase, S. *Angew. Chem. Int. Ed. Engl.* **1989**, 28, 329
f) Slanina, Z. *Chem. Phys. Lett.* **1989**, 161, 175

7 Bjarnason, A.; Arnason, I. *Angew. Chem. Int. Ed. Engl.* **1992**, 31, 1633

8 Stock, A.; Pohland, E. *Dtsch. Chem. Ges.* **1926**, 59, 2215

9 a) Dias, H. V. R.; Power, P. P. *Angew. Chem. Int. Ed. Engl.* **1987**, 26, 1270
b) Dias, H. V. R.; Power, P. P. *J. Ame. Chem. Soc.* **1989**, 111, 144
c) Power, P. P. *Angew. Chem. Int. Ed. Engl.* **1990**, 29, 449
d) Waggoner, K. M.; Hope, H.; Power, P. P. *Angew. Chem. Int. Ed. Engl.* **1988**, 27, 1699
e) Waggoner, K. M.; Power, P. P. *J. Ame. Chem. Soc.* **1991**, 113, 3385
f) Hope, H.; Pestana, D. C.; Power, P. P. *Angew. Chem. Int. Ed. Engl.* **1990**, 29, 449

10 Hope, H.; Pestana, D. C.; Power, P. P. *Angew. Chem. Int. Ed. Engl.* **1991**, 30, 691

11 Fink, W. H.; Richards, J. C. *J. Ame. Chem. Soc.* **1991**, 113, 3393

12 a) Homodesmic reaction is a reaction that conserves the type and number of bonds to calculate resonance energy. For example, the resonance energy of benzene can be calculated from the following: $3\ CH_2{=}CH{-}CH{=}CH_2 \rightarrow C_6H_6 + 3\ CH_2{=}CH_2$
b) George, P.; Trachtman, M.; Bock, C. W.; Brett, A. M. *Theoret. Chim. Acta* **1975**, 38, 121
b) George, P.; Trachtman, M.; Bock, C. W.; Brett , A. M. *J. Chem. Soc., Perkin Trans.* **1976**, 2, 1222
c) George, P.; Trachtman, M.; Bock, C. W.; Brett, A. M. *Tetrahedron* **1976**, 32, 1357
d) see for example reference 5

13 Matsunaga, N.; Cundari, T. R.; Schmidt, M. W.; Gordon, M. S. *Theoret. Chim. Acta* **1992**, 83, 57

14 Sekiguchi, A.; Kubota, C.; Sakurai, H. *Angew. Chem. Int. Ed. Engl.* **1989**, 28, 55

15 Sekiguchi, A.; Yatabe, T.; Kubota, C.; Sakurai, H. *J. Ame. Chem. Soc.* **1993**, 115, 5853

16 a) Schmidt, M. W.; Baldridge, K. K.; Boatz, J. A.; Elbert, S. T.; Gordon, M. S.; Jensen, J. H.; Koseki, S.; Matsunaga, N.; Nugyen, K. A.; Su, S.; Windus, T. L.;

Dupuis, M.; Montgomery Jr., J. A. *J. Comput. Chem.* **1993**, 14, 1347
b) contact Mike Schmidt at mike@si.fi.ameslab.gov concerning this program

17 a) B-O, Al-S: Stevens, W. J.; Basch, H.; Krauss, M. *J. Chem. Phys.* **1984**, 81, 6026
b) Zn-Ge: Stevens, W. J.; Krauss, M.; Jasien, P. G. *Can. J. Chem.* **1992**, 70, 612

18 a) Ditchfield, R.; Hehre, W. J.; Pople, J. A. *J. Chem. Phys.* **1971**, 54, 724
b) Dill, J. D.; Pople, J. A. *J. Chem. Phys.* **1975**, 62, 2921
c) Hehre, W. J.; Ditchfield, R.; Pople, J. A. *J. Chem. Phys.* **1972**, 56, 2257
d) Francl, M. M.; Pietro, W. J.; Hehre, W. J.; Binkley, J. S.; Gordon, M. S.; DeFrees, D. J.; Pople, J. A. *J. Chem. Phys.* **1982**, 77, 3654
e) Gordon, M. S. *Chem. Phys. Lett.* **1980**, 76, 163

19 d-polarization exponents used for basis-A and basis-B are: B=0.6, C=N=0.8, Al=0.325, Si=0.395, P=0.55, Ga=0.207, Ge=0.246, As=0.293
and for basis-C are: B=0.401, C=0.626, N=0.913, Al=0.325, Si=0.395, P=0.55, Ga=0.141, Ge=0.202, As=0.273

20 a) Gordon, M. S.; Nugyen, K. A.; Carroll, M. T. *Polyhedron* **1991**, 10, 1247
b) Nugyen, K. A.; Carroll, M. T.; Gordon, M. S. *J. Ame. Chem. Soc.* **1991**, 113, 7924

21 a) Cundari, T. R.; Gordon, M. S. *J. Ame. Chem. Soc.* **1992**, 114, 539
b) Cundari, T. R.; Gordon, M. S. *Organomet.* **1992**,11, 55
c) Cundari, T. R. *J. Ame. Chem. Soc.* **1992**, 114, 7889

22 Frisch, M. J.; Trucks, G. W.; Head-Gordon, M.; Gill, P. M. W.; Wong, M. W.; Foresman, J. B.; Johnson, B. G.; Schlegel, H. B.; Robb, M. A.; Gonzalez, C.; Martin, R. L.; Fox, D. J.; Defrees, D. J.; Baker, J.; Stewart, J. J. P.; Pople, J. A.; GAUSSIAN 92, Gausian, Inc. Pittsburgh, PA, 1992

23 Krishnan, R.; Binkley, J. S.; Seeger, R.; Pople, J. A. *J. Chem. Phys.* **1980**, 72, 650

24 Binning Jr., R. C.; Curtiss, L. A. *J. Comput. Chem.* **1990**, 11, 1206
These bases are augmented with d-polarization functions listed in ref. 19 and p-polarization functions for hydrogen (0.75).

25 a) Carsky, P.; Hess Jr., B. A.; Schaad, L. J. *J. Comput. Chem.* **1984**, 5, 280
b) Møller, C.; Plesset, M. S. *Phys. Rev.* **1934**, 46, 618

26 Pipek, J.; Mezey, P. Z. *J. Chem. Phys.* **1989**, 90, 4916

27 Bader, R. F. W. *Atoms in Molecules--A Quantum Theory*, University of Oxford, Oxford, 1990

28 a) Rauk, A.; Allen, L. C.; Clementi, E. *J. Chem. Phys.* **1970**, 52, 4133
b) Moc, J.; Morokuma, K. *Inorg. Chem.* **1994**, 33, 551
c) Dixon, D. A.; Arduengo III, A. J. *J. Ame. Chem. Soc.* **1987**, 109, 338

29 a) Morehouse, R. J.; Christiansen, J. J.; Gordy, W. *J. Chem. Phys.* **1966**, 45, 1751
b) Jackel, G. S.; Christiansen, J. J.; Gordy, W. *J. Chem. Phys.* **1967**, 47, 4274

30 Moc, J.; Rudzinski, J. M.; Ratajczak, H. *Chem. Phys.* **1992**, 159, 197

31 Schmidt, M. W.; Truong, P. N.; Gordon, M. S. *J. Ame. Chem. Soc.* **1987**, 109, 5217

32 Windus, T. L.; Gordon, M. S. *J. Ame. Chem. Soc.* **1992**, 114, 9559

33 a) Gonzales, C.; Schlegel, H. B. *J.Phys.Chem.* **1990**, 94, 5523
b) Gonzales, C.; Schlegel, H. B. *J.Chem.Phys.* **1991**, 95, 5853

34 Karl, R. R.; Wang, Y. C.; Bauer, S. H. *J. Mol. Struct.* **1975**, 25, 17

35 We found essentially no difference in the values of electron density and the positions of critical points obtained with basis-B and basis-C.

36 Pauling, L. *The Natutre of The Chemical Bond* , 3rd Ed., Cornell University Press, New York, 1960

37 Foust, A. F.; Foster, M. S.; Dahl, L. F. *J. Ame. Chem. Soc.* **1969**, 91, 5631

38 Harmony, M. D.; Laurie, V. W.; Kuczkowski, R. L.; Scwendeman, R. H.; Lovas, F. J.; Lafferty, W. J.; Maki, A. G. *J. Physc. Chem. Ref. Data* **1979**, 8, 630

39 Boyd, R. J.; Choi, S. C.; Hale, C. C. *Chem. Phys. Lett.* **1984**, 112, 136

Table 1. Geometries of chair conformers for $X_3Y_3H_6$ compounds[a]

$X_3Y_3H_6$	XY	HX	HY	YXY	XYX	HXY	HYX	XYY-pl[b]	YXX-pl[b]	H-XYY[c]	H-YXX[c]	Hessian[d]
Si_6H_6	2.232	1.485		118.8		119.0		161.0		17.8		+
$Si_3Ge_3H_6$	2.308	1.492	1.543	111.4	118.6	114.4	116.1	143.2	140.6	42.9	30.5	+
Ge_6H_6	2.385	1.545		112.5		113.0		133.5		45.2		*i*
	[2.396]	[1.564]		[111.4]		[112.2]		[130.2]		[47.8]		[+]
$B_3P_3H_6$	1.910	1.204	1.408	120.4	109.0	119.5	105.9	138.7	143.0	7.6	61.9	+
$B_3As_3H_6$	2.027	1.192	1.507	121.1	103.4	119.1	100.9	128.8	136.8	8.2	72.2	+
$Al_3P_3H_6$	2.315	1.584	1.415	117.1	106.8	121.3	103.2	129.6	134.3	5.8	67.4	+
$Al_3As_3H_6$	2.422	1.583	1.513	119.3	98.8	120.2	97.0	118.9	129.4	6.0	79.2	+
$Ga_3P_3H_6$	2.312	1.567	1.407	118.6	102.9	120.5	100.5	124.6	132.2	6.2	73.0	+
$Ga_3As_3H_6$	2.414	1.569	1.513	119.6	97.8	120.0	96.8	117.6	129.0	6.4	79.6	+

[a]The geometries are obtained at the RHF/basis-A level of theory. The values in square brakets are the geometries obtained at the MP2/basis-A level of theory. Bond lengths are in Å, and bond angles are in degrees.

[b]Plane-plane torsion angles: XYY-pl refers to the torsion angle between the planes formed by $X_1Y_2Y_2$ and $Y_2Y_2X_2X_2$, and YXX-pl refers to the torsion angle between the planes formed by $Y_1X_2X_2$ and $Y_2Y_2X_2X_2$. The dotted lines represent the bisectors of these planes.

[c]Bond-plane torsion angles: H-XYY refers to the torsion angle of the bond H-X_1 with respect to the plane $X_1Y_2Y_2$. H-YXX refers to the torsion angle of the bond H-Y_1 with respect to the plane $Y_1X_2X_2$.

[d]+ indicates that the compound is a minimum on the potential energy surface, and *i* indicates a number of imaginary frequency (*i* is a transition state).

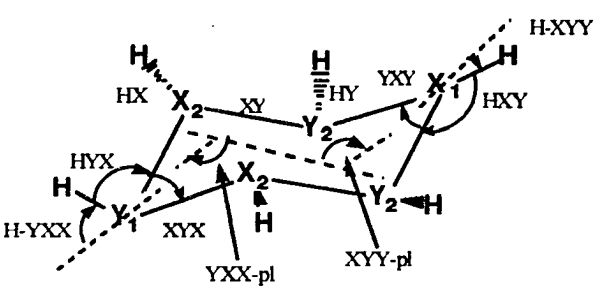

Table 2. Geometries of boat conformers for $X_3Y_3H_6$ compounds[a]

$X_3Y_3H_6$	X_2Y_2	X_1Y_2	X_2Y_1	HX_1	HX_2	HY_1	HY_2	$Y_2X_1Y_2$	$X_2Y_1X_2$	$Y_1X_2Y_2$	$X_2Y_2X_1$	H-YXX[b]	H-YXX[b]	XYYX[c]	YXXY[c]	Hessian[d]
Ge_6H_6	2.385	2.385		1.544	1.544			112.5		112.4		45.2		133.3		***2i***
$B_3P_3H_6$	1.912	1.909	1.892	1.203	1.202	1.404	1.408	117.7	116.7	121.2	110.8	11.5	44.2	134.9	164.9	+
$B_3As_3H_6$	2.038	2.031	2.012	1.203	1.203	1.511	1.516	116.0	110.9	123.2	104.8	11.9	60.0	122.2	157.0	+
$Al_3P_3H_6$	2.319	2.317	2.299	1.583	1.582	1.410	1.416	113.8	117.0	118.8	107.3	8.4	48.7	122.2	159.2	+
$Al_3As_3H_6$	2.447	2.437	2.423	1.591	1.590	1.508	1.516	112.7	105.8	112.4	98.7	7.0	69.0	109.5	146.7	+
$Ga_3P_3H_6$	2.320	2.314	2.301	1.566	1.566	1.403	1.408	113.0	111.8	120.8	104.0	8.5	59.1	117.1	154.2	+
$Ga_3As_3H_6$	2.430	2.416	2.408	1.568	1.570	1.509	1.515	112.4	104.8	123.0	98.7	7.2	70.8	109.5	147.0	+

[a]The geometries are obtained at the RHF/basis-A level of theory. Bond lengths are in Å, and bond angles are in degree.

[b]Bond-plane torsion angles: H-XYY refers to the torsion angle of the bond H-X_1 with respect to the plane $X_1Y_2Y_2$. H-YXX refers to the torsion angle of the bond H-Y_1 with respect to the plane $Y_1X_2X_2$. The dotted lines represent the bisectors of the planes formed from either $X_1Y_2Y_2$, $Y_1X_2X_2$, or $X_2X_2Y_2Y_2$.

[c]Plane-plane torsion angles: XYYX refers to the torsion angle between the planes formed by $X_1Y_2Y_2$ and $Y_2Y_2X_2X_2$, and YXXY refers to the torsion angle between the planes formed by $Y_1X_2X_2$ and $Y_2Y_2X_2X_2$.

[d]+ indicates that the compound is a minimum, and *i* indicates the number of imaginary frequency (***2i*** is a second-order saddle point).

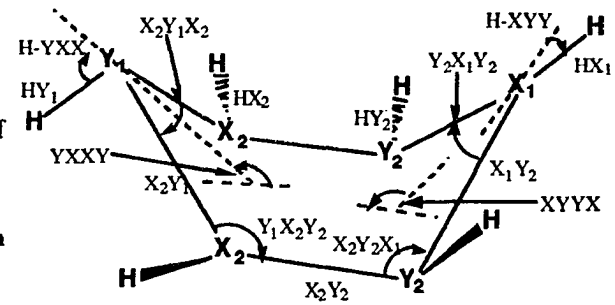

Table 3. Geometries of $X_3Y_3H_6$ Inorganic Benzenes[a]

$X_3Y_3H_6$	X-Y	X-H	Y-H	YXY	XYX	Hessian[b]
C_6H_6[c]	1.406 (1.396)	1.091 (1.083)		120.0 (120.0)		+
$Si_3C_3H_6$	1.766	1.483	1.094	121.3(Si)	118.7(C)	+
$Ge_3C_3H_6$	1.828 [1.845]	1.527 [1.540]	1.080 [1.097]	121.4(Ge) [121.0]	118.6(C) [119.0]	+ [+]
Si_6H_6	2.223	1.483		120.0		*i*
$Si_3Ge_3H_6$	2.262	1.475	1.523	119.2(Si)	120.8(Ge)	*i*
Ge_6H_6	2.306 [2.324]	1.521 [1.539]		120.0 [120.0]		3*i* [3*i*]
$B_3N_3H_6$[d]	1.434 [1.442] (1.44)	1.209 [1.217] (1.20)	1.008 [1.027] (1.00)	117.5 [117.0] (118.)	122.5 [123.0] (121.)	+ [+]
$B_3P_3H_6$[e]	1.868 (1.84)	1.198	1.397	116.6 (115.)	123.4 (124.)	3*i*
$B_3As_3H_6$	1.956	1.186	1.482	116.0	124.0	3*i*
$Al_3N_3H_6$[f]	1.787 (1.78)	1.584	1.016	114.2 (115.)	125.8 (125.)	+
$Al_3P_3H_6$	2.275	1.578	1.405	112.8	127.1	3*i*
$Al_3As_3H_6$	2.359	1.573	1.489	112.4	127.6	3*i*

Table 3. continued.

$Ga_3N_3H_6$	1.814	1.564	1.006	114.0	126.0	+
$Ga_3P_3H_6$	2.264	1.556	1.393	113.4	126.6	***3i***
$Ga_3As_3H_6$	2.345	1.554	1.489	112.8	127.2	***3i***

[a]X refers to the more electropositive elements. XYX and YXY are internal ring angles. Bond lengths are in Å and angles are in degrees. The values in parenthesis are experimental geometries. The values in square brakets are obtained at the MP2/basis-A level of theory. All other values are obtained at the RHF/basis-A level of theory.

[b]+ indicates that the compound is a minimum on the potential energy surface, and ***i*** indicates a number of imaginary frequency (***i*** is a transition state and ***3i*** is a third-order saddle point).

[c]see Reference 38 (p.717)

[d]see Reference 39 (reference therein)

[e]see Reference 9a-c,f

[f]see Reference 9d,e

Table 4. Calculated vibrational frequencies of XH_3 and YH_3 (X=B, Al or Ga and Y=N, P or As)[a]

mode		NH_3	PH_3	AsH_3
	a_1	1236	1132	1030
	e	1799	1248	1112
	a_1	3604	2582	2305
	e	3748	2585	2316
angle[b]		105.8	95.4	93.7
barrier[c]		6.5	34.9	42.6
imag. mode[d]	a_2"	1002(5.30)	1249(17.38)	1273(21.50)

mode		BH_3	AlH_3	GaH_3
	a_2"	1200(10.54)	758(8.30)	764(8.80)
	e'	1260	836	840
	a_1'	2652	1994	1972
	e'	2767	1995	2016

[a]Vibrational frequencies (in cm^{-1}) are calculated at the RHF/SBK(d) level of theory. The values in parenthesis are the force constants (in mdyn/Å).

[b]The H-Y-H angle. Values are in degrees.

[c] Inversion barrier (in kcal/mol) is calculated at the MP2/SBK(d)//RHF/SBK(d) level of theory.

[d]Imaginary frequencies (in cm^{-1}) of the planar YH_3. The values in parenthesis are the force constants (in mdyn/Å).

Table 5. Relative energies of chair conformers[a]

	RHF//RHF/basis-A[b]			MP2//RHF/basis-A[b]		
$X_3Y_3H_6$	basis-A	basis-B	basis-C	basis-A	basis-B	basis-C
Si_6H_6	-0.1	-0.0	-0.1	-1.6	-2.2	-3.0
$Si_3Ge_3H_6$	-3.9	4.2	-3.4	-6.5	1.1	-4.8
Ge_6H_6[c]	-15.8	1.9	-4.2	-19.3	-4.0	-10.7
$B_3P_3H_6$	-9.3	-6.8	-5.7	-1.7	1.0	-0.2
$B_3As_3H_6$	-22.8	-23.7	-14.2	-9.0	-9.6	-0.7
$Al_3P_3H_6$	-8.9	-8.5	-8.2	-12.0	-11.1	-13.6
$Al_3As_3H_6$	-24.0	-14.1	-17.7	-26.6	-16.9	-21.2
$Ga_3P_3H_6$	-17.7	-24.0	-15.7	-21.8	-26.4	-20.9
$Ga_3As_3H_6$	-32.6	-30.6	-25.7	-35.4	-32.8	-29.0

[a]The energies (harmonic ZPE's, multiplied by 0.89, incorporated) are relative to the planar structures. Values are in kcal/mol.
[b]The RHF//RHF/basis-A (or MP2//RHF/basis-A) means that the single-point RHF (or MP2) energy is calculated with the geometries obtained with the RHF/basis-A level of theory.
[c]The compound is not a minimum on the PES; it is a transition state (see text).

Table 6. Relative energies of boat conformers[a]

	RHF//RHF/basis-A[b]			MP2//RHF/basis-A[b]		
$X_3Y_3H_6$	basis-A	basis-B	basis-C	basis-A	basis-B	basic-C
Ge_6H_6[c]	-0.7	6.2	-4.0	-0.3	3.9	-10.4
$B_3P_3H_6$	-5.7	-3.8	-2.8	2.3	3.7	3.2
$B_3As_3H_6$	-13.3	-16.5	-9.9	3.6	-1.6	4.6
$Al_3P_3H_6$	-6.4	-6.2	-5.9	-8.4	-7.8	-10.2
$Al_3As_3H_6$	-17.2	-10.8	-14.4	-24.6	-12.5	-16.7
$Ga_3P_3H_6$	-13.5	-18.7	-12.1	-15.8	-20.0	-15.9
$Ga_3As_3H_6$	-27.6	-26.6	-21.4	-29.0	-27.8	-23.5

[a]The energies (harmonic ZPE's multiplied by 0.89, incorporated) are relative to the planar structures. Values are in kcal/mol.

[b]The RHF//RHF/basis-A (or MP2//RHF/basis-A) means that the single-point RHF (or MP2) energy is calculated with the geometries obtained with the RHF/basis-A level of theory.

[c]The compound is not a minimum on the PES; it is a second-order saddle point (see text).

Table 7a. Geometries of $X_3Y_3H_6$ prismane analogs (bond lengths)[a]

$X_3Y_3H_6$	HX_1	HX_2	HY_1	HY_2	X_1Y_1	X_2Y_2	X_1Y_2	X_2Y_1	X_2X_2	Y_2Y_2	Hessian[b]
C_6H_6	1.090				1.556		1.518				+
$Si_3C_3H_6$	1.485	1.487	1.093	1.091	1.886	1.906	1.861	1.994	2.239	1.630	+
$Ge_3C_3H_6$	1.532	1.542	1.093	1.092	1.969	1.986	1.963	2.026	2.393	1.574	+
	[1.573]	[1.599]	[1.112]	[1.113]	[1.932]	[2.012]	[2.082]	[2.055]	[2.977]	[1.471]	[+]
Si_6H_6	1.489				2.383		2.365				+
$Si_3Ge_3H_6$	1.484	1.483	1.532	1.532	2.436	2.436	2.427	2.431	2.364	2.493	+
Ge_6H_6	1.537				2.487		2.494				+
	[1.562]				[2.496]		[2.522]				[+]
$B_3N_3H_6$	1.200	1.202	1.008	1.011	1.509	1.680	1.558	1.622	1.664	1.475	+
	[1.209]	[1.212]	[1.028]	[1.034]	[1.526]	[1.675]	[1.574]	[1.646]	[1.684]	[1.522]	[+]
$B_3P_3H_6$	1.196	1.200	1.406	1.412	2.004	2.111	2.006	2.045	1.733	2.191	*i*
$B_3As_3H_6$	1.181	1.190	1.491	1.516	2.009	2.164	2.188	2.265	1.690	2.805	**2*i***
$Al_3N_3H_6$	1.570	1.592	1.013	1.012	1.827	2.020	1.904	2.030	2.400	1.520	+
$Al_3P_3H_6$	1.575	1.587	1.408	1.410	2.368	2.518	2.419	2.537	2.527	2.258	+
$Al_3As_3H_6$	1.570	1.583	1.495	1.505	2.466	2.619	2.521	2.636	2.534	2.518	*i*
$Ga_3N_3H_6$	1.545	1.569	1.006	1.006	1.849	2.048	1.962	2.090	2.356	1.509	+
$Ga_3P_3H_6$	1.550	1.565	1.400	1.401	2.348	2.506	2.444	2.570	2.459	2.251	*i*
$Ga_3As_3H_6$	1.552	1.566	1.498	1.507	2.440	2.602	2.545	2.666	2.468	2.512	**2*i***

[a]The geometries are obtained at the RHF/basis-A level of theory. The values in square brakets are the geometries obtained at the MP2/basis-A level of theory. Bond lengths are in Å.
[b]+ indicates that the compound is a minimum on the potential energy surface, and *i* indicates a number of imaginary frequency (*i* is a transition state and **2*i*** is a second-order saddle point).

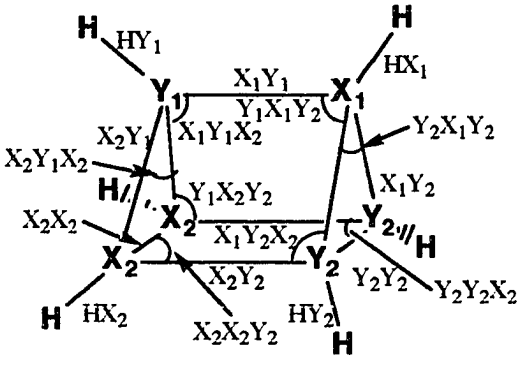

Table 7b. Geometries of $X_3Y_3H_6$ prismane analogs (bond angles)[a]

$X_3Y_3H_6$	$Y_2X_1Y_2$	$Y_1X_1Y_2$	$X_2Y_1X_2$	$X_1Y_1X_2$	$X_2X_2Y_2$	$Y_1X_2Y_2$	$Y_2Y_2X_2$	$X_1Y_2X_2$
C_6H_6	60.0	90.0						
$Si_3C_3H_6$	52.0	88.9	70.3	90.8	80.8	85.9	99.2	92.8
$Ge_3C_3H_6$	47.3	86.6	72.4	92.4	78.1	84.4	101.9	93.8
	[41.4]	[86.3]	[92.8]	[89.8]	[68.0]	[85.0]	[112.0]	[86.9]
Si_6H_6	60.0	90.0						
$Si_3Ge_3H_6$	61.8	90.8	58.2	89.2	91.5	90.7	88.5	89.3
Ge_6H_6	60.0	90.0						
	[60.0]	[90.0]						
$B_3N_3H_6$	56.5	93.3	60.9	92.8	86.8	84.3	93.2	89.6
	[57.8]	[92.4]	[60.8]	[92.9]	[87.5]	[84.6]	[92.5]	[90.0]
$B_3P_3H_6$	66.2	87.8	50.2	94.6	96.2	84.0	83.8	91.6
$B_3As_3H_6$	79.7	87.4	43.8	93.5	104.9	81.8	75.0	91.6
$Al_3N_3H_6$	47.0	86.6	72.4	99.2	77.4	78.4	102.6	95.1
$Al_3P_3H_6$	55.7	82.9	59.7	100.1	86.9	77.6	93.0	99.3
$Al_3As_3H_6$	59.9	82.0	57.4	101.0	89.8	77.0	90.2	100.0
$Ga_3N_3H_6$	45.2	86.1	68.6	97.8	78.1	77.9	101.9	95.7
$Ga_3P_3H_6$	54.8	83.2	57.2	100.0	87.6	77.6	92.4	99.2
$Ga_3As_3H_6$	59.2	82.6	55.1	100.6	90.5	77.3	89.5	99.6

[a]The geometries are obtained at the RHF/basis-A level of theory. The values in square brakets are the geometries obtained at the MP2/basis-A level of theory. Bond angles are in degrees.

Table 8. Torsion angles of prismanes[a]

species	X_2	angle 1	Y_2	angle 2
B-N	B	85.3	N	87.8
B-P	B	80.4	P	97.1
B-As	B	74.6	As	105.0
Al-N	Al	84.7	N	90.1
Al-P	Al	77.4	P	98.9
Al-As	Al	75.2	As	101.5
Ga-N	Ga	83.4	N	91.3
Ga-P	Ga	77.2	P	99.1
Ga-As	Ga	75.3	As	101.3
C-C		90.0		
C-Si	C	88.7	Si	91.5
C-Ge	C	89.0	Ge	91.8
Si-Si		90.0		
Si-Ge	Si	89.9	Ge	90.1
Ge-Ge		90.0		

[a]Angles are in degrees. The angles are formed between the trapezoidal $X_2X_2Y_2Y_2$ and the triangles $X_1Y_2Y_2$ and $Y_1X_2X_2$ of the strucutre **1**. Angle 1 is related to the bending of X_2 atoms, and angle 2 is related to the bending of Y_2 atoms.

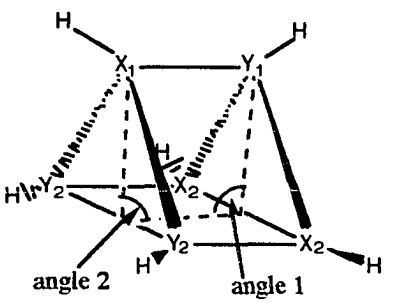

Table 9. Relative energies of prismanes[a]

	RHF//RHF/basis-A[b]			MP2//RHF/basis-A[b]		
X-Y	basis-A	basis-B	basis-C	basis-A	basis-B	basis-C
C-C	111.7	123.2	123.6	102.5	116.4	113.9
Si-C	42.7	43.8	48.4	27.6	33.9	35.3
Ge-C	42.8	23.2	40.3	29.3	12.2	27.2
Si-Si	-23.5	-21.0	-15.0	-24.0	-18.3	-13.6
Si-Ge	-12.0	-22.3	-9.8	-11.0	-20.8	-6.4
Ge-Ge	-19.1	-49.4	-9.8	-21.4	-50.1	-11.1
B-N	185.0	185.9	187.1	161.2	162.8	162.6
B-P	93.0	98.2	96.4	70.5	76.2	71.2
B-As	48.9	45.9	59.6	24.9	22.4	33.0
Al-N	102.4	95.5	101.4	88.3	84.8	90.7
Al-P	39.4	41.2	41.4	21.7	23.3	22.8
Al-As	26.3	28.8	31.9	7.9	10.6	12.9
Ga-N	86.1	64.0	82.1	73.4	79.8	96.4
Ga-P	34.8	15.3	37.7	15.5	-2.8	19.1
Ga-As	22.5	4.4	28.5	1.4	-15.3	8.3

[a] The energies (harmonic ZPE, calculated at the RHF/basis-A level of theory, multiplied by 0.89 is incorporated) are relative to the planar structures. Values are in kcal/mol.

[b] The RHF//RHF/basis-A (or MP2//RHF/basis-A) means that the single-point RHF (or MP2) energy is calculated with the geometries obtained by the RHF/basis-A level of theory.

Table 10. Electron density at the critical points[a]

Bond or Ring			ρ_c	
	N	B	Al	Ga
bonds	X_1Y_1	0.1691	0.0875	0.1252
	X_1Y_2	0.1302	0.0664	0.0885
	Y_1X_2	0.1255	0.0466	
	X_2Y_2	0.0996	0.0557	0.0792
	Y_2Y_2	0.2843	0.2562	0.2639
	X_2X_2	0.1597	0.0466	0.0662
rings	$X_1Y_2Y_2$	0.1240	0.0591	0.0752
	$Y_1X_2X_2$	0.1254		0.0508
	P	B	Al	Ga
bonds	X_1Y_1	0.1249	0.0605	0.0802
	X_1Y_2	0.1065		0.0584
	Y_1X_2	0.0999		0.0491
	X_2Y_2	0.0832	0.0412	0.0555
	Y_2Y_2	0.1176	0.1084	0.1106
	X_2X_2	0.1537	0.0593[b]	0.0661
rings	$X_1Y_2Y_2$	0.0894	0.0419	0.0480
	$Y_1X_2X_2$	0.0951	0.0392	0.0400
	As	B	Al	Ga
bonds	X_1Y_1	0.1283	0.0570	0.0747
	X_1Y_2	0.0841		0.0528
	Y_1X_2	0.0741		0.0447
	X_2Y_2	0.0947	0.0380	0.0511
	Y_2Y_2	No stationary point[c]	0.0792	0.0804
	X_2X_2	0.1650	0.0599[b]	0.0662
rings	$X_1Y_2Y_2$	No stationary point[c]	0.0388	0.0433
	$Y_1X_2X_2$	0.0741	0.0370	0.0372
	C	C	Si	Ge
bonds	X_1Y_1	0.2424	0.1145	0.1223
	X_1Y_2	0.2437	0.1085	0.1131
	Y_1X_2	0.2437	0.1033	0.1107
	X_2Y_2	0.2424	0.1134	0.1210
	Y_2Y_2	0.2437	0.1993	0.2253
	X_2X_2	0.2437		0.0686
rings	$X_1Y_2Y_2$	0.1968	0.0970	0.0994
	$Y_1X_2X_2$	0.1968	0.0773	0.0636

Table 10. continued.

	Si	Si	Ge	Ge-Ge
bonds	X_1Y_1	0.0882	0.0820	0.0764
	X_1Y_2	0.0866	0.0787	0.0734
	Y_1X_2	0.0866	0.0804	0.0734
	X_2Y_2	0.0882	0.0820	0.0764
	Y_2Y_2	0.0866	0.0882(Si-Si)	0.0734
	X_2X_2	0.0866	0.0722(Ge-Ge)	0.0734
rings	$X_1Y_2Y_2$	0.0596	0.0528(Si-Ge-Ge)	0.0496
	$Y_1X_2X_2$	0.0596	0.0559(Ge-Si-Si)	0.0496

[a]Values are in au. The electron density is calculated from the RHF wavefunction using the basis-C. The empty cell indicates where the critical points were not located.

[b]The values obtained have three negative eigenvalues.

[c]There is no stationary point on the surface of interest (See Figure 8).

Table 11. Summary of the lowest and highest energy isomers[a]

$X_3Y_3H_6$	lowest	highest
C-C	benzene	prismane
Si-C	benzene	prismane
Ge-C	benzene	prismane
Si-Si	prismane	benzene/chair
Si-Ge	chair	benzene
Ge-Ge	prismane	benzene
B-N	benzene	prismane
B-P	chair	C_1[b]
B-As	chair	C_1[b]
Al-N	benzene	prismane
Al-P	chair	prismane
Al-As	chair	C_1[b]
Ga-N	benzene	prismane
Ga-P	chair	C_1[b]
Ga-As	chair	boat

[a]The listed isomers are minima on the potential energy surface.
[b]C_1 denotes the structure obtained by following the imaginary normal modes. See text.

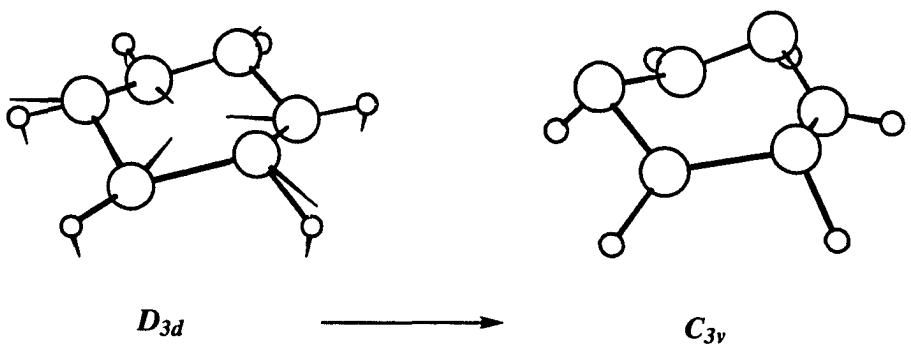

Figure 1. Normal Mode of Ge-Ge Chair Conformer and the Related Minimum. The chair conformer (a transition state) is shown on the left along with its normal mode vectors (64 cm^{-1}) corresponding to the negative eigenvalue of hessian. The structure on the right, which is a minimum at the RHF/basis-A level of theory, is obtained by following the IRC.

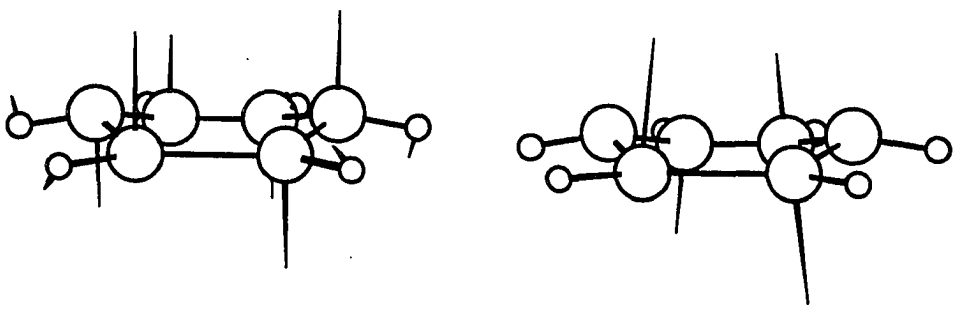

Figure 2. Normal Modes of Ge-Ge Boat Conformers
The arrows indicate the normal mode vectors corresponding to the negative eigenvalues (117.1 and 9.5 cm^{-1}) of energy hessian.

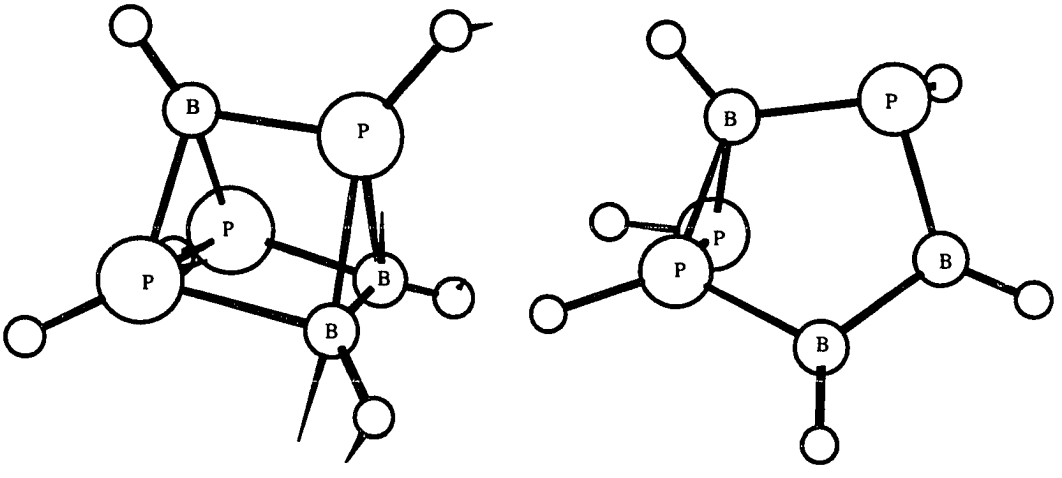

229 cm^{-1}

Figure 3. B-P prismane and related minimum
The arrows on the prismane indicate the normal mode vector corresponding to the negative eigenvalue of energy hessian. The molecule on the right is obtained by following IRC.

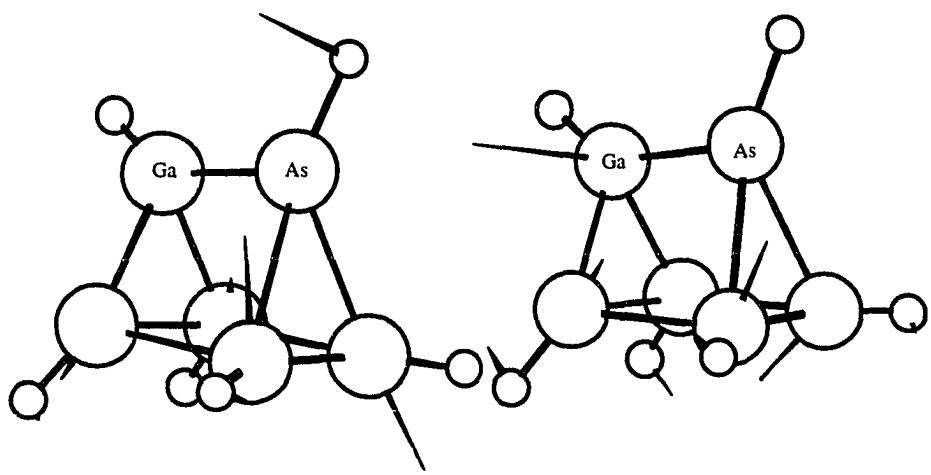

141 cm^{-1} 49 cm^{-1}

Figure 4. Ga-As prismane and its normal modes
The arrows on the prismane indicate the normal mode vector corresponding to the negative eigenvalues of energy hessian.

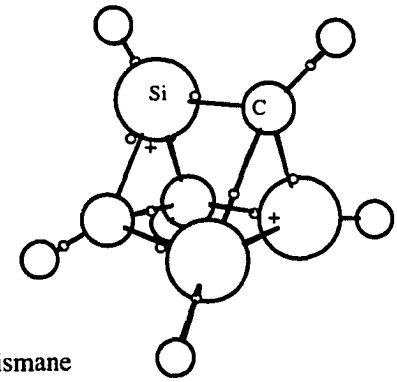

Si-C prismane

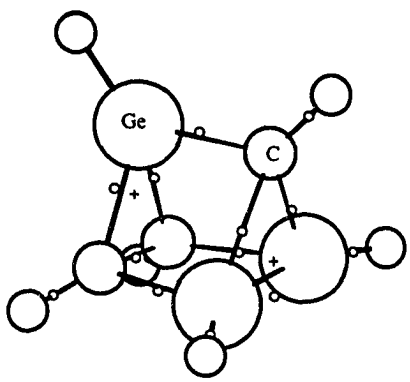

Ge-C prismane

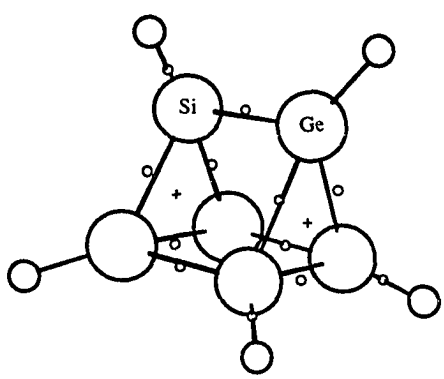

Si-Ge prismane

Figure 5. Positions of Critical Points.
A smaller circle represents the position of a bond critical point, and "+" represents the position of a ring critical point. The ring critical points are searched for the rings formed by $X_1Y_2Y_2$ and $Y_1X_2X_2$

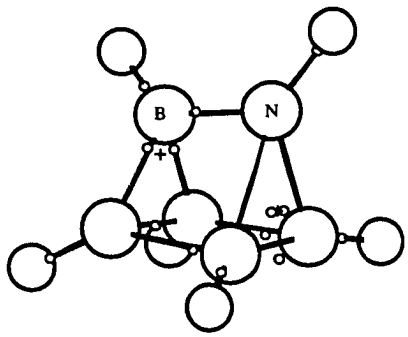

B-N prismane

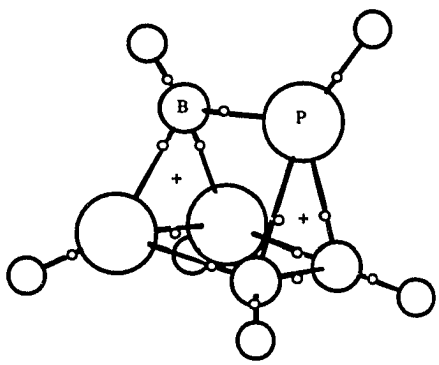

B-P prismane

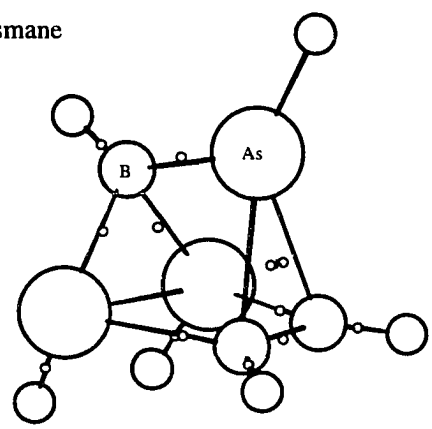

B-As prismane

Figure 5. Continued.

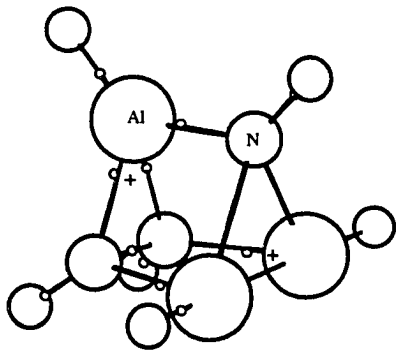

Al-N prismane

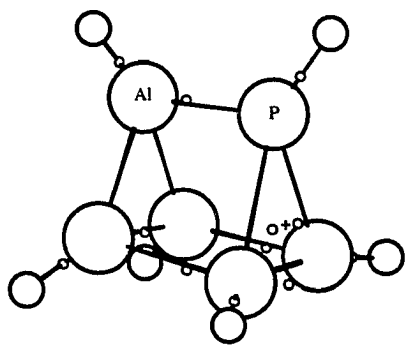

Al-P prismane

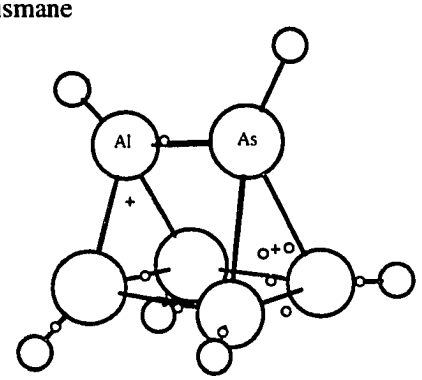

Al-As prismane

Figure 5. Continued.

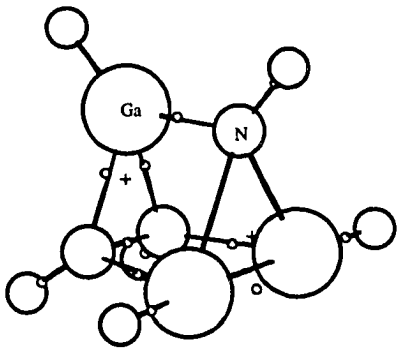

Ga-N prismane

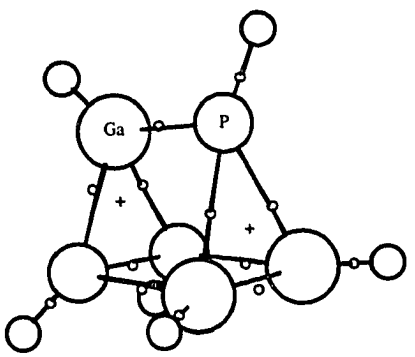

Ga-P prismane

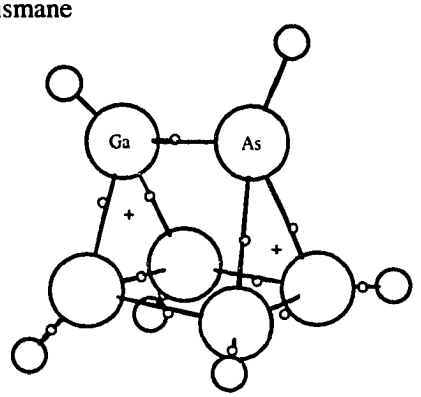

Ga-As prismane

Figure 5. Continued.

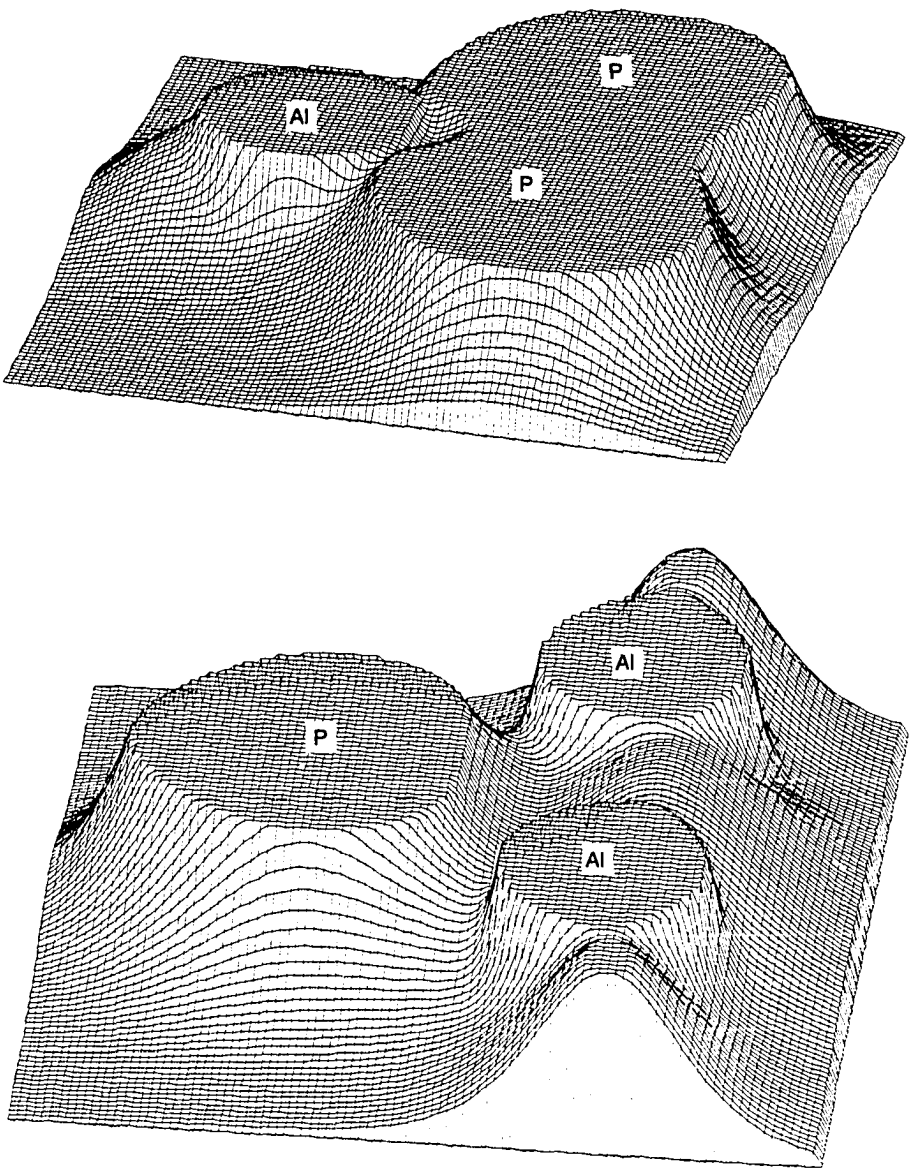

Figure 6. Total electron density map of Al-P prismane
The electron density shown here is on the plane of Al-P-P and P-Al-Al. Although, the bond critical points for the bonds X_1-Y_2, Y_1-X_2 and X_2-X_2 were not found, the figures show the significant electron density present.

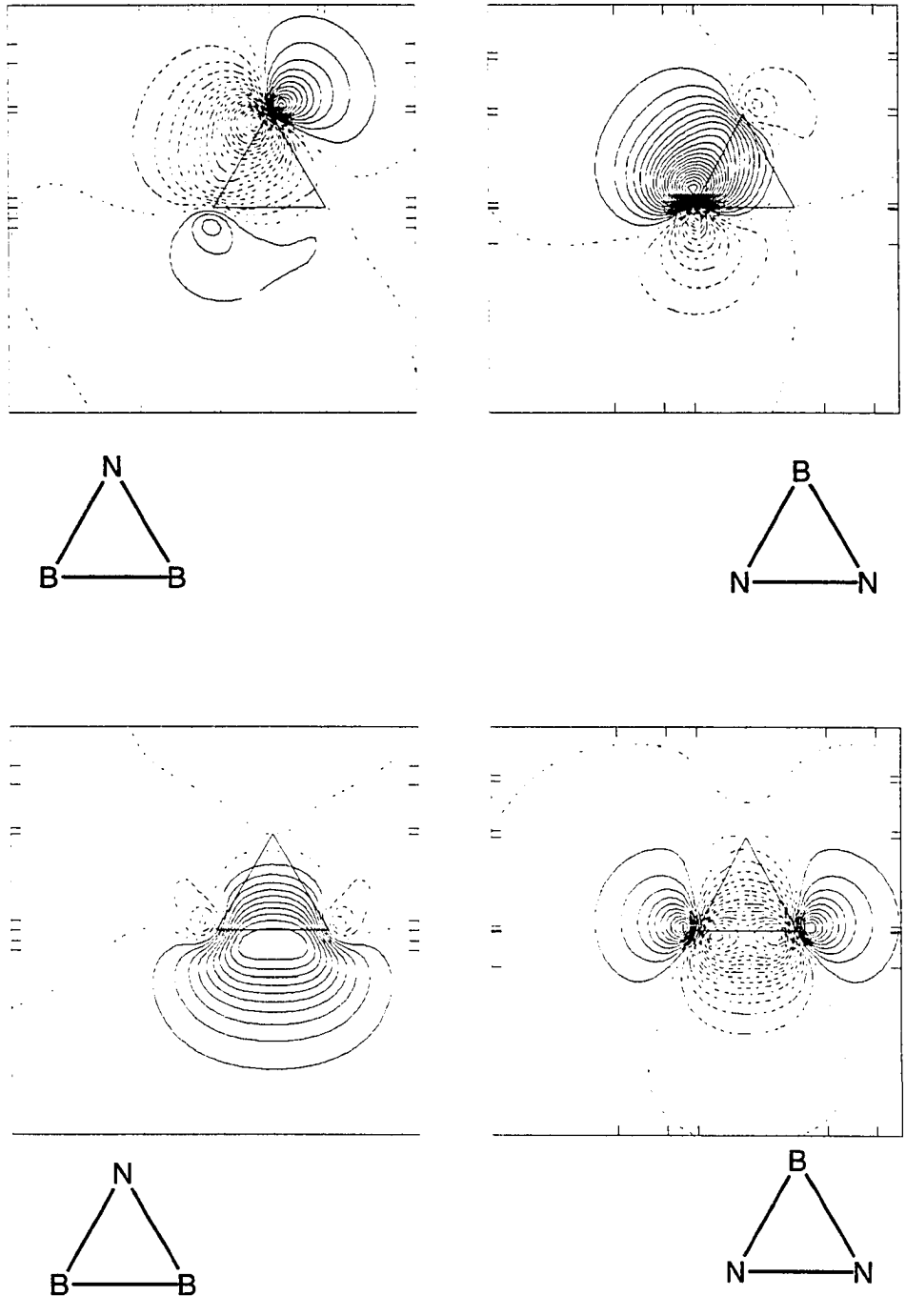

Figure 7a. Localized orbitals of B-N prismane.
The successive contours are drawn with 0.025 $bohr^{-3/2}$.

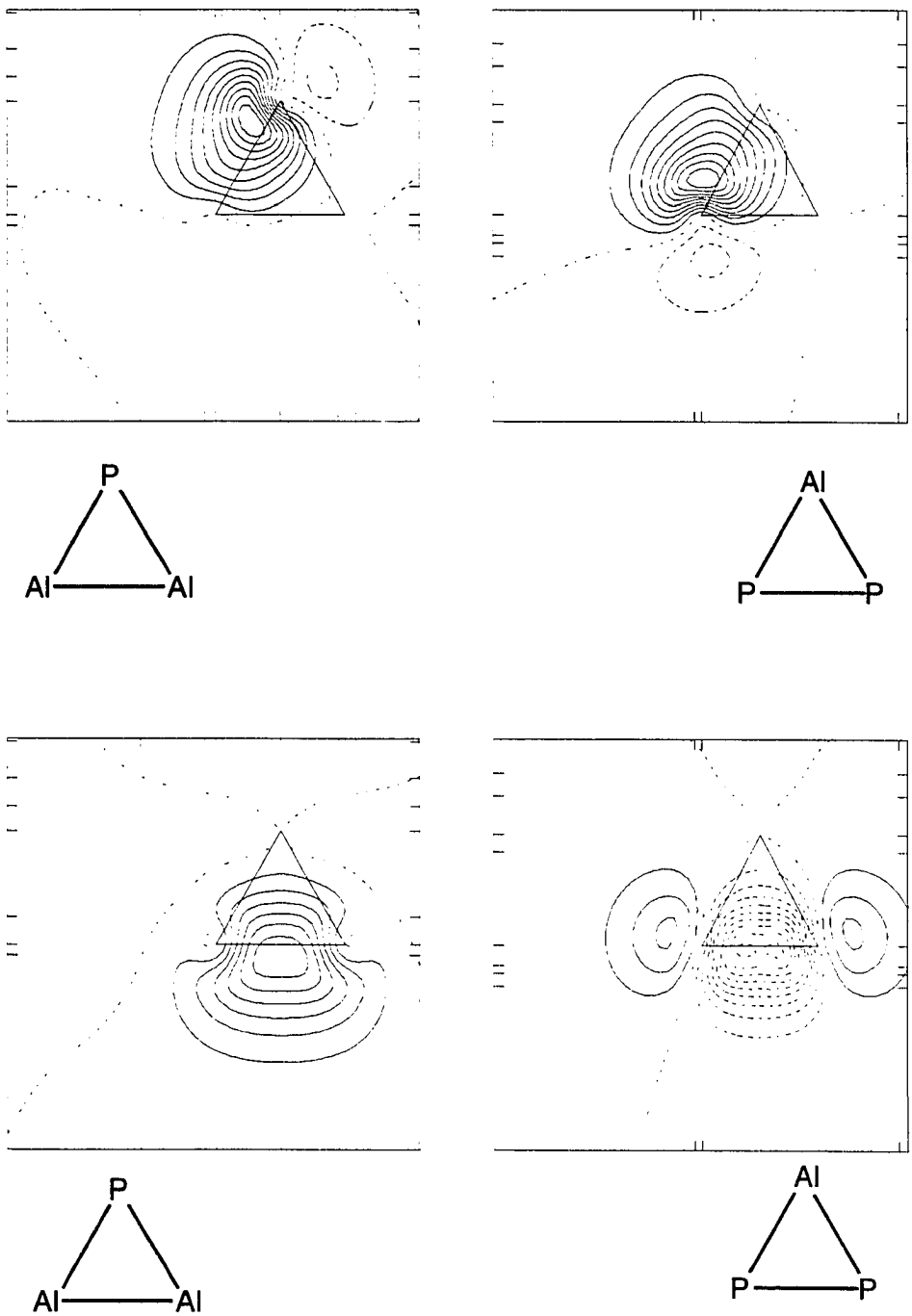

Figure 7b. Localized orbitals of Al-P prismane.
The successive contours are drawn with 0.025 bohr$^{-3/2}$.

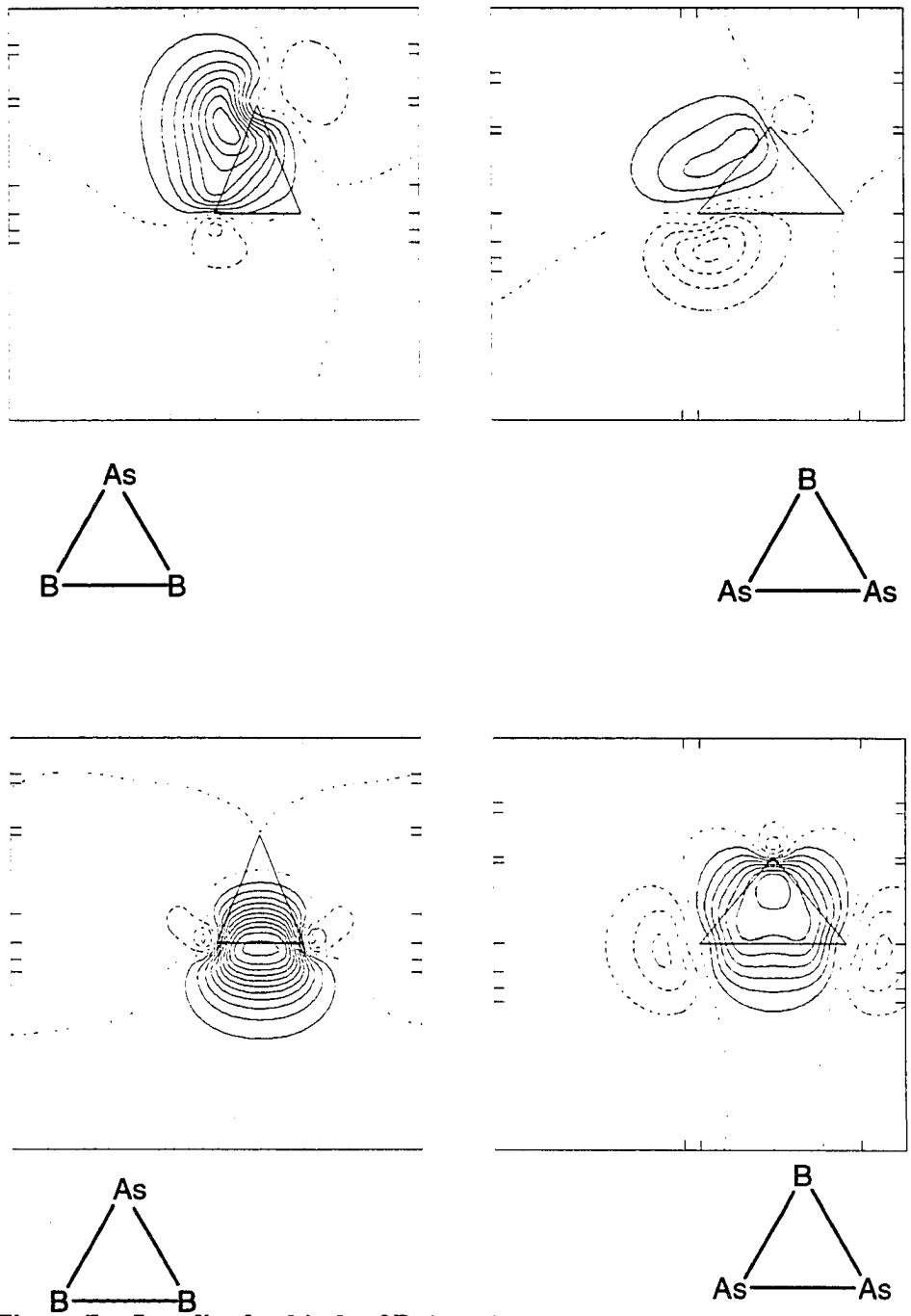

Figure 7c. Localized orbitals of B-As prismane.
The successive contours are drawn with 0.025 bohr$^{-3/2}$.
Notice the three-center bonding.

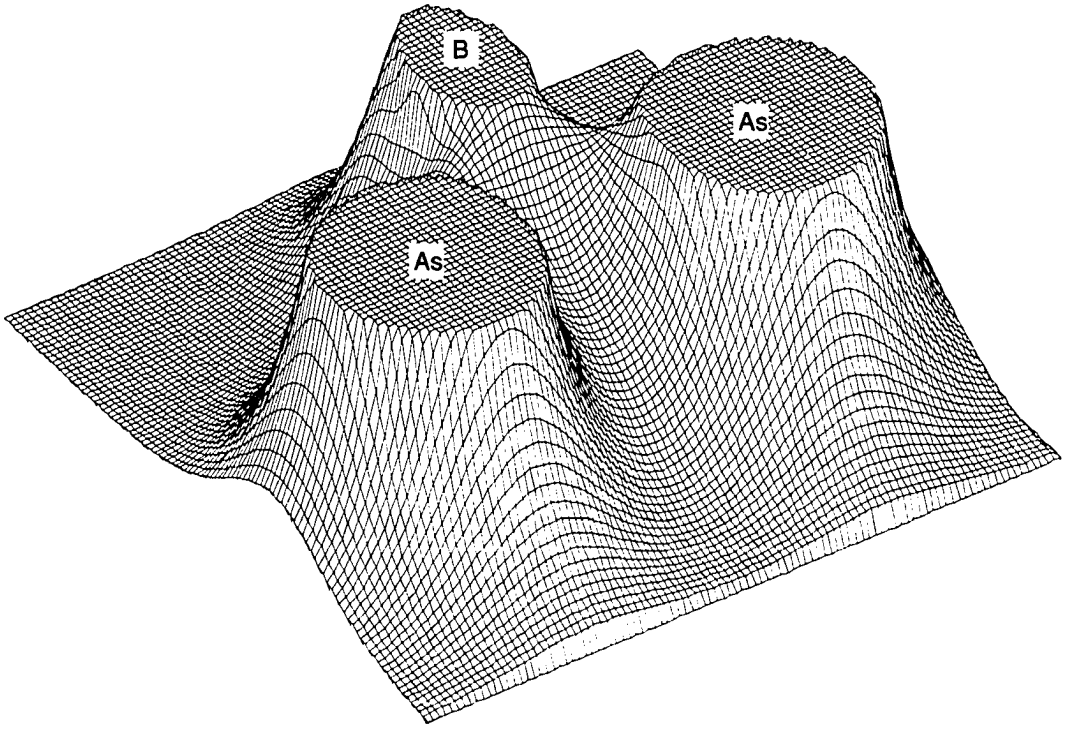

Figure 8. Total electron density map of B-As prismane

Supplementary material

(All values are in Å)

Cartesian Coordinates of Chair Conformers
Geometries obtained at the RHF/basis-A

B-P conformer

P	-.957085	1.657719	.534134
P	-.957085	-1.657719	.534134
P	1.914169	.000000	.534134
B	.897971	-1.555331	.090706
B	.897971	1.555331	.090706
B	-1.795942	.000000	.090706
H	-1.509616	2.614731	-.338517
H	-1.509616	-2.614731	-.338517
H	3.019231	.000000	-.338517
H	1.462642	-2.533371	-.325646
H	1.462642	2.533371	-.325646
H	-2.925285	.000000	-.325646

B-As conformer

As	-1.019137	1.765197	.685298
As	-1.019137	-1.765197	.685298
As	2.038274	.000000	.685298
B	.918374	-1.590670	.117080
B	.918374	1.590670	.117080
B	-1.836748	.000000	.117080
H	-1.548610	2.682272	-.386852
H	-1.548610	-2.682272	-.386852
H	3.097220	.000000	-.386852
H	1.451520	-2.514106	-.415908
H	1.451520	2.514106	-.415908
H	-2.903039	.000000	-.415908

Al-P conformer

Al	-1.073285	1.858985	.028885
Al	-1.073285	-1.858985	.028885
Al	2.146571	.000000	.028885
P	1.140294	-1.975047	-.638720
P	1.140294	1.975047	-.638720
P	-2.280588	.000000	-.638720
H	-1.773982	3.072626	.767372
H	-1.773982	-3.072626	.767372
H	3.547963	.000000	.767372
H	1.694076	-2.934226	.242348
H	1.694076	2.934226	.242348
H	-3.388153	.000000	.242348

Al-As conformer

Al	-1.062169	1.839731	-.106389
Al	-1.062169	-1.839731	-.106389
Al	2.124338	.000000	-.106389
As	1.206828	-2.090288	-.917038
As	1.206828	2.090288	-.917038
As	-2.413657	.000000	-.917038
H	-1.706901	2.956440	.811191
H	-1.706901	-2.956440	.811191
H	3.413803	.000000	.811191
H	1.710222	-2.962191	.213018
H	1.710222	2.962191	.213018
H	-3.420444	.000000	.213018

Ga-P conformer

P	-1.147290	1.987165	.800404
P	-1.147290	-1.987165	.800404
P	2.294580	.000000	.800404
Ga	1.043540	-1.807464	.085118
Ga	1.043540	1.807464	.085118
Ga	-2.087080	.000000	.085118
H	-1.660062	2.875312	-.163174
H	-1.660062	-2.875312	-.163174
H	3.320124	.000000	-.163174
H	1.714868	-2.970238	-.722837
H	1.714868	2.970238	-.722837
H	-3.429735	.000000	-.722837

Ga-As conformer

As	-1.204732	2.086658	.923985
As	-1.204732	-2.086658	.923985
As	2.409465	.000000	.923985
Ga	1.049984	-1.818625	.104834
Ga	1.049984	1.818625	.104834
Ga	-2.099967	.000000	.104834
H	-1.705764	2.954470	-.210239
H	-1.705764	-2.954470	-.210239
H	3.411528	.000000	-.210239
H	1.683846	-2.916507	-.819328
H	1.683846	2.916507	-.819328
H	-3.367693	.000000	-.819328

Si-Si conformer

Si	-1.920511	-1.108808	.124770
Si	1.920511	-1.108808	.124770
Si	.000000	-2.217615	-.124770
Si	1.920511	1.108808	-.124770
Si	-1.920511	1.108808	-.124770

Si	.000000	2.217615	.124770
H	-3.201316	-1.848281	-.008004
H	3.201316	-1.848281	-.008004
H	.000000	-3.696562	.008004
H	3.201316	1.848281	.008004
H	-3.201316	1.848281	.008004
H	.000000	3.696562	-.008004

Si-Ge conformer

Ge	-1.100993	1.906976	.166613
Ge	-1.100993	-1.906976	.166613
Ge	2.201986	.000000	.166613
Si	1.146210	-1.985294	-.355639
Si	1.146210	1.985294	-.355639
Si	-2.292420	.000000	-.355639
H	-1.870318	3.239486	.053926
H	-1.870318	-3.239486	.053926
H	3.740637	.000000	.053926
H	1.850753	-3.205598	.135314
H	1.850753	3.205598	.135314
H	-3.701506	.000000	.135314

Ge-Ge conformer

Ge	-1.983209	-1.145006	.334243
Ge	1.983209	-1.145006	.334243
Ge	.000000	-2.290012	-.334243
Ge	1.983209	1.145006	-.334243
Ge	-1.983209	1.145006	-.334243
Ge	.000000	2.290012	.334243
H	-3.282596	-1.895208	-.058637
H	3.282596	-1.895208	-.058637
H	.000000	-3.790415	.058637
H	3.282596	1.895208	.058637
H	-3.282596	1.895208	.058637
H	.000000	3.790415	-.058637

==========

Cartesian Coordinates of Chair Conformers
Geometries obtained at the MP2/basis-A

==========

Ge-Ge conformer

Ge	1.96119	1.13156	0.35593
Ge	-1.99992	1.13152	0.3559
Ge	-0.01938	2.27472	-0.3638
Ge	-1.99966	-1.15561	-0.36276
Ge	1.96111	-1.15526	-0.36344
Ge	-0.01901	-2.29929	0.35565
H	3.2648	1.88379	-0.06761

H	-3.30353	1.8839	-0.06749
H	-0.01935	3.78007	0.05926
H	-3.30343	-1.90802	0.0597
H	3.26438	-1.90818	0.06015
H	-0.01943	-3.80426	-0.06846

==========

Cartesian Coordinates of Boat Conformers
Geometries obtained at the RHF/basis-A

==========

B-P analog

P	1.686045	0.265816	0.000000
P	-1.134314	-0.339810	-1.633836
P	-1.134314	-0.339810	1.633836
B	-1.913370	0.266383	0.000000
B	0.763573	-0.106189	-1.610492
B	0.763573	-0.106189	1.610492
H	2.982112	-0.273938	0.000000
H	-1.621855	0.461865	-2.683218
H	-1.621855	0.461865	2.683218
H	-2.992180	0.798215	0.000000
H	1.377137	-0.144694	-2.643568
H	1.377137	-0.144694	2.643568

B-As analog

As	-1.351933	0.076586	-1.721621
As	-1.351933	0.076586	1.721621
As	1.665677	0.862599	0.000000
B	0.671972	0.302592	-1.657406
B	0.671972	0.302592	1.657406
B	-2.022620	0.919012	0.000000
H	-1.695201	1.100091	-2.785749
H	-1.695201	1.100091	2.785749
H	2.961425	0.086028	0.000000
H	1.286350	0.182857	-2.684435
H	1.286350	0.182857	2.684435
H	-2.949116	1.685813	0.000000

Al-P analog

P	-1.232317	-.723483	1.941151
P	-1.232317	-.723483	-1.941151
P	2.065999	.349976	.000000
Al	1.043928	-.282390	1.960386
Al	1.043928	-.282390	-1.960386
Al	-2.097513	.198569	.000000
H	-1.708351	.107502	2.983645
H	-1.708351	.107502	-2.983645
H	3.414911	-.061260	.000000

H	1.873766	-.336877	3.306321
H	1.873766	-.336877	-3.306321
H	-3.337300	1.183438	.000000

Al-As analog

As	-1.350836	-.920537	2.028973
As	-1.350836	-.920537	-2.028973
As	2.017622	.736935	.000000
Al	1.022716	-.334563	1.933137
Al	1.022716	-.334563	-1.933137
Al	-2.092651	.206596	.000000
H	-1.704150	.138256	3.054107
H	-1.704150	.138256	-3.054107
H	3.417271	.174285	.000000
H	1.923159	-.550801	3.225711
H	1.923159	-.550801	-3.225711
H	-3.123380	1.418049	.000000

Ga-P analog

P	1.263808	-.783833	-1.942624
P	-1.968745	.560770	.030894
P	1.270898	-.891318	1.916151
GA	-.981910	-.335254	1.906395
GA	2.105680	.125102	.012076
GA	-.984065	-.212650	-1.899772
H	1.712010	.106836	-2.937109
H	-3.296913	.107366	.016677
H	1.713126	-.050211	2.955469
H	-1.819579	-.468650	3.222740
H	3.296913	1.141318	.037932
H	-1.820842	-.253059	-3.222740

Ga-As analog

As	-1.342275	-.919310	2.010696
As	-1.342275	-.919310	-2.010696
As	2.003587	.759829	.000000
Ga	1.014960	-.332543	1.904398
Ga	1.014960	-.332543	-1.904398
Ga	-2.081172	.201186	.000000
H	-1.681664	.145420	3.033897
H	-1.681664	.145420	-3.033897
H	3.393036	.171089	.000000
H	1.900359	-.559440	3.180752
H	1.900359	-.559440	-3.180752
H	-3.095508	1.397721	.000000

Ge-Ge analog

Ge	1.186277	.594972	-1.978046
Ge	1.186277	.594972	1.978046

Ge	-1.097291	1.285121	-1.988082
Ge	-1.097291	1.285121	1.988082
Ge	2.347136	1.251225	.000000
Ge	-2.239999	.626392	.000000
H	1.942763	.956171	-3.283076
H	1.942763	.956171	3.283076
H	-1.847737	.875464	-3.282265
H	-1.847737	.875464	3.282265
H	3.836299	.817147	.000000
H	-3.743221	1.009254	.000000

==========

Cartesian Coordinates of Inorganic Prismanes
Geometries obtained at the RHF/basis-A

==========

B-N prismane

N	0.839083	1.132154	0.000000
H	1.503668	1.889463	0.000000
B	-0.669343	1.171760	0.000000
H	-1.455431	2.078060	0.000000
N	-0.793957	-0.195436	0.737337
N	-0.793957	-0.195436	-0.737337
B	0.881555	-0.282280	0.832271
B	0.881555	-0.282280	-0.832271
H	1.419904	-0.416421	1.898136
H	1.419904	-0.416421	-1.898136
H	-1.581509	-0.653536	1.174884
H	-1.581509	-0.653536	-1.174884

B-P prismane

B	.849662	1.299458	.000000
H	1.556193	2.264467	.000000
P	-1.138423	1.049917	.000000
H	-2.081370	2.093449	.000000
B	-1.070557	-.800914	.866775
B	-1.070557	-.800914	-.866775
H	-1.764379	-1.229817	1.747205
H	-1.764379	-1.229817	-1.747205
P	.984207	-.375663	1.095417
P	.984207	-.375663	-1.095417
H	2.162152	-.956298	1.613986
H	2.162152	-.956298	-1.613986

B-As prismane

B	.826059	1.473447	.000000
H	1.564074	2.396050	.000000
As	-1.159479	1.164523	.000000
H	-2.189428	2.242902	.000000

B	-.974921	-.928813	.844752
B	-.974921	-.928813	-.844752
H	-1.703406	-1.307154	1.706968
H	-1.703406	-1.307154	-1.706968
As	.983867	-.198558	1.402620
As	.983867	-.198558	-1.402620
H	2.078313	-1.213163	1.133066
H	2.078313	-1.213163	-1.133066

Al-N prismane

Al	.668594	1.178564	.000000
H	1.565538	2.467424	.000000
N	-1.111176	.765531	.000000
H	-1.923847	1.370798	.000000
Al	-.993352	-.867855	1.199404
Al	-.993352	-.867855	-1.199404
H	-1.321265	-.767879	2.753573
H	-1.321265	-.767879	-2.753573
N	.951132	-.544703	.759754
N	.951132	-.544703	-.759754
H	1.768435	-1.019739	1.120989
H	1.768435	-1.019739	-1.120989

Al-P prismane

Al	.991839	1.656564	.000000
H	1.918030	2.930858	.000000
P	-1.315075	1.122928	.000000
H	-2.302160	2.127214	.000000
Al	-1.265045	-1.077100	1.263402
Al	-1.265045	-1.077100	-1.263402
H	-1.899457	-1.294596	2.701376
H	-1.899457	-1.294596	-2.701376
P	1.176084	-.474303	1.129164
P	1.176084	-.474303	-1.129164
H	2.346567	-1.181837	1.471615
H	2.346567	-1.181837	-1.471615

Al-As prismane

Al	1.049138	1.748243	.000000
H	1.970527	3.019763	.000000
As	-1.349514	1.177692	.000000
H	-2.369495	2.270521	.000000
Al	-1.316433	-1.133797	1.267130
Al	-1.316433	-1.133797	-1.267130
H	-1.987178	-1.411777	2.673566
H	-1.987178	-1.411777	-2.673566
As	1.206064	-.429800	1.258940
As	1.206064	-.429800	-1.258940
H	2.451646	-1.241845	1.489884

H	2.451646	-1.241845	-1.489884

Ga-N prismane

Ga	1.184843	-.846439	.000000
H	2.299626	-1.916234	.000000
N	.947835	.987258	.000000
H	1.667848	1.690513	.000000
Ga	-.777823	1.051895	-1.178164
Ga	-.777823	1.051895	1.178164
H	-.684268	1.423657	-2.699434
H	-.684268	1.423657	2.699434
N	-.623197	-.945669	-.754645
N	-.623197	-.945669	.754645
H	-1.169738	-1.707675	-1.117843
H	-1.169738	-1.707675	1.117843

Ga-P prismane

Ga	1.599329	-1.138272	.000000
H	2.702601	-2.227135	.000000
P	1.306181	1.191364	.000000
H	2.449908	1.998348	.000000
Ga	-.944416	1.356238	-1.229544
Ga	-.944416	1.356238	1.229544
H	-1.106578	2.042482	-2.627138
H	-1.106578	2.042482	2.627138
P	-.569568	-1.119900	-1.125418
P	-.569568	-1.119900	1.125418
H	-1.408377	-2.191129	-1.461144
H	-1.408377	-2.191129	1.461144

Ga-As prismane

Ga	.992652	1.796791	.000000
H	1.967617	3.004688	.000000
As	-1.379228	1.225349	.000000
H	-2.326973	2.385943	.000000
Ga	-1.312549	-1.137182	1.234048
Ga	-1.312549	-1.137182	-1.234048
H	-2.010381	-1.424133	2.606294
H	-2.010381	-1.424133	-2.606294
As	1.185178	-.407947	1.256108
As	1.185178	-.407947	-1.256108
H	2.415162	-1.246215	1.493433
H	2.415162	-1.246215	-1.493433

C-C prismane

C	.876699	.000000	.778264
C	.876699	.000000	-.778264
H	1.682035	.000000	1.512588
H	1.682035	.000000	-1.512588

C	-.438350	.759244	.778264
H	-.841017	1.456685	1.512588
C	-.438350	-.759244	.778264
H	-.841017	-1.456685	1.512588
C	-.438350	.759244	-.778264
H	-.841017	1.456685	-1.512588
C	-.438350	-.759244	-.778264
H	-.841017	-1.456685	-1.512588

Si-C prismane

C	1.032561	1.238721	0.000000
H	1.834693	1.981315	0.000000
Si	-0.848233	1.380982	0.000000
H	-1.761717	2.552129	0.000000
C	-0.939605	-0.289076	-0.815246
C	-0.939605	-0.289076	0.815246
H	-1.745631	-0.851395	1.289569
H	-1.745631	-0.851395	-1.289569
Si	0.940546	-0.348440	-1.119547
Si	0.940546	-0.348440	1.119547
H	1.651023	-0.499635	-2.417326
H	1.651023	-0.499635	2.417326

Ge-C prismane

C	1.090165	1.234655	.000000
H	1.890931	1.978986	.000000
Ge	-.865441	1.464490	.000000
H	-1.852592	2.636097	.000000
C	-.958839	-.331100	-.787148
C	-.958839	-.331100	.787148
H	-1.766487	-.873869	1.283415
H	-1.766487	-.873869	-1.283415
Ge	.982869	-.397137	-1.196668
Ge	.982869	-.397137	1.196668
H	1.645876	-.466967	-2.587492
H	1.645876	-.466967	2.587492

Si-Si prismane

Si	1.365312	.000000	1.191313
H	2.495250	.000000	2.160957
Si	1.365312	.000000	-1.191313
H	2.495250	.000000	-2.160957
Si	-.682656	1.182395	1.191313
H	-1.247625	2.160950	2.160957
Si	-.682656	-1.182395	1.191313
H	-1.247625	-2.160950	2.160957
Si	-.682656	1.182395	-1.191313
H	-1.247625	2.160950	-2.160957
Si	-.682656	-1.182395	-1.191313

H	-1.247625	-2.160950	-2.160957

Si-Ge prismane

Si	1.062148	1.489427	.000000
H	1.887589	2.722209	.000000
Ge	-1.363455	1.261319	.000000
H	-2.478754	2.311014	.000000
Si	-1.129686	-.850362	1.181936
Si	-1.129686	-.850362	-1.181936
H	-2.028784	-1.552588	2.130146
H	-2.028784	-1.552588	-2.130146
Ge	1.290274	-.579946	1.246656
Ge	1.290274	-.579946	-1.246656
H	2.318718	-1.018152	2.293992
H	2.318718	-1.018152	-2.293992

Ge-Ge prismane

Ge	1.439872	0.000000	1.243628
H	2.615566	0.000000	2.233511
Ge	1.439872	0.000000	-1.243628
H	2.615566	0.000000	-2.233511
Ge	-0.719936	1.246966	1.243628
H	-1.307783	2.265147	2.233511
Ge	-0.719936	1.246966	-1.243628
H	-1.307783	2.265147	-2.233511
Ge	-0.719936	-1.246966	1.243628
H	-1.307783	-2.265147	2.233511
Ge	-0.719936	-1.246966	-1.243628
H	-1.307783	-2.265147	-2.233511

==========

Cartesian Coordinates of Inorganic Prismanes
Geometries obtained at the MP2/basis-A

==========

B-N prismane

N	.844510	1.129595	.000000
B	-.680556	1.182505	.000000
N	-.791168	-.191288	-.761021
N	-.791168	-.191288	.761021
B	.879563	-.284430	-.841924
B	.879563	-.284430	.841924
H	1.538412	1.887520	.000000
H	-1.465906	2.101948	.000000
H	1.424445	-.406077	-1.917618
H	1.424445	-.406077	1.917618
H	-1.595880	-.678784	1.189181
H	-1.595880	-.678784	-1.189181

Ge-C prismane

C	1.100158	.734503	.000000
Ge	-.780059	1.180330	.000000
C	-1.098183	-.741367	-.735347
C	-1.098183	-.741367	.735347
Ge	.765438	-.642606	-1.488700
Ge	.765438	-.642606	1.488700
H	1.951401	1.450051	.000000
H	-1.902789	2.282238	.000000
H	.530444	.166809	-2.847617
H	.530444	.166809	2.847617
H	-1.992606	-1.102400	1.290507
H	-1.992606	-1.102400	-1.290507

Ge-Ge prisamane

Ge	-.723589	1.248140	1.246864
Ge	-.719397	-1.274396	1.246934
Ge	1.462897	-.000000	-1.248834
Ge	-.719564	1.249923	-1.248840
Ge	-.723379	-1.272568	-1.248796
Ge	1.463243	-.000000	1.246889
H	-1.316501	2.270622	2.267768
H	-1.309893	-2.300554	2.265581
H	2.646031	-.000000	-2.268459
H	-1.307943	2.276564	-2.268402
H	-1.316854	-2.297434	-2.267082
H	2.646373	-.000000	2.266510

CHAPTER 4. MULTISTATE POTENTIAL ENERGY SURFACES OF XH_2 (X=C, Si, Ge, Sn, AND Pb) MOLECULES AND SPIN-ORBIT COUPLING

A paper to be submitted to *J. Phys. Chem.*

Nikita Matsunaga[§], Shiro Koseki[‡], and Mark S. Gordon[§]

Abstract

Potential energy surfaces of the $^1A_1$ and $^3B_1$ states for XH_2 molecules (X=C, Si, Ge, Sn, Pb) are investigated with *ab initio* full valence multiconfigurational self-consistent field wavefunctions, using effective core potentials. Spin-orbit coupling is also calculated to construct relativistic potential energy surfaces. The relativistic potential energy surfaces are compared with the adiabatic non-relativistic potentials. Simple one dimensional Landau-Zener transition probabilities are calculated at the minimum energy crossing points of the XH_2 molecules to estimate intersystem crossing probabilities.

Introduction

Spin-orbit coupling is the major mechanism that connects two adiabatic potential energy surfaces of different spin. This coupling arises due to the interaction between the spin magnetic moment and the orbital motion of an electron around a nucleus. It lifts the degeneracy of a triplet state, for example, into three sub-states, and with correct symmetries of the spatial and spin parts of the wavefunction these two states may couple. Spin-orbit coupled states should then give a more realistic view of potential energy surfaces, and it is certainly essential to include spin-orbit coupling in a calculation of potential energy surfaces (PES) of molecules containing heavy elements. For example, one could not possibly obtain even a qualitatively correct dissociation curve of CH_3I[1], due to the spin-orbit splitting of iodine into $^2P_{1/2}$ and $^2P_{3/2}$.

Although the formalism for evaluating spin-orbit coupling matrix elements is available[2] for molecular calculations, there are still a limited number of such calculations, especially as applied to potential energy surfaces[1,3] or chemical reactions[4] of polyatomic molecules.

§ Iowa State University
‡ Department of Chemistry, Faculty of Education, Mie University, Tsu, 514, Japan

The effective core potential (ECP) method that projects out core-electron contributions is a powerful way to include heavier elements in calculations on large systems. We have successfully applied ECP's to a number of systems, including main-group[5,6] and transition metal complexes[7]. The ECP method has also been used in the calculations of spin-orbit coupling in order to avoid the rather large computational expense in studying heavy element containing molecules[8].

The spin-orbit coupling of two different spin states is determined by using the relativistic Breit-Pauli Hamiltonian[9]. Recently, we have utilized the one-electron Breit-Pauli Hamiltonian and systematically deduced the effective nuclear charges of second and third period main group elements using an all-electron basis set[10]. We also reported the effective nuclear charges derived from effective core potentials[11] developed by Stevens *et al.*[12] for second to fifth period alkaline earth and main group elements.

Another method utilizing ECP's to calculate spin-orbit integrals is due to Ermler *et al*[13]. These authors have noted that the difference between the two j-dependent relativistic effective potentials, obtained by fitting to atomic full relativistic Dirac-Hartree-Fock calculations, corresponds to the spin-orbit operator in the core region. Therefore, the gaussian exponents used in the usual ECP integral calculations can be used to define a spin-orbit operator for the core space.

CH_2 is unique among the group IV XH_2 molecules, in that the ground state is a triplet state. The experimental singlet-triplet splitting is in the range 8.5-9.0 kcal/mol[14]. A number of accurate theoretical calculations are also available[15], in which the calculated singlet-triplet splittings converge close to the experimental values. The lowest singlet state in the remaining group IV XH_2 species is lower in energy than the lowest triplet states. Several theoretical calculations at various levels of theory have been reported for SiH_2. The most accurate of these place the singlet-triplet splitting at 19-21 kcal/mol[16].

There are only a handful of theoretical studies[17] dealing with the singlet-triplet splitting and the stationary points on the PES of GeH_2, SnH_2 and PbH_2. The spin-orbit effects are explicitly treated in some of these studies[17e,18,19]. Electron diffraction derived structures, although they are not dihydrides (XR_2, X = Ge, Sn; R = $CH(SiMe_3)_2$) have also been reported[20]. These are the only experimental XH_2 related structures for heavier Group IV A elements in the gas phase.

The energetics, as well as geometries, are affected by large spin-orbit coupling

between singlet and triplet states of the heavier group IV XH_2 compounds. It is certainly interesting to learn how the relativistic PES of XH_2 are different from the adiabatic non-relativistic PES. Here we report potential energy surfaces of XH_2 (X=C, Si, Ge, Sn and Pb) possessing C_{2v} symmetry, in which the adiabatic and spin-orbit states of these XH_2 species are compared. The Landau-Zener transition model was also utilized to gain more insight into how transitions between the two states might occur.

Computational Approach

The potential energy surfaces of the XH_2 species are prepared with full optimized reaction space (FORS) multiconfiguration self-consistent field (MCSCF or CASSCF) calculations defined by Ruedenberg *et al.*[21] using the GAMESS quantum chemistry package[22]. The active space is a full valence space *i.e.* six electrons are distributed among six orbitals in the active space. These six orbitals correspond to the two bonding and two antibonding XH bonds, X lone pair and X empty p orbital for a singlet state.

Effective core potentials (ECP), which utilize the averaged relativistic core potentials, of Stevens *et al.*[12] are used throughout this paper. Since some of the relativistic effects in the core region, especially contraction of orbitals, are already described with the potentials, geometries obtained with the ECP are expected to be better than those obtained with all-electron basis sets for heavier elements. The lowest singlet ($X\ ^1A_1$) and the lowest triplet ($A\ ^3B_1$) state potential energy surfaces of XH_2 were constructed for a range of bond distances and bond angles, retaining C_{2v} symmetry.

Spin-orbit coupling is calculated by using the one-electron part of the microscopic Breit-Pauli Hamiltonian[9]

$$H_{SO} = \frac{e^2 \mathrm{h}}{2m^2c^2} \sum_{i,\alpha} \frac{Z_\alpha^{eff}}{r_{i\alpha}^3} (\mathbf{r}_{i\alpha} \times \mathbf{p}_i) \cdot \mathbf{s}_i \qquad (1)$$

where i runs over all electronic coordinates and α runs over all nuclear coordinates. Z^{eff} is an adjustable parameter which is determined systematically by adjusting Z^{eff} so that the fine structure splittings of the lowest Π states of diatomic hydrides (XH) are reproduced. Z^{eff} for carbon, silicon, germanium and tin are 3.90, 168, 1312, and 5500, respectively[11]. Z^{eff} for lead (18200) is chosen to reproduce the fine structure splitting of Pb atom.

The matrix elements are calculated using the Breit-Pauli spin-orbit operator in eq (1), and are placed in a Hamiltonian matrix (4 x 4 in this case) which is complex. This matrix is diagonalized to obtain the eigenvalues of the four spin-mixed states.

The transition probability is estimated by using a Landau-Zener model[23] for intersystem crossing. The transition probability P_{LZ} can be given by

$$1 - P_{LZ} = 1 - e^{-2\delta} \tag{2}$$

where

$$\delta = \frac{\pi |H_{ij}|^2}{h\nu |\Delta g_{ij}|} \tag{3}$$

and where H_{ij} is the spin-orbit coupling matrix element between two adiabatic states i and j, v is the velocity with which the system is passing through the singlet-triplet crossing region, and Δg_{ij} is the difference in the gradients of the two adiabatic states i and j. The transition probability was calculated for a range of kinetic energies.

Results and Discussion

The stationary points on the adiabatic PES and the relativistic PES of XH_2 are compared with available experiments and relativistic Dirac-Hartree-Fock (DHF)[24] calculations in Table 1. The bond lengths of adiabatic XH_2 singlet states calculated with the MCSCF/SBK(d,p) level of theory are 0.4 - 0.7 Å longer than those for the triplet states. Except for CH_2, the bond angle at which the minimum on the adiabatic PES occurs for singlets is ≈ 90°, and for triplet the angle is ≈ 120°. The geometries obtained from the relativistic PES for SiH_2 and GeH_2 do not differ from the adiabatic PES. This is due to the fact that the spin-orbit coupling is smaller than in the heavier XH_2 species, even though the position of the crossing seam is closer to the triplet minima of SiH_2 and GeH_2 than to the singlet minima. For CH_2 the adiabatic triplet state crosses right at the position of the singlet minimum on the adiabatic surface. Hence a small change in the singlet state geometry results upon mixing of the states by spin-orbit coupling, even though the spin-orbit coupling in CH_2 is the smallest among the XH_2 molecules in the region where the crossing occurs. The MCSCF/SBK(d,p) bond lengths are longer than the corresponding DHF values.

Since there is no two-electron spin-other-orbit coupling term in the DHF calculation,

the DHF and MCSCF/SBK(d,p) should be in close agreement, except for the fact that our ECP results contain non-dynamical correlation through the MCSCF wavefunctions. Also, the ECP basis set is constructed so as to reproduce the position of the maximum in the atomic radial wavefunctions taken from the DHF calculations[12]. Therefore, relativistic effects, such as inner-shell contractions, are already included in the ECP. The possible source of any difference in geometry obtained with MCSCF/SBK(d,p) and the DHF calculations should be due to the non-dynamical correlation.

The calculated bond angles are consistently in better agreement with other *ab initio* calculations than the bond lengths, except for PbH_2, in which both triplet geometrical parameters are not in as good agreement. In the present study, the spin-orbit Hamiltonian contains only four elements; therefore, together with the lack of dynamical correlation in the MCSCF wave functions, the discrepancy could come from the omission of higher lying states which may mix with the $^1A_1$ and $^3B_1$ states. For CH_2 to SnH_2, it is more important to consider including dynamical electron correlation, since the effect of spin-orbit coupling on geometries is much smaller than for PbH_2.

Table 2 shows the calculated vibrational frequencies of adiabatic singlet and triplet states. In general, the triplet states have smaller bending frequencies than the corresponding singlet states, since the triplet bond angles are larger, and the triplet bend potentials are flatter. The stretching frequencies are larger in the triplet, due to the shorter triplet bond lengths. Among the three vibrational states the bending mode has lowest frequencies, and the symmetric stretch is smaller than that of the asymmetric stretch, except for SnH_2, where the two stretching frequencies are nearly degenerate. This accidental degeneracy allows the two modes to appear as local Sn-H bond stretches.

Potential energy surfaces of XH_2 have been prepared for a range of bond lengths and bond angles. Contour maps of the adiabatic potential energy surfaces of XH_2 are plotted in Figures 1 - 5 for X=C, Si, Ge, Sn and Pb, respectively. In each case, the angle was varied from 60° to 180°. The variation in bond lengths are different for each species. In each figure, the crossing seam between the singlet and triplet is drawn by a bold line. In CH_2 the crossing of singlet and triplet occurs almost exactly at the position of the singlet minimum. As the X atom becomes heavier, the crossing seam moves away from the position of a minimum on one of the surfaces.

It can been seen from Figures 1 - 5 that the distances between two contour lines is narrower in the angular direction in all adiabatic triplets. Similarly, the adiabatic singlet has

narrower contours along the bond distance axis, except for SiH_2 and PbH_2. The contour map of the adiabatic singlet SiH_2 and PbH_2 are almost concentric.

The singlet and triplet surfaces can be coupled through spin-orbit coupling. The non-zero matrix element that contributes to the spin-orbit coupling in a C_{2v} XH_2 molecule is the term arising from the x components of angular momentum and the x and y components of spin angular momentum operators, respectively (see Appendix for explanation):

$$<A_1|l_x|B_1><1|s_{x,y}|3>$$

where <1| and |3> denote singlet and triplet spin functions, respectively. The choice of axis here is such that the atoms in XH_2 molecules are on the X-Z plane in cartesian space. The rest of the matrix elements are zero in C_{2v} symmetry. The Hamiltonian matrix for mixing these singlet and triplet substates should have the form

$$\begin{array}{c} \\ \langle 0,0| \\ \langle 1,1| \\ \langle 1,0| \\ \langle 1,-1| \end{array} \begin{array}{c} \begin{array}{cccc} |0,0\rangle & |1,1\rangle & |1,0\rangle & |1,-1\rangle \end{array} \\ \begin{pmatrix} {}^1E-\varepsilon & x & 0 & x \\ x & {}^3E-\varepsilon & 0 & 0 \\ 0 & 0 & {}^3E-\varepsilon & 0 \\ x & 0 & 0 & {}^3E-\varepsilon \end{pmatrix} \end{array} \qquad (4)$$

where the bra and ket denote | M, M_s> (M is the total spin angular momentum quantum number and M_s is the z component of the spin quantum number), x denotes the non-zero matrix elements and ${}^1E$ and ${}^3E$ are the adiabatic singlet and triplet energies, respectively. Due to the coupling of singlet and a substate of triplet through the non-zero matrix elements, an avoided crossing between two states out of the four occurs where the adiabatic singlet and triplet states cross. The three spin functions of the triplet can be expressed as $2^{-1/2}(\alpha\beta+\beta\alpha)$, $2^{-1/2}(\alpha\alpha+\beta\beta)$ and $2^{-1/2}(\alpha\alpha-\beta\beta)$. These transform as A_2, B_1 and B_2, respectively[25d,17c]. Hence the overall symmetry of the substates of the triplet are B_2, A_1 and A_2, denoted as ${}^3B_1(B_2)$, ${}^3B_1(A_1)$ and ${}^3B_1(A_2)$. Similarly, the singlet is denoted ${}^1A_1(A_1)$. Mixing of two substates occurs if the overall symmetry of the two wavefunctions transform according to the same irreducible representation; here, ${}^1A_1(A_1)$ and ${}^3B_1(A_1)$ mix, and an

avoided crossing occurs. The wavefunctions describing the other two states, $^3B_1(B_2)$ and $^3B_1(A_2)$, can only couple with other high lying states with overall symmetry B_2 and/or A_2. Therefore, these two states are degenerate in the present study, and are described exclusively by triplet character. To lift these degenerate levels, requires the inclusion of higher lying states to form a larger Hamiltonian.

The singlet-triplet energy differences are compared in Table 3. This table lists the energy differences for both adiabatic and relativistic singlet and triplet states. The adiabatic singlet-triplet energy gap for the heavier XH_2 molecules becomes larger, except for SnH_2. The latter is actually smaller than that of GeH_2 by 1.2 kcal/mol. The relativistic singlet-triplet splitting does not differ from the adiabatic ones for CH_2, SiH_2 and GeH_2, since the spin-orbit coupling in these molecules are relatively small. In SnH_2 the relativistic singlet-triplet splitting is about 1 kcal/mol larger than the adiabatic value. On the other hand, the splitting becomes almost 6 kcal/mol larger for PbH_2 when the relativistic effects are introduced.

The contour maps for the relativistic XH_2 PES are shown in Figures 6 - 10. Only the $^1A_1(A^1)$ and $^3B_1(A_1)$ states are presented here, as the middle two levels possess exclusively triplet character (*vide supra*) in the present study. Since there is a coupling between singlet and triplet, one side of the crossing seam on the relativistic PES is predominantly singlet character and the other side of the crossing seam possesses predominantly triplet character. This is especially clear for the species with relatively smaller spin-orbit coupling. For example, CH_2 in Figure 6b shows steeper contours below the crossing seam than the ones shown in Figure 1a, in which the lower part of the triplet is connected. Similarly, the $^3B_1(A_1)$ PES in Figure 6b clearly shows adiabatic triplet character above the crossing seam and singlet character below the crossing seam. This becomes less apparent as X becomes heavier and the crossing seam moves to larger HXH angles.

A cross sectional view of the PES is more revealing. Figure 13 shows the cross section of the PES of CH_2 at the fixed bond distance 1.15 Å and the PES of PbH_2 at the fixed bond distance 1.885 Å. Following the top curve (denoted with the squares) of Figure 3a from smaller to larger angle, the curve dramatically changes its character from triplet to singlet. The leading configurations of the wavefunction at a 90° bond angle on the upper curve have triplet character ($2^{-1/2}[\alpha\alpha+\beta\beta]$ combination), accounting for 84.6% of the wavefunction. The lower curve consists of 90.8% singlet character ($2^{-1/2}[\alpha\beta-\beta\alpha]$). At 110°

the upper curve consists of 90.8% singlet character, and the lower curve contains 83.5% triplet character.

Figure 11 also shows spin-orbit coupling matrix elements along the bending coordinates. The spin-orbit coupling for CH_2 becomes larger as the angle becomes larger, and it reaches its maximum value at 135°. Then, it gradually decreases until 135°, then sharply decreases to zero at 180° due to symmetry (see Appendix for more explanation). The spin-orbit coupling trend in PbH_2 is similar to that of CH_2, but the maximum occurs at a smaller angle (80°) and gradually decreases to 175°, then drops steeply to zero at 180°.

The minimum energy crossing occurs at 1.15 Å and 100° for CH_2, 1.5Å and 127.9° for SiH_2, 1.56Å and 135.7° for GeH_2, 1.65Å and 134.5° for SnH_2, and 1.75Å and 146.3° for PbH_2. Figure 12 shows the energetics and the spin-orbit coupling matrix elements along the crossing seam in each XH_2. As can be seen from the figure, the minimum energy crossing occurs at the bond length corresponding to the equilibrium structure on XH_2 upper states ($^1A_1$ for CH_2 and $^3B_1$ for the rest), except for PbH_2, in which the crossing occurs at a bond length that is shorter than that at the singlet stationary point (1.812Å). The spin-orbit coupling between $^1A_1(A_1)$ and $^3B_1(A_1)$ along the crossing seam is more or less constant. The spin-orbit couplings in CH_2 and SiH_2 are similar; the spin-orbit coupling is less than 0.5 kcal/mol, with that in SiH_2 slightly larger than CH_2. The spin-orbit coupling in GeH_2 is about 3 kcal/mol. As can be seen from the matrix elements, shown in Figure 12, the coupling actually becomes smaller until 1.8Å, then increases again, but the spin-orbit coupling is essentially constant. For SnH_2, the coupling is 6.7 - 5.5 kcal/mol, and the trend is to that found for GeH_2. The coupling for PbH_2 is 24 - 17 kcal/mol; again there is a decrease in coupling then it increases.

The transition probability for intersystem crossing using a simple one dimensional Landau-Zener model[23] was calculated for kinetic energies ranging from zero to 2.0 eV. Figure 13 shows the transition probabilities calculated at the minimum energy crossing points for XH_2 species. A probability of unity means that the transition would take place. As can be seen from the figure, CH_2 and SiH_2 have a similar transition profile, in which the transition would take place only in a small kinetic energy region. On the other hand, transition is accessible at any kinetic energy in SnH_2 and PbH_2. Strong spin-orbit coupling and larger mass in SnH_2 and PbH_2 for given kinetic energy *both* contribute to larger intersystem crossing probability. GeH_2 is an intermediate case for which the transition is accessible in a range of kinetic energy.

Conclusions

The PES of adiabatic and spin-orbit coupled states of XH_2 (X=C, Si, Ge, Sn and Pb) species have been compared. The geometries of SiH_2 and GeH_2 at the stationary points on the relativistic PES do not differ from the ones on the adiabatic PES due to small spin-orbit coupling. For CH_2, the singlet-triplet crossing seam lies at the position of the singlet minimum; therefore a small change in geometry is observed. The triplet state of SnH_2 is shifted 0.004Å in bond length and 1.6° in bond angle on the relativistic PES. Due to the strong spin-orbit coupling, the geometries of PbH_2 are shifted 0.005Å and 1° for the singlet and 0.015Å and 3.4° for the triplet.

Due to the coupling of singlet and triplet, the relativistic PES appears as predominantly singlet at one side and triplet at the other separated by the crossing seam. If the coupling is strong, as found in PbH_2, the relativistic PES can differ drastically from adiabatic PES .

The spin-orbit coupling affects the singlet-triplet splitting only for SnH_2 by 1 kcal/mol and 6 kcal/mol for PbH_2. The splittings in CH_2, SiH_2 and GeH_2 are not affected.

The bond length at which the minimum energy crossing occurs is closer to that of the corresponding higher energy states (singlet for CH_2 and triplet for the others). The energy separation between the spin-orbit coupled states is less than 1 kcal/mol for CH_2 and SiH_2, and for GeH_2 it is about 3 kcal/mol. For SnH_2, the energy separation is 5.5 - 6.7 kcal/mol, and 17 - 24 kcal/mol for PbH_2.

Transition probabilities for intersystem crossing are calculated using Landau-Zener model. The intersystem crossing occurs only for relatively small kinetic energy regions in CH_2 and SiH_2. However, for SnH_2 and PbH_2 transition is readily accessible at any kinetic energy due to the strong spin-orbit coupling and larger mass. GeH_2 is an intermediate case where the transition is accessible in a range of kinetic energy.

Appendix

The spin-orbit mattrix element between $^1A_1$ and $^3B_1$ states in C_{2v} symmetry can be expressed as[25]

$$\left\langle {}^1A_1 \left| H_{SO} \right| {}^3B_1 \right\rangle = \left\langle {}^1A_1 \left| l \bullet s \right| {}^3B_1 \right\rangle \qquad \text{(A1)}$$

By utilizing second quantization notation, $l \bullet s$ can be written as

$$l \bullet s = l_z s_z + \frac{1}{2} l^+ s^- + \frac{1}{2} l^- s^+ \qquad \text{(A2)}$$

where l_z is the cartesian z-component of the orbital angular momentum operator and s_z is the cartesian z-component of the spin angular momentum operator. l^+ and l^- are the raising and lowering operators for orbital angular momentum, respectively, and are defined as

$$\begin{aligned} l^+ &\equiv l_x + i l_y \\ l^- &\equiv l_x - i l_y \end{aligned} \qquad \text{(A3)}$$

Similarly, s^+ and s^- are the raising and lowering spin angular momentum operators, respectively.

$$\begin{aligned} s^+ &\equiv s_x + i s_y \\ s^- &\equiv s_x - i s_y \end{aligned} \qquad \text{(A4)}$$

Substituting (A2) into (A1) gives

$$\left\langle {}^1A_1 \middle| l \bullet s \middle| {}^3B_1 \right\rangle = \langle A_1 | l_z | B_1 \rangle \langle 1 | s_z | 3 \rangle + \langle A_1 | l^+ | B_1 \rangle \langle 1 | s^- | 3 \rangle + \langle A_1 | l^- | B_1 \rangle \langle 1 | s^+ | 3 \rangle \qquad \text{(A5)}$$

Here |1> and |3> denote appropriate singlet and triplet spin functions. The three triplet spin functions are $2^{-1/2}(\alpha\beta+\beta\alpha)$, $2^{-1/2}(\alpha\alpha+\beta\beta)$ and $2^{-1/2}(\alpha\alpha-\beta\beta)$, and these transform as A_2, B_1 and B_2 irreducible representations in C_{2v} symmetry[25]. The l_x, l_y and l_z operators transform as B_1, B_2 and A_1 irreducible representations, respectively. A spin operator transforms as a rotation; therefore the s_x, s_y and s_z operators transform as B_2, B_1 and A_2, respectively, in C_{2v} symmetry. Substituting (A3) and (A4) into (A5), and using the fact that the spin-orbit Hamiltonian is totally symmetric, the non-zero spin-orbit matrix element between $^1A_1$ and $^3B_1$ is

$$\left\langle {}^1A_1 \middle| l \bullet s \middle| {}^3B_1 \right\rangle = \langle A_1 | l_x | B_1 \rangle \langle 1 | s_y | 3 \rangle \neq 0 \quad \text{for triplet spin function } \alpha\alpha+\beta\beta$$

$$\left\langle {}^1A_1 \middle| l \bullet s \middle| {}^3B_1 \right\rangle = \langle A_1 | l_x | B_1 \rangle \langle 1 | s_x | 3 \rangle \neq 0 \quad \text{for triplet spin functioin } \alpha\alpha-\beta\beta$$

The non-zero spin-orbit matrix elements between $^1A_1$ and $^3B_1$ states arises from the term containing the l_x angular momentum operator and the s_y spin operator for the $\alpha\alpha+\beta\beta$ triplet spin function and the s_x operator for the $\alpha\alpha-\beta\beta$ spin functions.

Similar group theoretical arguments can be applied to deduce that the matrix element connecting $^1\Delta_g$ and $^3\Sigma_g^-$ states of $D_{\infty h}$ XH_2 molecules is zero.

Acknowledgements

This work was supported by grants from Air Force Office of Scientific Research (F49620-95-1-0077) and the National Science Foundation (CHE-93-13717). The authors wish to acknowledge helpful discussions with Drs. Tetsuya Taketsugu and Satoshi Yabushita during the course of this project. The authors also wish to acknowledge Dr. Greg Atchity for providing us with a contouring program CNTOUR in ALIS system of programs.

References

1 a) Yabushita, S.; Morokuma, K. *Chem. Phys. Lett.* **1988**, 153, 517
b) Amatatsu, Y.; Morokuma, K.; Yabushita, S. *J. Chem. Phys.* **1991**, 94, 4858

2 a) King, H. F.; Furlani, T. R. *J. Comput. Chem.* **1988**, 9, 771
b) Furlani, T. R. Ph. D. dissertation, State University of New York at Buffallo, Buffallo, 1984
c) Abegg, P. W. *Mol. Phys.* 1975, 30, 579
d) McMurchie, L. E.; Davidson, E. R. *J. Comput. Phys.* **1976**, 26, 218.

3 a) Furlani, T. R.; King, H. F. *J. Chem. Phys.*, **1985**, 82, 5577
b) Caldwell, R. A.;Carlacci, L.; Doubleday, C. E.; Furlani, T. R.; King, H. F.; McIver, J. W. *J. Ame. Chem. Soc.* **1988**, 110, 6901.

4 a) Manaa, M. R.; Yarkony, D. R. *J. Chem. Phys.* **1991**, 95, 1808
b) Nguyen, K. A.; Gordon, M. S.; Montgomery, J. A.; Michels, H. H.; Yarkony, D. R. *J. Chem. Phys.* **1993**, 98, 3845.

5 a) Matsunaga, N.; Cundari, T. R.; Schmidt, M. W.; Gordon, M. S. *Theoretica Chimica Acta* **1992**, 83, 57
b) Matsunaga, N.; Gordon, M. S. *J. Amer. Chem. Soc.* **1994**, 116, 11407

6 a) Gordon, M. S.; Nugyen, K. A.; Carroll, M. T. *Polyhedron* **1991**, 10, 1247
b) Nguyen, K. A.; Carroll, M. T.; Gordon, M. S. *J. Ame. Chem. Soc.* **1991**, 113, 7924

7 a) Cundari, T. R.; Gordon, M. S. *J. Ame. Chem. Soc.* **1992**, 114, 539
b) Cundari, T. R.; Gordon, M. S. *Organomet.* **1992**,11, 55
c) Cundari, T. R. *J. Ame. Chem. Soc.* **1992**, 114, 7889

8 a) J. S. Cohen, W. R. Wadt, P. J. Hay, *J. Chem. Phys.* **1979**, 71, 2955
b) W. R. Wadt, *Chem. Phys. Lett.* **1982**, 89, 245

9 Langhoff, S. R.; Kern, C. W. in *Modern Theoretical Chemistry*, Vol 4, Schaefer, H. F. Ed., Plenum Press, New York, 1977, p. 381.

10 Koseki, S.; Schmidt, M. W.; Gordon, M. S. *J. Phys. Chem.* **1992**, 96, 10768

11 Koseki, S.; Schmidt, M. W.; Gordon, M. S.; Matsunaga, N. *J. Phys. Chem.*, in press, 1995

12 a) Stevens, W. J.; Basch, H.; Krauss, M. *J. Chem. Phys.* **1984**, 81, 6026
b) Stevens, W. J.; Basch, H.; Krauss, M.; Jaisen, P. *Can. J. Chem.* **1992**, 70, 612
c) Cundari, T. R.; Stevens, W. J. *J. Chem. Phys.* **1993**, 98, 5555

13 Ermler, W. C.; Lee, Y. S.; Christiansen, P. A.; Pitzer, K. S. *Chem. Phys. Lett.* **1981**, 81, 70

14 a) McKellar, A. R. W.; Bunker, P. R.; Sears, T. J.; Evenson, K. M.; Saykally, R. J.; Langhoff, S. R. *J. Chem. Phys.* **1983**, 79, 5251
b) Leopold, D. G.; Murray, K. K.; Stevens Miller, A. E.; Lineberger, W. C. *J. Chem. Phys.* **1985**, 83, 4849

15 a) Li, X.; Piecuch, P.; Paldus, J. *Chem. Phys. Lett.* **1994**, 224, 267
b) Reynolds, P. J.; Dupuis, M.; Lester, Jr., W. A. *J. Chem. Phys.* **1985**, 82, 1983
c) Bauschlicher, Jr., C. W.; Langhoff, S. R.; Taylor, P. R. *J. Chem. Phys.* **1987**, 87, 387

16 a) Colvin, M. E.; Grev, R. S.; Schaefer, H. F. *Chem. Phys. Lett.* **1983**, 99, 399
b) Rice, J. E.; Handy, N. C. *Chem. Phys. Lett.* **1984**, 107, 365
c) Gordon, M. S. *Chem. Phys. Lett.* **1985**, 114, 348
d) Balasubramanian, K.; McLean, A. D. *J. Chem. Phys.* **1986**, 85, 5117
e) Gordon, M. S.; Gano, D. R.; Binkley, J. S.; Frisch, M. J. *J. Ame. Chem. Soc.*, **1986**, 108, 2191
f) Koseki, S.; Gordon, M. S. *J. Mol. Spectrosc.* **1987**, 123, 392
g) Selmani, A.; Salahub, D. R. *J. Chem. Phys.* **1988**, 89, 1529

17 a) Olbrich, G. *Chem. Phys. Lett.* **1980**, 73, 110
b) Barthelat, J.-C.; Roch, B. S.; Trinquier, G.; Satge, J. *J. Ame. Chem. Soc.* **1980**, 102, 4080
c) Philips, R. A.; Buenker, R. J.; Beardsworth, R.; Bunker, P. R.; Jensen, p.; Kraemer, W. P. *Chem. Phys. Lett.* **1985**, 118, 60
d) Pettersson, L. G. M.; Siegbahn, P. E. M. *Chem. Phys.* **1986**, 105, 355
e) Balasubramanian, K. *J. Chem. Phys.* **1988**, 89, 5731
f) see ref. 16 e).

18 a) Balasubramanian, K. *Chem. Phys. Lett.* **1986**, 127, 585
b) see ref. 17 e).

19 a) see ref. 17 e).
b) Schwerdtfeger, P.; Silberbach, H.; Miehlich, B. *J. Chem. Phys.* **1989**, 90, 762

20 Fjeldberg, T.; Haaland, A.; Schilling, B. E. R.; Lappert, M. F.; Thorne, A. J. *J. Chem. Soc. Dalton Trnas.* **1986**, 1551

21 Ruedenberg, K.; Schmidt, M. W.; Gilbert, M. M.; Elbert, S. T. *Chem. Phys.* **1982**, 71, 41, 51 and 65.

22 a) Schmidt, M. W.; Baldridge, K. K.; Boatz, J. A.; Elbert, S. T.; Gordon, M. S.; Jensen, J. H.; Koseki, S.; Matsunaga, N.; Nguyen, K. A.; Su, S.; Windus, T. L.; Dupuis, M.; Montgomery Jr., J. A. *J. Comput. Chem.* **1993**, 14, 1347
b) contact Mike Schmidt at mike@si.fi.ameslab.gov concerning this program

23 Nakamura, H. *J. Chem. Phys.* **1987**, 87, 4031

24 Dyall, K. G. *J. Chem. Phys.* **1992**, 96 1210

25 a) Sidman, J. W. *J. Chem. Phys.* **1958**, 29, 644
b) Hall, W. R.; Hameka, H. F. *J. Chem. Phys.* **1973**, 58, 226
c) Langhoff, S. R. *J. Chem. Phys.* **1974**, 61, 3881
d) Pitzer, R. M.; Winter, N. W. *J. Phys. Chem.* **1988**, 92, 3061

26 Dubois, I. *Can. J. Phys.* **1968**, 46, 2485

Table 1. Comparison of MCSCF/SBK(d,p) stationary points of XH_2 adiabatic and spin-mixed potential energy surfaces with Dirac-Hartree-Fock (DHF) relativistic calculations[a].

	Adiabatic		Relativistic		Experimental or other theoretical calculations	
XH_2	$^1A_1$	$^3B_1$	$^1A_1$	$^3B_1$	$^1A_1$	$^3B_1$
CH_2						
bond length	1.152	1.116	1.150	1.116	1.11[b],1.11[c]	1.07[b],1.08[c]
bond angle	98.9	129.8	100.1	129.8	102.[b],102.0[c]	134.[b],132.9[c]
SiH_2						
bond length	1.555	1.511	1.555	1.511	1.516[d],1.519[e]	1.484[e]
bond angle	93.4	118.3	93.4	118.3	92.8[d],92.5[e]	118.5[e]
GeH_2						
bond length	1.620	1.559	1.620	1.559	1.600[f],1.587[g] 1.575[h]	1.549[f],1.534[g]
bond angle	92.3	118.9	92.3	118.9	91.8[f],91.5[g] 92.96[h]	118.9[f],119.8[g]
SnH_2						
bond length	1.793	1.730	1.793	1.734	1.785[g],1.759[h]	1.730[g]
bond angle	92.4	118.4	92.4	116.8	91.1[g],92.55[h]	114.9[g]
PbH_2						
bond length	1.885	1.812	1.880	1.827	1.869[g],1.817[h]	1.865[g]
bond angle	90.6	118.6	91.5	115.2	90.5[g],92.29[h]	109.8[g]

[a]Bond lengths are in Å, and bond angles are in degrees.
[b]experimental, see ref. 14a.
[c]MRCI, see ref. 15c.
[d]experimental, see ref. 26.
[e]second-order CI, see ref. 16d.
[f]MRDCI/ECP, see ref. 17d.
[g]spin-orbit CI, see ref. 17e.
[h]Dirac-Hartree-Fock, see ref. 24.

Table 2. Calculated Vibrational Frequencies[a] of XH_2

XH_2	Bending	Symm. Str.	Asymm. Str.
$CH_2(^1A_1)$	1403.2	2766.4	2811.4
$CH_2(^3B_1)$	1139.2	3021.8	3215.6
$SiH_2(^1A_1)$	1005.2	1667.6	1970.9
$SiH_2(^3B_1)$	872.1	2107.5	2167.0
$GeH_2(^1A_1)$	936.5	1822.3	1827.2
$GeH_2(^3B_1)$	819.0	1964.6	2036.4
$SnH_2(^1A_1)$	792.5	1627.3	1627.4
$SnH_2(^3B_1)$	687.1	1747.4	1796.2
$PbH_2(^1A_1)$	721.3	1463.3	1487.7
$PbH_2(^3B_1)$	636.7	1456.8	1606.1

[a]The values are calculated from the (6,6)MCSCF/SBK(d,p) level of theory, and they are in cm^{-1}.

Table 3. Singlet-triplet splittings of adiabatic and relativistic potential energies of XH_2[a]

XH_2	adiabatic $^1A_1$-$^3B_1$	relativistic $^1A_1(A_1)$-$^3B_1(A_1)$
CH_2	10.6	10.6
SiH_2	-16.8	-16.8
GeH_2	-23.9	-24.1
SnH_2	-22.7	-23.7
PbH_2	-33.4	-39.1

[a]The energy of $^1A_1$ state with respect to $^3B_1$ in kcal/mol. A positive value indicates that the triplet is energetically more stable. The geometries of each stationary points are used for adiabatic states. For the relativistic splittings, the geometries are optimized by fitting parabolas to the calculated single point energies.

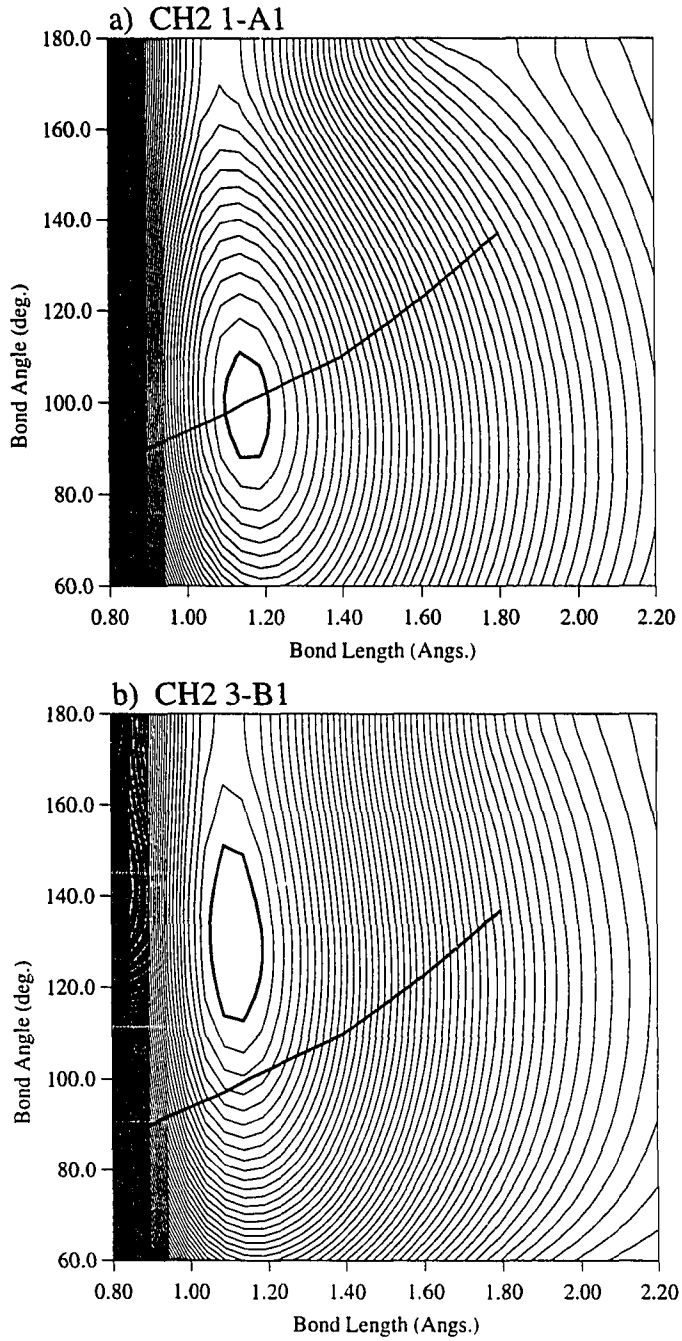

Figure 1. Contour maps of adiabatic potential energy surfaces of CH_2. The plots are C_{2v} potential energy surfaces of a) $^1A_1$ state and b) $^3B_1$ state. Successive contour lines are incremented by 0.005 hartree. The bold contours indicate -6.555 and -6.570 hartree for singlet and triplet states, respectively. The bold lines indicate crossing seams.

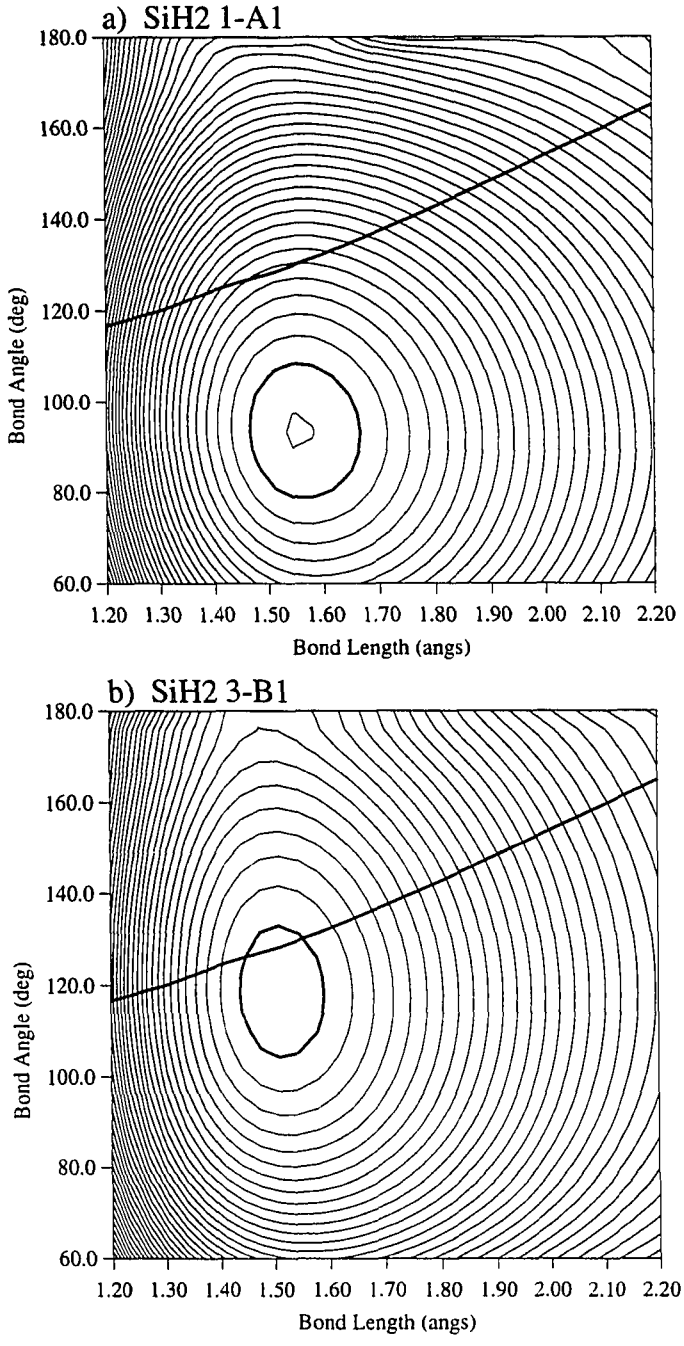

Figure 2. Contour maps of adiabatic potential energy surfaces of SiH_2. The plots are C_{2v} potential energy surfaces of a) $^1A_1$ state and b) $^3B_1$ state. Successive contour lines are incremented by 0.005 hartree. The bold contours indicate -4.880 and -4.855 hartree for singlet and triplet states, respectively. The bold lines indicate crossing seams.

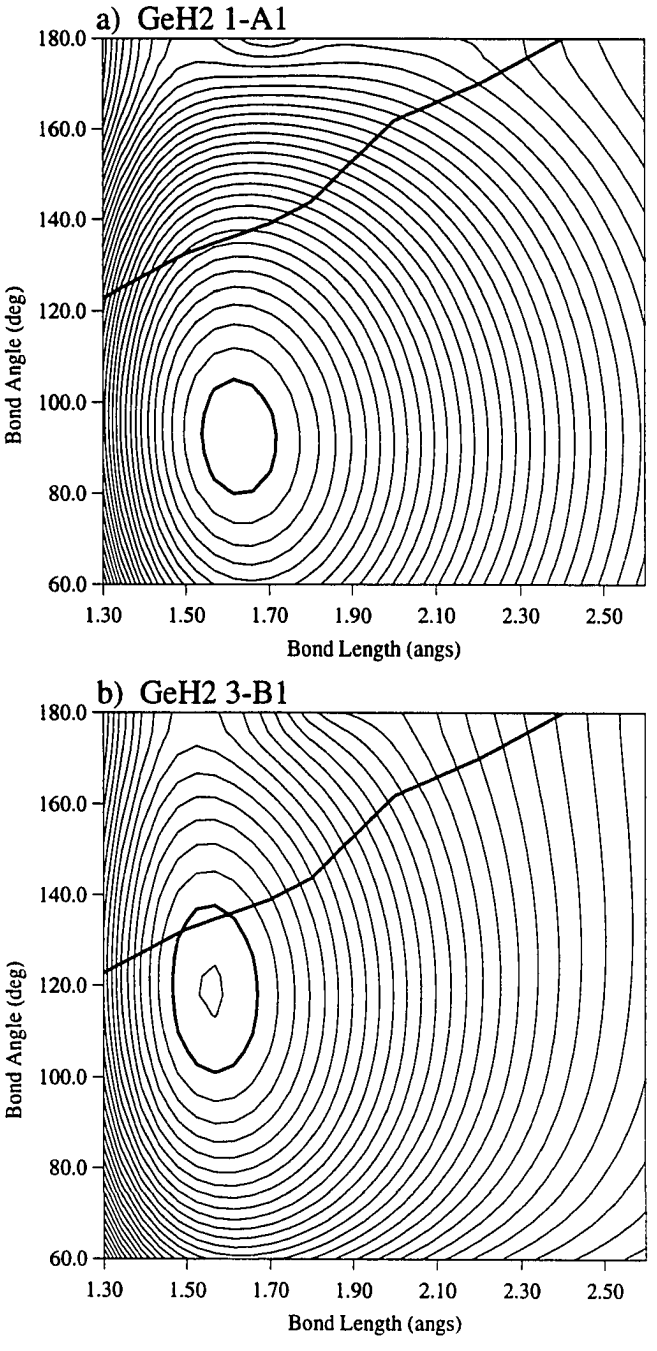

Figure 3. Contour maps of adiabatic potential energy surfaces of GeH_2. The plots are C_{2v} potential energy surfaces of a) $^1A_1$ state and b) $^3B_1$ state. Successive contour lines are incremented by 0.005 hartree. The bold contours indicate -4.855 and -4.815 hartree for singlet and triplet states, respectively. The bold lines indicate crossing seams.

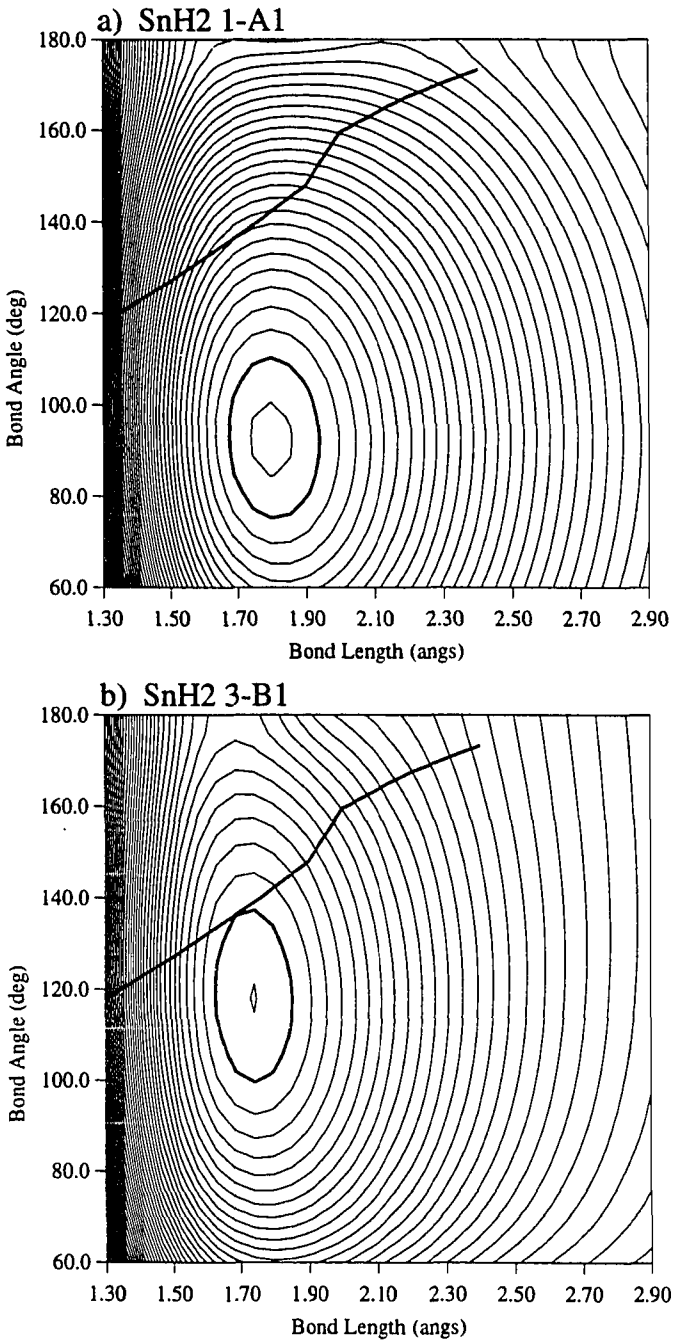

Figure 4. Contour maps of adiabatic potential energy surfaces of SnH_2. The plots are C_{2v} potential energy surfaces of a) $^1A_1$ state and b) $^3B_1$ state. Successive contour lines are incremented by 0.005 hartree. The bold contours indicate -4.445 and -4.410 hartree for singlet and triplet states, respectively. The bold lines indicate crossing seams.

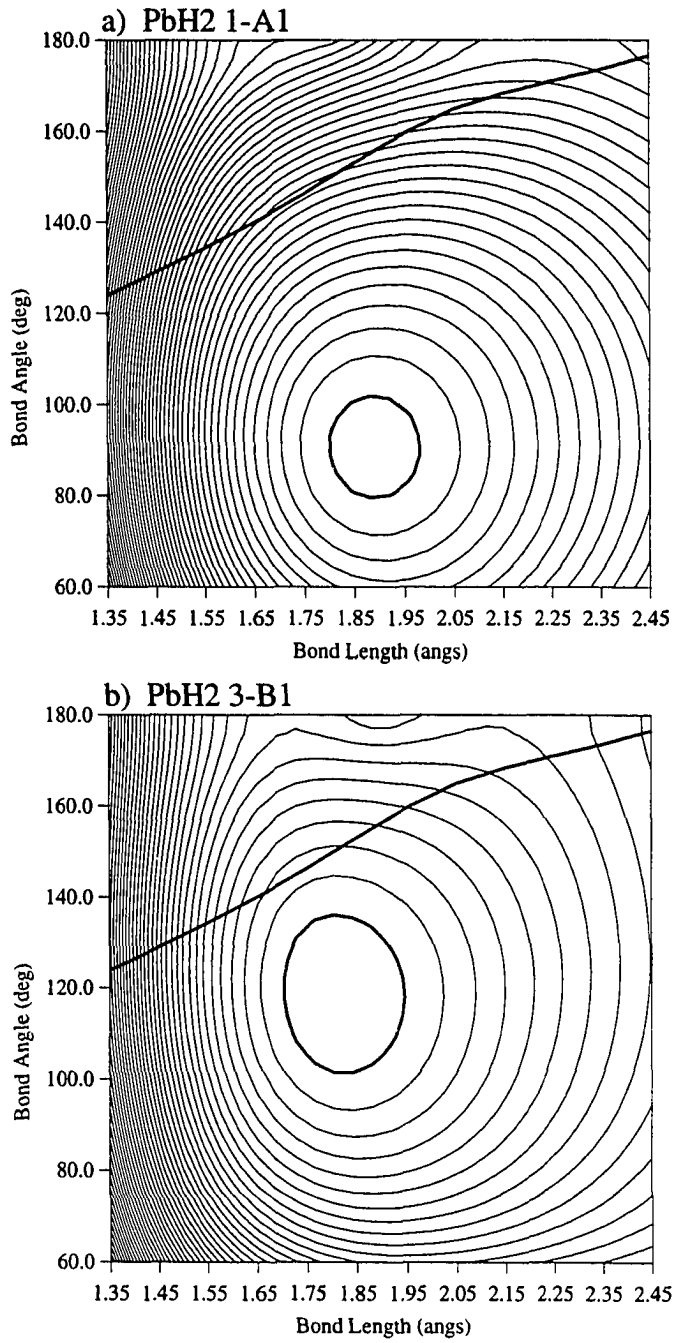

Figure 5. Contour maps of adiabatic potential energy surfaces of PbH_2. The plots are C_{2v} potential energy surfaces of a) $^1A_1$ state and b) $^3B_1$ state. Successive contour lines are incremented by 0.005 hartree. The bold contours indicate -4.520 and -4.465 hartree for singlet and triplet states, respectively. The bold lines indicate crossing seams.

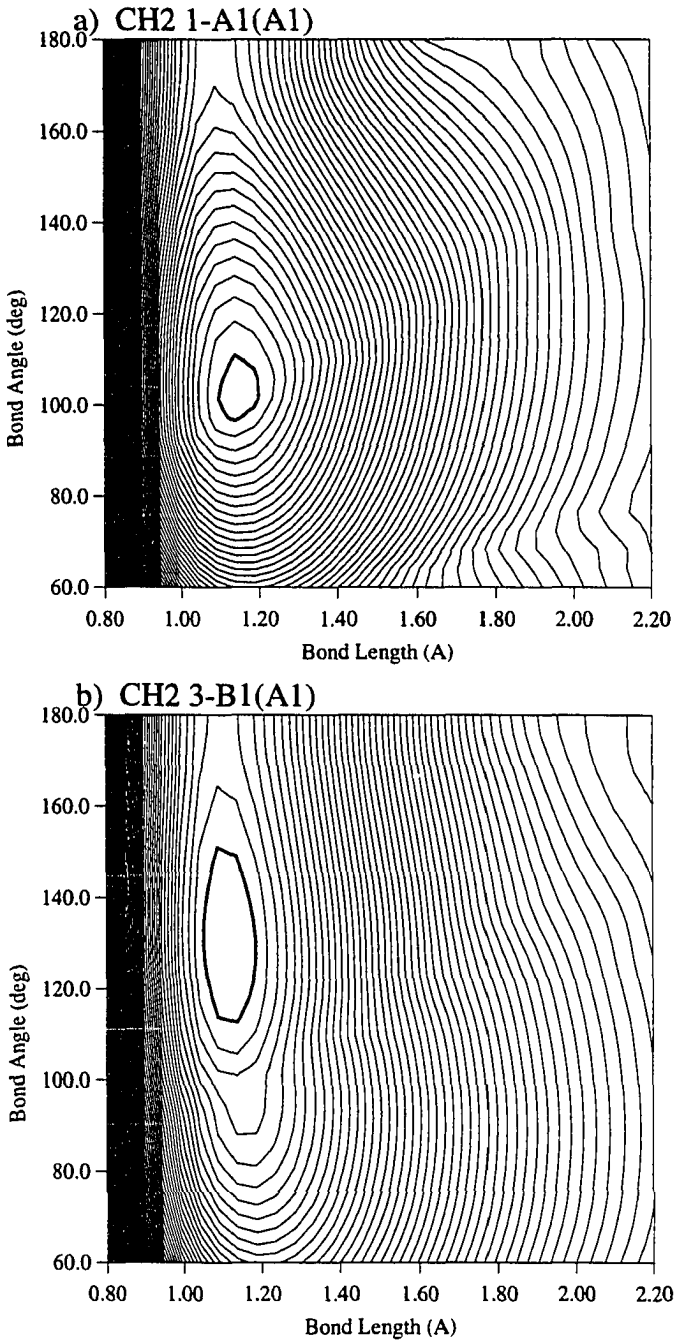

Figure 6. Contour maps of relativistic potential energy surfaces of CH_2. The plots are C_{2v} potential energy surfaces of a) $^1A_1(A_1)$ state and b) $^3B_1(A_1)$ state. Successive contour lines are incremented by 0.005 hartree. The bold contours indicate -6.555 and -6.570 hartree for singlet and triplet states, respectively.

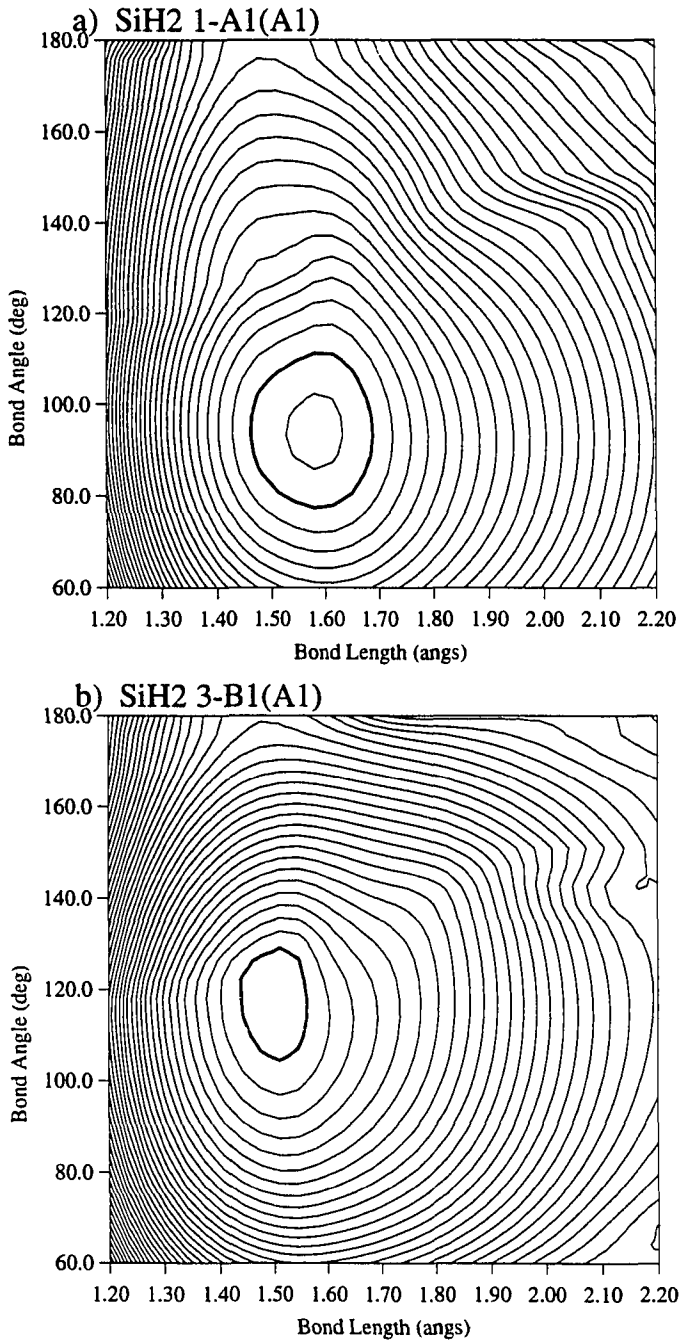

Figure 7. Contour maps of relativistic potential energy surfaces of SiH_2.
The plots are C_{2v} potential energy surfaces of a) $^1A_1(A_1)$ state and b) $^3B_1(A_1)$ state. Successive contour lines are incremented by 0.005 hartree. The bold contours indicate -4.880 and -4.855 hartree for singlet and triplet states, respectively.

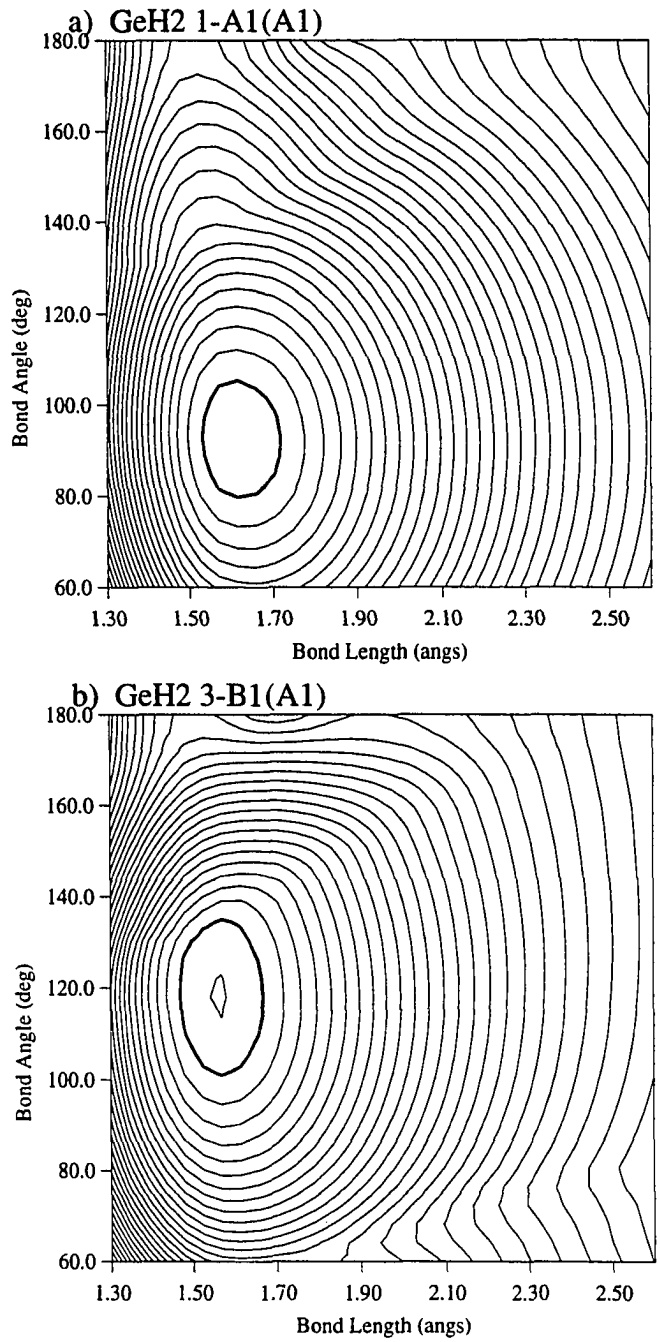

Figure 8. Contour maps of relativistic potential energy surfaces of GeH_2.
The plots are C_{2v} potential energy surfaces of a) $^1A_1(A_1)$ state and b) $^3B_1(A_1)$ state. Successive contour lines are incremented by 0.005 hartree. The bold contours indicate -4.855 and -4.815 hartree for singlet and triplet states, respectively.

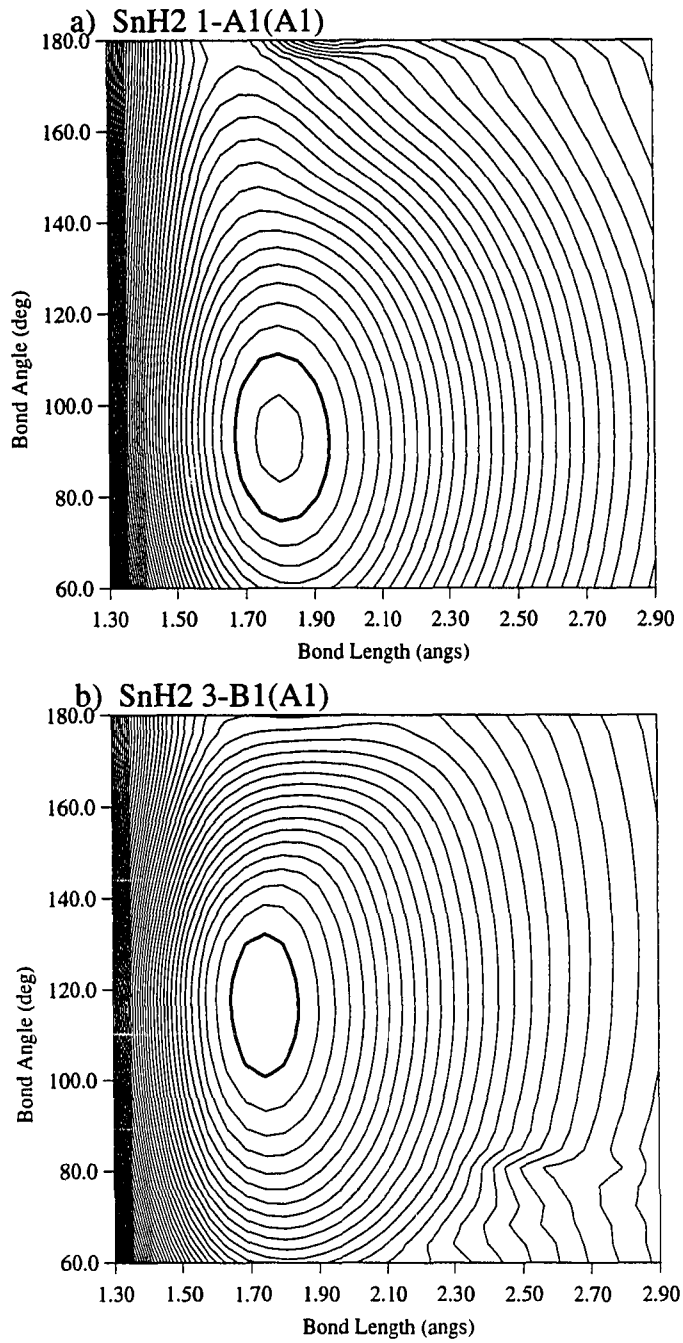

Figure 9. Contour maps of relativistic potential energy surfaces of SnH_2.
The plots are C_{2v} potential energy surfaces of a) $^1A_1(A_1)$ state and b) $^3B_1(A_1)$ state. Successive contour lines are incremented by 0.005 hartree. The bold contours indicate -4.445 and -4.410 hartree for singlet and triplet states, respectively.

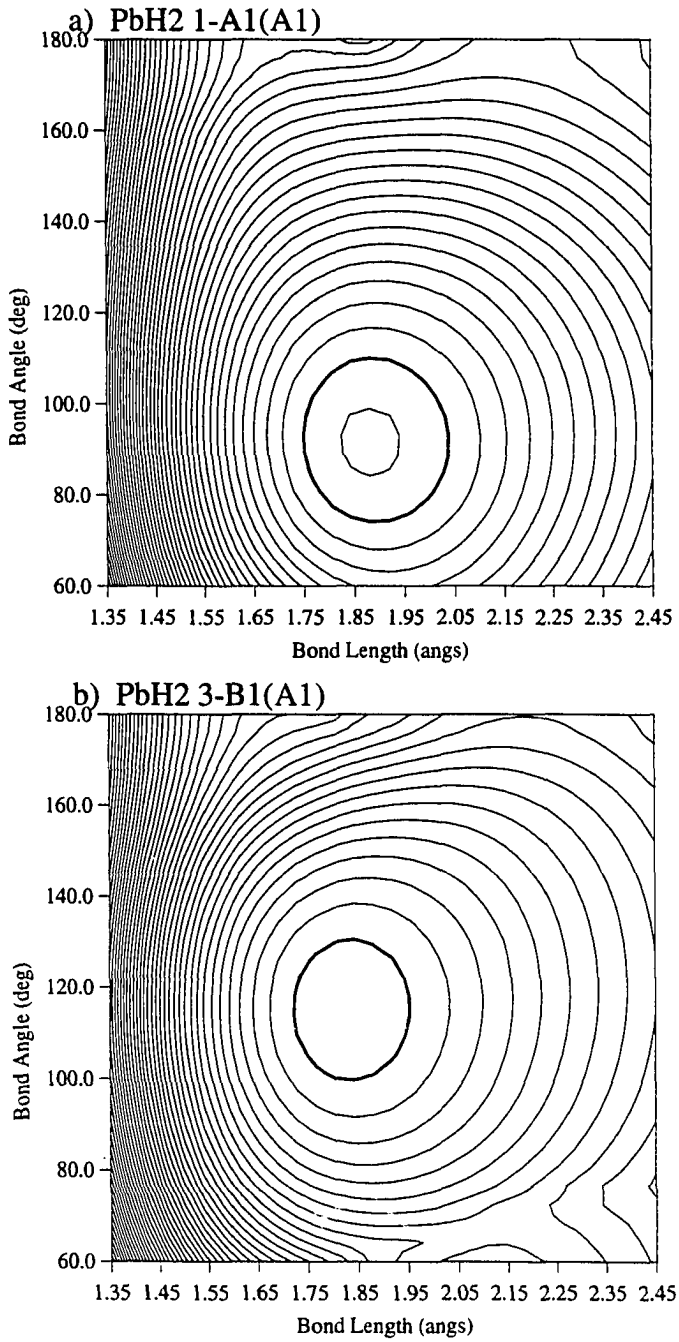

Figure 10. Contour maps of relativistic potential energy surfaces of PbH_2. The plots are C_{2v} potential energy surfaces of a) $^1A_1(A_1)$ state and b) $^3B_1(A_1)$ state. Successive contour lines are incremented by 0.005 hartree. The bold contours indicate -4.520 and -4.460 hartree for singlet and triplet states, respectively.

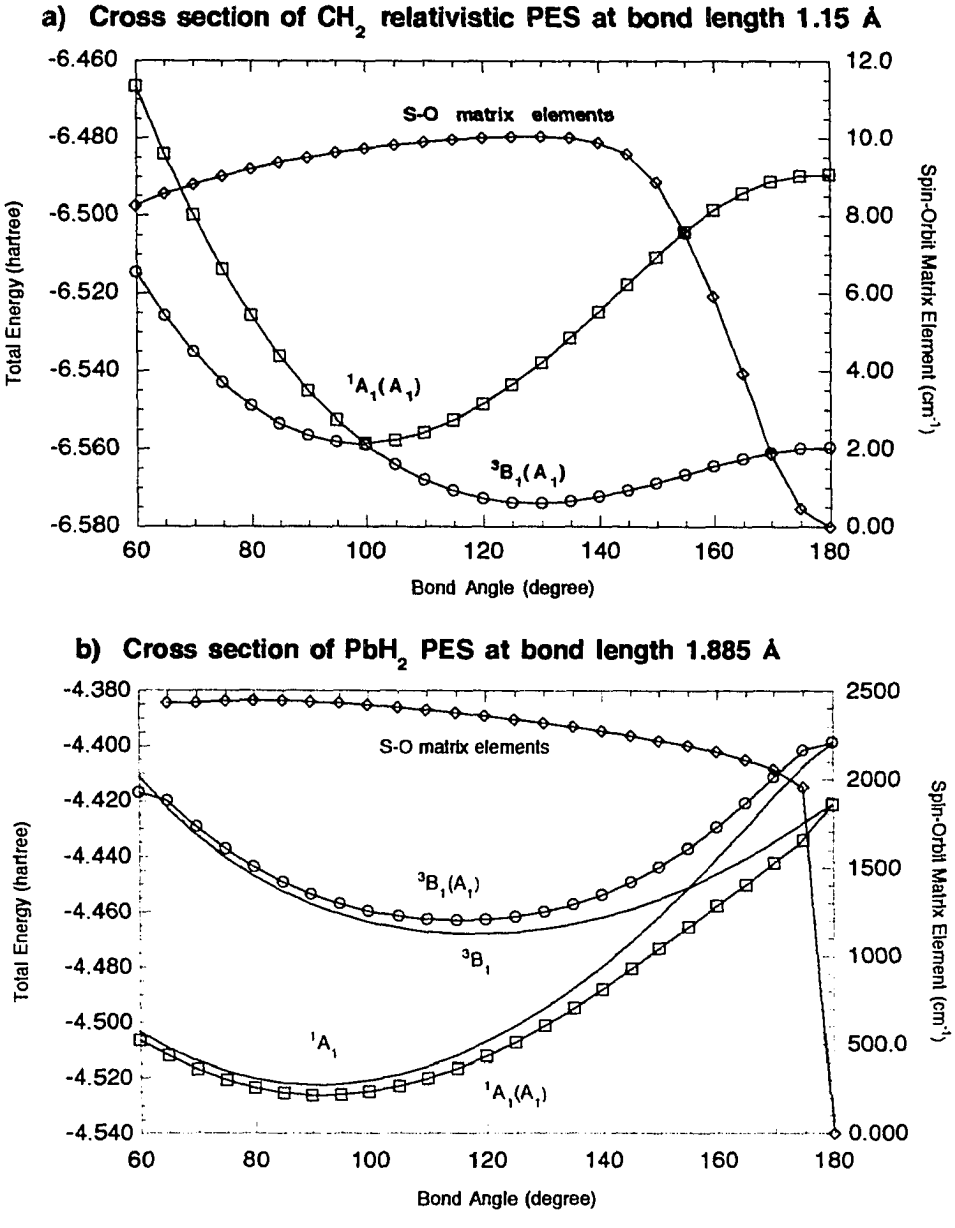

Figure 11. Cross sectional view of PES of CH_2 and PbH_2. The cross section of a) relativistic PES of CH_2 at the bond length 1.15 Å is plotted. Also the spin-orbit coupling matrix elements are shown. b) PbH_2 PES (bond length 1.885 Å), in which both the adiabatic and relativistic curves, as well as the matrix elements are shown. Note the difference in the scale on the right vertical axis.

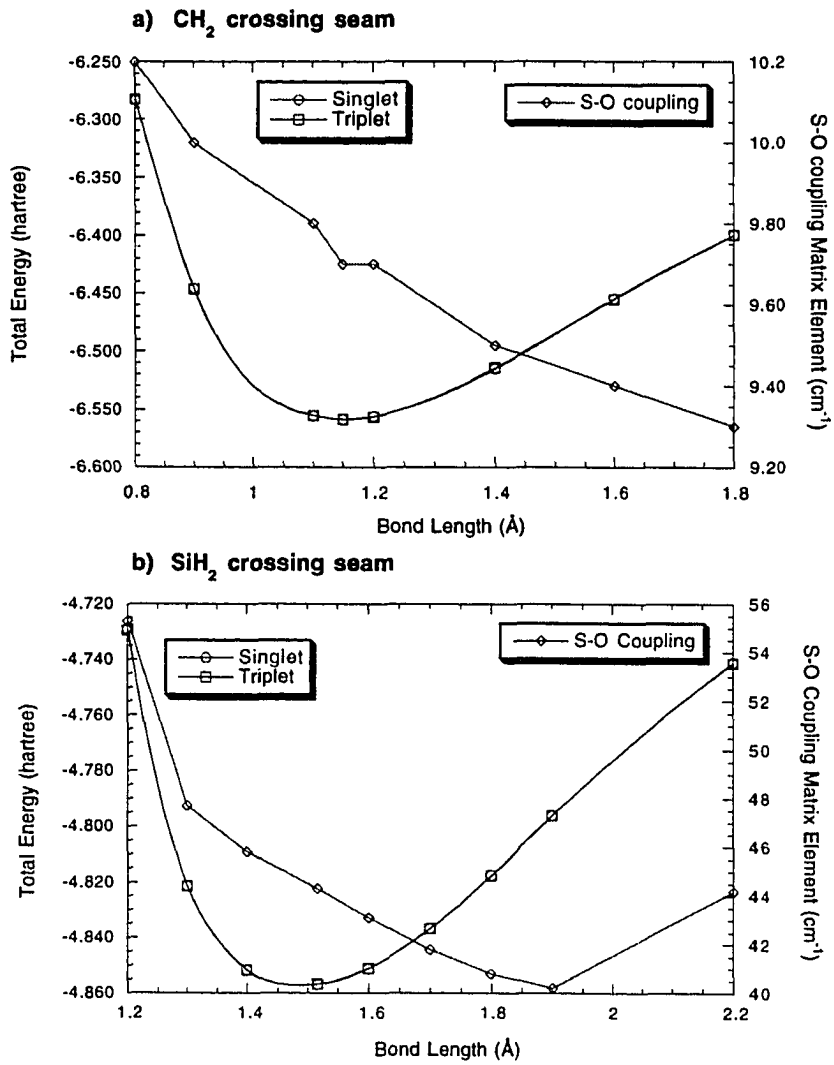

Figure 12. Energies and spin-orbit coupling matrix elements at crossing seam. Energetics (in hartree) and spin-orbit matrix elements (cm^{-1}) of XH_2 species at crossing seam are plotted against bond lengths. a) CH_2, b) SiH_2, c) GeH_2, d) SnH_2 and e) PbH_2

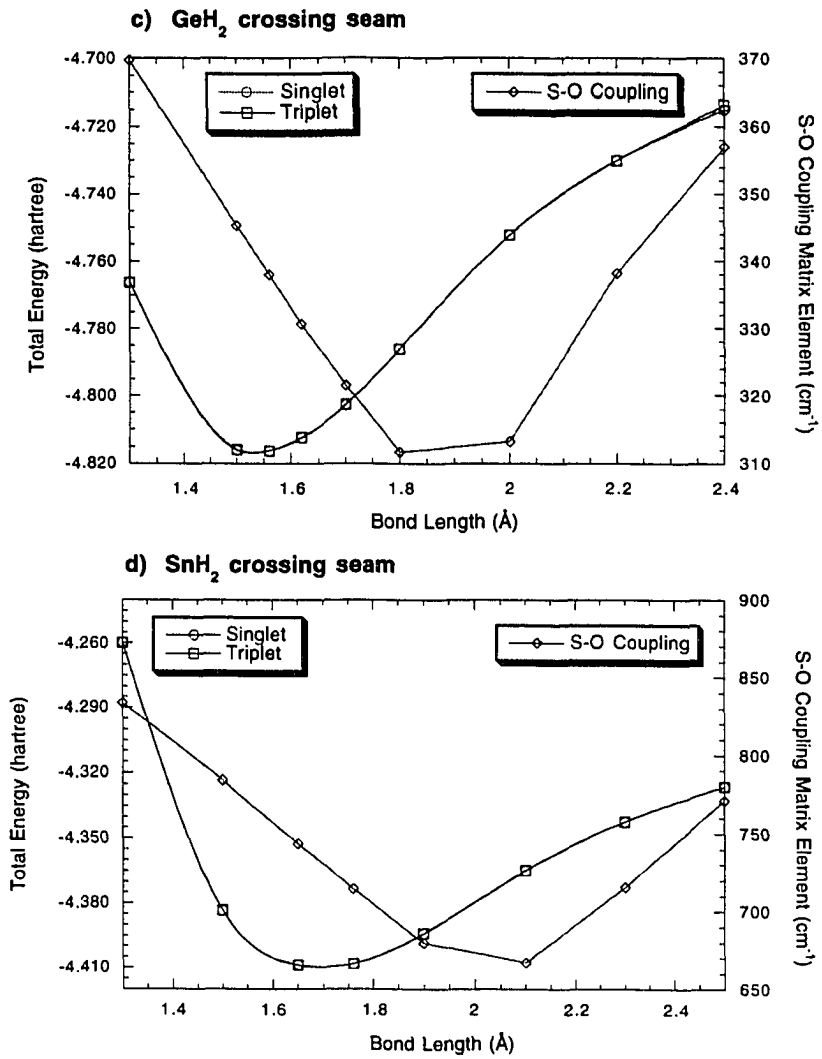

Figure 12. continued.

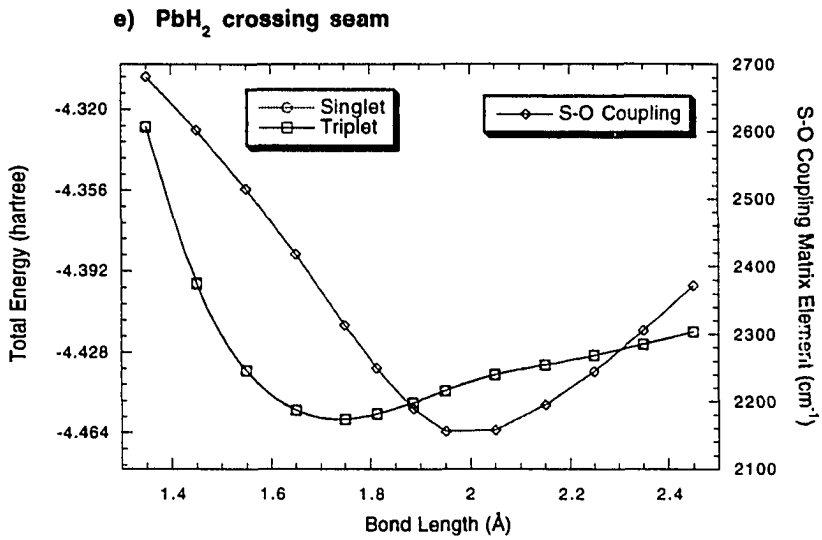

Figure 12. continued.

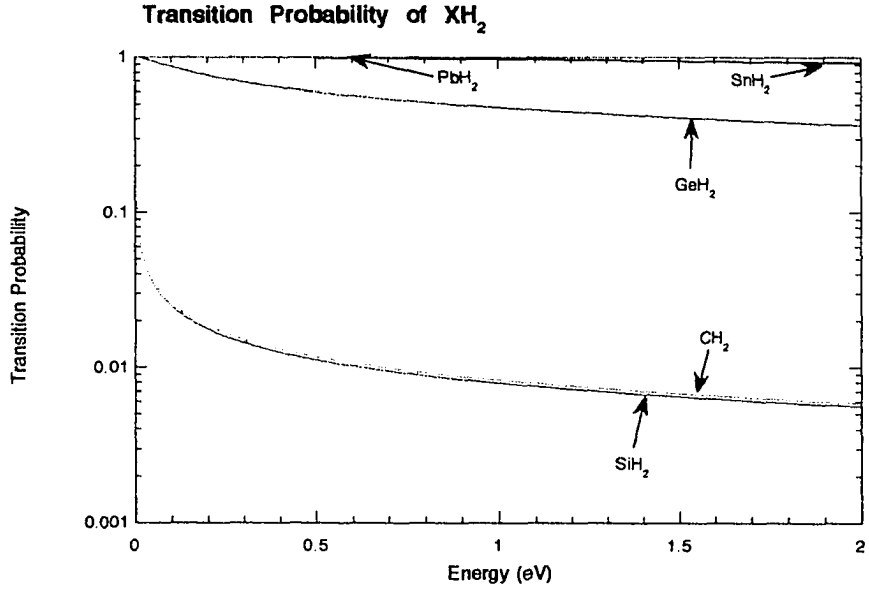

Figure 13. Transition probability of XH_2. Transition probability is calculated at the minimum energy crossing point of the C_{2v} potential energy surfaces using the Landau-Zener model.

CHAPTER 5. ONGOING AND FUTURE WORK: POTENTIAL ENERGY SURFACES OF HIGH ENERGY B-N PRISMANE

Introduction

Our previous calculations[1] have shown that the B-N analog of prismane is a high energy minimum on the $B_3N_3H_6$ potential energy surface (PES). The relative energy of the B-N prismane with respect to planar borazine, including zero-point energy correction, is 163 kcal/mol using second-order perturbation theory (MP2)[2] and the 6-311G(d,p)[3] basis set. Such a high energy species may therefore be considered as a potential high energy density material (HEDM)[4].

Figure 1 summarizes the characteristics and requirements for HEDM. A HEDM is characterized as a metastable minimum on its potential energy surface, connected by means of a minimum energy path through a transition state to a more stable minimum. These two minima should be separated by a large energy gap (ΔH is large) so that a large energy release can be achieved upon chemical transformation. A HEDM should also be kinetically stable: The PES surrounding the metastable minimum should have a high barrier, so that the molecule is stable enough to be synthesized and also to be stored. Third, the molecular weight of a typical HEDM candidate is small. One performance measure is obtained through the specific impulse[5] (I_{sp}), which is inversely proportional to the square root of the molecular weight, and directly proportional to the energy release achieved by the chemical transformation. The last critical requirement is that no crossing of states should occur that could lead to non-adiabatic transformations, for example vibronic coupling, and relativistic spin-orbit coupling to undesired products.

One way to consider a reaction between the B-N prismane and borazine is a symmetry-forbidden isomerization reaction (**Scheme 1**).

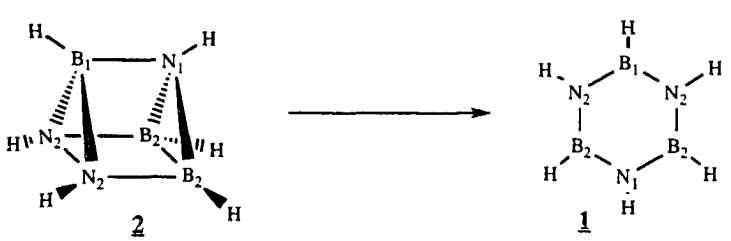

Scheme 1

This isomerization reaction is expected to have a large energy barrier, based on symmetry conservation rules[6]. In the case of all-carbon prismane, Palmer *et al.*[7] suggested that there might not be any transition state directly connecting prismane to benzene due to the expected high energy barrier. Much of the synthetic work in prismane has been done using photochemical processes[8], which supports the implication of Palmer *et al.* However, B-N prismane possesses only C_s symmetry, instead of D_{3h} as in all-carbon prismane. Therefore, it is possible that the B-N prismane could isomerize to borazine more readily than the all-carbon prismane does.

Here we present preliminary results for the potential energy surfaces of B-N prismane and related molecules, in an attempt to aid synthetic efforts and to search possible decomposition/isomerization paths.

Computational Approach

The geometries were optimized with the restricted Hartree-Fock (RHF) method using the GAMESS[9] quantum chemistry program. The basis sets used here include the Stevens-Basch-Krauss-Jasien (SBKJ) effective core potentials (ECP) and basis sets[10] augumented withe the d-polarization functions[11] for all heavy atoms and the -31G basis[12] for hydrogen. The 6-31G(d,p) basis[12] is also used to obtain geometries and energetics; all heavy atoms in are augumeneted with d-polarization functions[11] and a set of p-polarization functions is added to the hydrogens[11].

Stationary points are verified as transition states or minima by diagonalizing an energy second-derivative matrix (hessian) to obtain harmonic vibrational frequencies. A minimum on the PES possesses all real vibrational frequencies, and a transition state has one and only one imaginary vibrational frequency; the remaining frequencies are all real. Second-order Møller-Plesset perturbation theory[2] (MP2) was used for refining the energetics.

The intrinsic reaction coordinate[13] (IRC: minimum energy path connecting a transition state with reactants and products) was followed by using the second-order Gonzalez-Schlegel method[14] with a 0.3 $amu^{-1/2}$bohr step size from each transition state.

In addition, a muliticonfigurational self-consistent field (MCSCF) wave function[15] was utilized in a search for a transition state that connects prismane and borazine. The STO-3G[16] basis set was used for the MCSCF calculation. The prismane active space consists of the three bonding and anti-bonding orbitals (corresponding to B_1-N_1, N_2-N_2 and

B_2-B_2 bonding and anti-bonding orbitals), constructed from the localized orbitals prescribed by Boys[17]. The six orbitals of the B-N prismane correspond to the six Π orbitals of borazine. This 6 electron-6 orbital active space generates 175 configuration state functions (CSF).

Bonding was analyzed with the total density analysis[18]. A bond critical point exists between two atoms if there is a "saddle point" in the electron density between the two atoms. At such a point the gradient of the electron density is zero, and the hessian of the electron density has one positive eigenvalue along the bond axis. The existence of a bond critical point implies the existence of a bond path (path of maximum electron density passing through the bond critical point), and the two atoms are said to be bonded. The hessian of the electron density at a ring critical point has two positive and one negative eigenvalues, with the density at the ring critical point being smaller than that of all the surrounding bond critical points.

Results and Discussion

Structures and Energetics The geometries of the B-N prismane and the related B-N structures along with the energies of each structure relative to the B-N prismane are shown in Figure 2. The normal modes corresponding to the negative eigenvalue (imaginary frequency) of the energy hessian for transition states are also shown in Figure 2. Some of the species could be considered as synthetic targets. For such molecules the vibrational frequencies and infrared intensities (provided only for the RHF/SBKJ(d) level of theory) are also included in the figure.

Borazine **1** is a highly symmetric molecule, possessing D_{3h} symmetry, and there is substantial delocalization of π electrons which can stabilize the structure[19]. Consequently, borazine **1** is 163 kcal/mol below B-N prismane at the MP2/6-311G(d,p) level of theory[1], and borazine is suspected to be the global minimum on the $B_3N_3H_6$ PES.

As can be seen from Figure 1, the effect of electron correlation on the relative energy is large. The relative energy obtained for borazine with the MP2/6-311G(d,p) level of theory is in good agreement with the MP2/SBK(d) results calculated for the $B_3N_3H_6$ PES in this work. Therefore, henceforth the MP2/SBK(d) energetics are considered without specifying the level of theory used in this section, unless otherwise stated.

The bond lengths of B-N bonds in prismane **2** are substantially longer than those of

borazine **1**. All the rectangular faces of the B-N prismane have up to about 5° deviations from the ideal angle of 90°. The two triangular faces deviate less than 4° from the ideal angle, 60°, found in all-carbon prismane.

Isomer **3** is a planar six-membered ring having a different nuclear arrangement from borazine; in addition to B-N bonds there are N-N and B-B bonds. This species is 66 kcal/mol more stable than the B-N prismane. It still lies about 100 kcal/mol above borazine, and therefore it can still be considered as a high-energy species.

Isomer **4** is closely related to the B-N prismane, by breaking the B_2-N_2 bond and stretching the B_1-N_1 bond to obtain **4**. **4** is 22 kcal/mol above the prismane structure, however, a transition state connecting **4** and **2** has not yet been found.

A transition state **5** lies about 10 kcal/mol above **4**,. This transition state is connected to **4** in one direction and is connected to structure **3** in the other direction according to the IRC calculated at the RHF/SBKJ(d) level of theory..

Structure **6** is a transition state in which both forward and reverse reaction paths lead to **3**. This isomerization reaction proceeds by the out-of-plane nitrogen inserting itself to either one of the nearest neighboring B-N bonds. This is a high-energy transition state, with a barrier height of over 90 kcal/mol.

Structure **7** is a minimum which connects with structure **3** through transition state **8**. Although structure **8** is isoenergetic with structure **7** at the RHF/SBKJ(d) level of theory, inclusion of electron correlation through MP2 preferentially lowers the minimum by few kcal/mol.

None of the species mentioned above appear to be directly connected to B-N prismane in an obvious manner. The only transition state found to date that is connected to the prismane structure **2** is the transition state **9**. The barrier height with respect to **2** is 45 kcal/mol. This transition state is characterized by elongated B_1-N_1 and two B_2-N_2 bonds; they are stretched 33 and 55%, respectively, from their values in equilibrium B-N prismane.

The other minimum associated with transition state **9** contains two three-membered ring species **10a** (*cyclic*-aminodiborane) and **10b** (*cyclic*-boradiimine). They are 30 kcal/mol above B-N prismane. Therefore, if one could obtain **10a** and **10b**, the barrier to overcome in order to obtain **2** is relatively small. Thus far, optimization with MP2/6-31G(d,p), using Gaussian 92[20], fails to locate the transition state **9**.

Another transition state that leads to **10a** and **10b** is structure **11**, which looks like a

B-N prismane with the B_1-N_1 bond elongated. However, the reverse reaction path leads to a planar five-membered $B_2N_3H_5$ ring + B-H, which sits on top of the ring (**12**). Transition state **11** is about 13 kcal/mol above **10a** + **10b**, and 65 kcal/mol above **12**. Structure **12** is a transition state. A minimum associated with **12** has not yet been identified.

Figure 2 summarizes the PES of B-N prismane obtained with the RHF/SBK(d) and MP2/SBKJ(d) level of theory (the values in parentheses). Thus far, there is no direct path that leads to borazine **1** from B-N prismane **2**.

Aside from the RHF wave functions, generalized valence bond (GVB)[21] and MCSCF wave functions have also been utilized. The Dewar-benzene analog of borazine is found at the MCSCF(6,6)/STO-3G level of theory, even though the RHF/SBKJ(d) failed to locate the structure. A transition state connecting the Dewar-benzene analog to B-N prismane is also found at the MCSCF(6,6)/STO-3G level. However, when the basis set is improved to 3-21G(d,p), these stationary points disappear. Presumably, both stationary points are artifacts of the minimal basis set.

Currently the MCSCF(6,6)/3-21G(d,p) wavefunction is being utilized to search for the transition state that leads from prismane to borazine.

Bonding in B-N prismane The bond critical points[18] found for the bonds B_1-N_2 and N_1-B_2 (of **Scheme 1**) are located inside the ring. The bond critical points of the N_1-B_2 bond can be found close to the ring critical point associated with the ring N_1-B_2-B_2. This can be interpreted to mean that the ring has small ring strain. One could think of N_1-B_2 as a "T-shaped" bond, although the total electron density contour map shows two distinct bond paths. On the other hand, the all-carbon prismane possesses bond critical points associated with the triangular face, located outside the ring. This suggests that the bonds are strained.

Figure 3 shows the electron density of B-N bonds in the B-N prismane at the bond critical points. As can be seen, the B_1-N_1 bond has the highest electron density among the B-N bonds, and the B_2-N_2 bond has the lowest value. If one correlates the value of electron density with the strength of the bond, then the bond B_1-N_1 is stronger than the B_2-N_2 bond.

Substituent Effects It is certainly important to identify the effect of substituents on the energetics of these species. The effect of substituents are studied by replacing one of hydrogens on either B_1 or N_1 with -Cl, -CH_3 or -SiH_3 groups. Thus far, the studied species are B-N prismane and borazine. Figure 4 shows the relative energies of substituted

prismanes with respect to corresponding benzene structures. It is apparent from the figure that there is no large substituent effect . Except for the -Cl group on B_1, all substitutions stabilize prismane, relative to borazine. Substitution on N_1 always stabilizes the prismane.

Further study

It has been implied by Palmer *et al.*[7] that there is no direct path which connects all-carbon prismane to benzene. They have shown, however, that the isomerization reaction of Dewar-benzene to benzene can proceed via non-adiabatic paths. The isomerization reaction undergoes a series of cascading reactions through several singlet excited states connected by conical intersections. Such reaction paths might be also important for the B-N prismane.

As a future study, we will be looking at non-adiabatic paths that could lead to isomerization of B-N prismane to borazine. Another important aspect that we should investigate is to search for decomposition/isomerization paths via triplet states.

It is also important to study the effect of substituents. We have presented preliminary results above showing the effect on B-N prismane and borazine. The substituents are placed only on either B_1 or N_1, and we would like to extend the study to substituting to other sites. Also we would like to determine the effect of substituents on the barrier height. This should help our understanding about the PES of $B_3N_3H_6$.

Conclusions

We have presented preliminary results on the PES of B-N prismane and related species. Thus far, there is no direct connection between B-N prismane and borazine. However, there is a path that leads to B-N prismane by addition of *cyclic*-aminodiborane and *cyclic*-boradiimine (**10a** and **10b**) at the RHF/SBK(d) level of theory.

Bonding in B-N prismane shows that the weakest bond among the B-N bonds are B_2-N_2 bonds, while the B_1-N_1 bond appears to be the strongest. Therefore the reaction path that leads directly to borazine in Scheme 1 may not be likely to occur.

The preliminary study on substituent effects show that the substituents do not affect the relative energies of prismanes and borazines. Further study, especially by substitutions at other sites will be of interest. Also, substituent effects on the barrier heights are certainly of interest.

Acknowledgements

This research is supported in part by the Air Force Office of Scientific Research (F49620-95-1-0077) and the National Science Foundation (CHE-93-13717). The generous computer time allocated for use of Cray YMP C90 by Waterways Experimental Station, Army Corps of Engineers at Vicksburg, Missouri, is also acknowledged.

References

1 Matsunaga, N.; Gordon, M. S. *J. Ame. Chem. Soc.* **1994**, 116, 11407

2 a) Møller, C.; Plesset, M. S. *Phys. Rev.* **1934**, 46, 618
b) Binkley, J. S.; Pople, J. A. *Int. J. Quantum Chem.* **1975**, 9, 229
c) Bartlett, R. J. *Ann. Rev. Phys. Chem.* **1981**, 32, 359

3 Krishnan, R.; Binkley, J.S.;Seeger, R.;Pople, J.A. *J. Chem. Phys.* **1980**, 72, 650

4 Proceeding of the High Energy Density Material Contractors Meeting at Crystal Bay, NV. Air Force Office of Scientific Research, 1994.

5 a) Sutton, G. P. "Rocket Propulsion Elements", Sixth Ed., John Wiley & Sons Inc., NY, 1992
b) Glassman; Sawyer "The Performance of Chemical Propellants", Technivision Services, Slough, England, 1970

6 Woodward, R. B.; Hoffmann R. *The Conservation of Orbital Symmetry*, Verlag Chemie GmbH, Weinheim/Bergstr, 1970

7 I. J. Palmer, I. N. Ragazos, F. Bernardi, M. Olivucci, M. A. Robb *J. Amer. Chem. Soc.* **115** (1993) 673.

8 Wilzbach, K. E.; Kaplan, L. *J. Ame. Chem. Soc.* **1965**, 87, 4004

9 Schmidt, M. W.; Baldridge, K. K.; Boatz J. A.; Elbert S. T.; Gordon, M. S.; Jensen, J. H.; Koseki, S.; Matsunaga, N.; Nguyen, K. A.; Su, S.; Windus, T. L.; Dupuis, M.; Montgomery, J. A. *J. Comput. Chem.* **1993**, 14, 1347

10 Stevens, W. J.; Basch, H.; Krauss, M.*J. Chem. Phys.* **81** (1984) 6026

11 We have used B=0.6, N=0.8 and H=1.1.

12 Ditchfield, R.; Hehre, W. J.; Pople, J. A. *J. Chem. Phys.* **54** (1971) 724

13 Minimum energy paths connecting reactants with products through transition states. Definition can be found in: Fukui, K. *J. Phys. Chem.*. **1970**, 74, 4161; see also Fukui, K. *Acc. Chem. Res.* **1971**, 14, 368

14 a) Gonzales, C.; Schlegel, H. B. *J.Phys.Chem.* **1990**, 94, 5523
b) Gonzales, C.; Schlegel, H. B. *J.Chem.Phys.* **1991**, 95, 5853

15 Ruedenberg, K.; Schmidt, M. W.; Gilbert, M. M.; Elbert, S. T. *Chem. Phys.* **1982**, 71, 41, 51 and 65.

16 Hehre, W. J.; Stewart, R. F.; Pople, J. A. *J. Chem. Phys.* **51** (1969) 2657

17 Boys, S. F. in Quantum Science of Atoms, Molecules, and Solids; Lowdin, P. O., Ed.; Academic Press, New York, 1966; p 253.

18 Bader, R. F. W. Atoms in Molecules–A Quantum Theory, University of Oxford, Oxford, 1990

19 Matsunaga, N.; Cundari, T. R.; Schmidt, M. W.; Gordon, M. S. *Theor. Chemica Acta*, **1992**, 83, 57

20 Frisch, M. J.; Trucks, G. W.; Head-Gordon, M.; Gill, P. M. W.; Wong, M. W.; Foresman, J. B.; Johnson, B. G.; Schlegel, H. B.; Robb, M. A.; Gonzalez, C.; Martin, R. L.; Fox, D. J.; Defrees, D. J.; Baker, J.; Stewart, J. J. P.; Pople, J. A.; GAUSSIAN 92, Gausian, Inc. Pittsburgh, PA, 1992

21 Bobrowicz, F. W.; Goddard, W.A. in Modern Theoretical Chemistry, Vol 3, Schaefer III, H.F. Ed., Chapter 4.

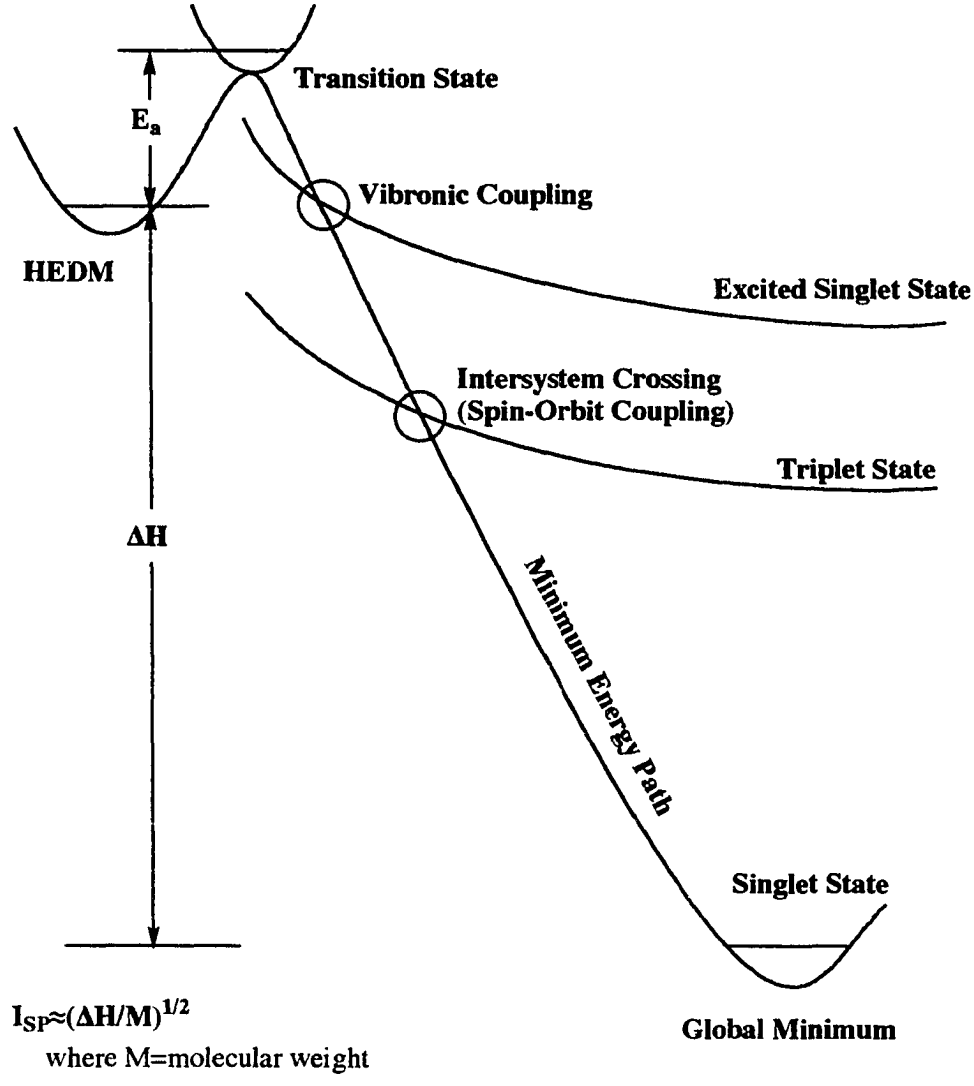

Figure 1. Characteristics and requirements of high energy density material (HEDM).

1

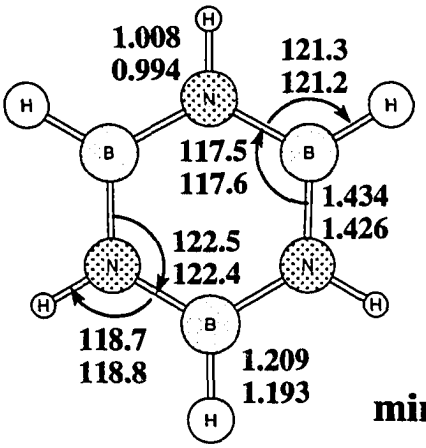

minimum

Relative Energies:

RHF/SBKJ(d)	**-185.0 kcal/mol**
MP2/SBKJ(d)	**-161.2**
RHF/6-31G(d,p)//RHF/6-31G(d,p)	**-186.0**

Vibrational Frequencies:

RHF/6-31G(d,p) vibrational frequencies (in cm^{-1})

295.8	295.8	407.3	555.1	555.1
737.0	737.0	761.8	912.1	991.9
991.9	1003.3	1004.9	1004.9	1022.7
1125.1	1142.8	1142.8	1300.3	1424.8
1495.5	1495.5	1590.6	1590.6	2708.5
2708.5	2722.0	3881.6	3883.1	3883.1

RHF/SBKJ(d) vibrational frequecies(in cm^{-1}) and intensities (in km/mol)

293.9(0.0)	293.9(0.0)	395.2(55.1)	543.0(0.1)	543.0(0.1)
714.5(0.0)	714.5(0.0)	752.8(98.9)	900.2(0.0)	975.3(0.3)
975.3(0.3)	986.2(0.0)	994.9(0.0)	994.9(0.0)	998.7(296.8)
1095.8(0.0)	1118.5(1.5)	1118.5(1.5)	1288.9(0.0)	1381.6(0.0)
1461.0(58.9)	1461.0(58.9)	1564.8(760.8)	1564.8(760.8)	2716.7(499.2)
2716.7(499.2)	2738.3(0.0)	3792.8(0.0)	3794.7(54.5)	3794.7(54.4)

Figure 2. Structure and energetics of B-N prismane and related molecules.
The relative energies with respect to B-N prismane are calculated at the geometries obtained by the RHF/SBKJ(d) level, unless otherwise stated by double-slash notation; A//B means that the energy is calculated at A level of theory at the geometry obtained by B level. Where appropriate as synthetic target, vibrational frequencies are also presented.

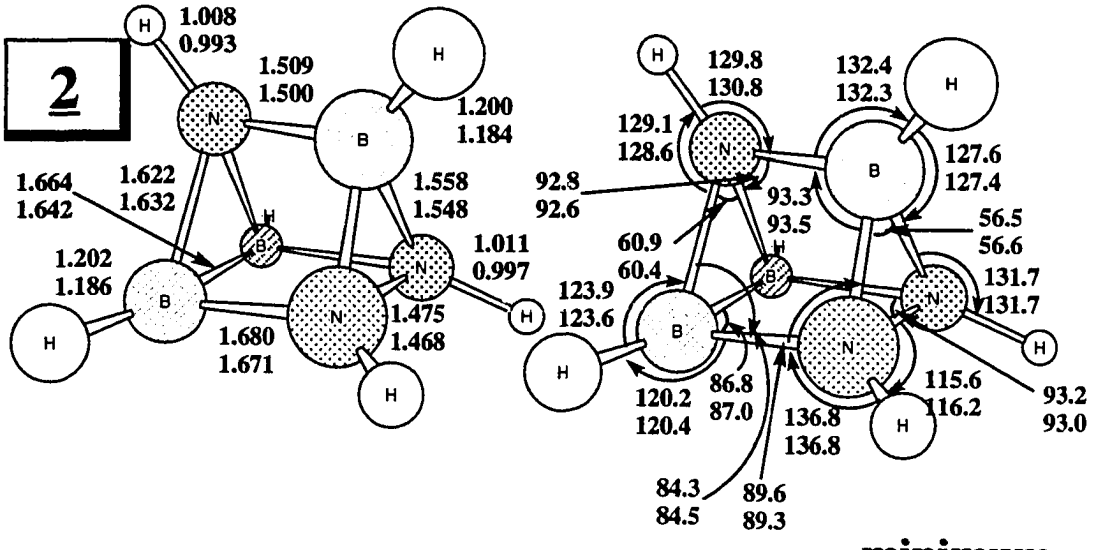

Relative Energies:

RHF/SBKJ(d)	**0.0 kcal/mol**
MP2/SBKJ(d)	**0.0**
RHF/6-31G(d)//RHF/6-31G(d,p)	**0.0**

Vibrational Frequencies:

RHF/6-31G(d,p) vibrational frequencies (in cm^{-1})

383.4	478.6	522.8	560.6	628.2
665.5	678.1	690.1	796.9	834.4
892.9	907.3	936.9	950.7	981.2
1024.1	1029.1	1040.1	1125.9	1169.6
1237.7	1250.2	1306.8	1451.8	2736.3
2758.0	2774.9	3858.6	3869.9	3888.3

RHF/SBKJ(d) vibrational frequencies (in cm^{-1}) and intensities (in km/mol)

370.8(1.6)	462.7(13.4)	483.4(1.9)	546.9(63.4)	623.1(21.5)
655.3(36.4)	664.8(25.4)	665.5(6.4)	767.0(0.1)	814.9(31.5)
879.0(50.6)	894.6(41.8)	916.2(9.2)	935.2(27.4)	960.6(57.9)
1007.2(30.5)	1017.5(132.0)	1020.7(39.7)	1099.2(15.9)	1157.5(96.5)
1205.7(50.2)	1227.1(220.3)	1277.5(114.3)	1425.3(25.3)	2721.1(321.9)
2745.1(186.2)	2763.8(169.7)	3789.3(19.6)	3799.4(19.9)	3805.1(94.8)

Figure 2. continued.

3

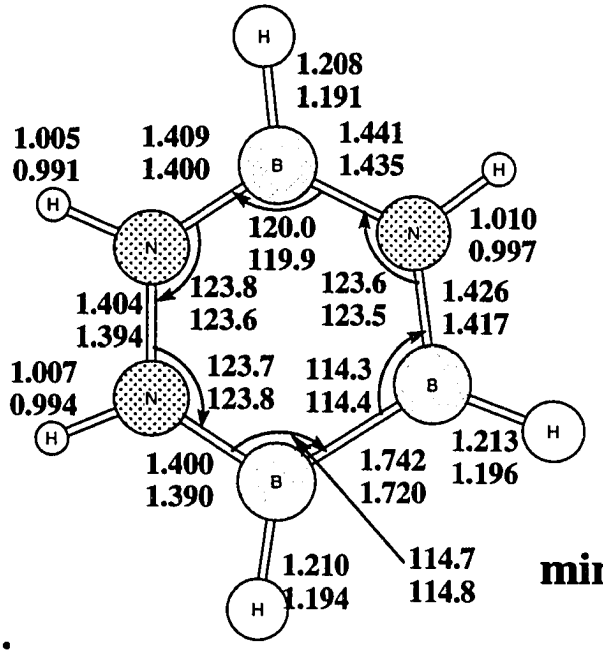

minimum

Relative Energies:

RHF/SBKJ(d)	**-86.3kcal/mol**
MP2/SBKJ(d)	**-66.4**
RHF/6-31G(d,p)//RHF/6-31G(d,p)	**-86.8**

Vibrational Frequencies:

RHF/6-31G(d,p) vibrational frequencies (in cm^{-1})

152.9	265.7	346.2	482.8	491.6
568.5	592.5	753.1	801.5	913.5
928.2	931.7	987.6	999.0	1005.4
1105.7	1129.9	1277.1	1335.4	1449.1
1512.2	1527.3	1613.3	1718.3	2671.4
2700.9	2730.5	3843.6	3879.7	3922.5

RHF/SBKJ(d) vibrational frequencies (in cm^{-1}) and intensities (in km/mol)

103.0(15.6)	245.3(9.8)	331.5(0.0)	475.7(28.7)	476.6(0.9)
556.3(0.8)	579.3(117.6)	739.5(2.1)	798.8(5.2)	895.5(4.0)
911.3(127.3)	919.6(5.0)	974.8(81.7)	982.6(5.4)	988.2(46.1)
1081.6(22.2)	1106.6(1.2)	1251.6(55.4)	1311.7(50.0)	1428.5(61.6)
1474.4(41.6)	1508.6(342.7)	1590.4(40.2)	1679.4(80.3)	2651.4(279.5)
2700.3(560.1)	2710.0(3.6)	3766.6(20.3)	3844.1(15.9)	3880.4(64.6)

Figure 2. continued.

4

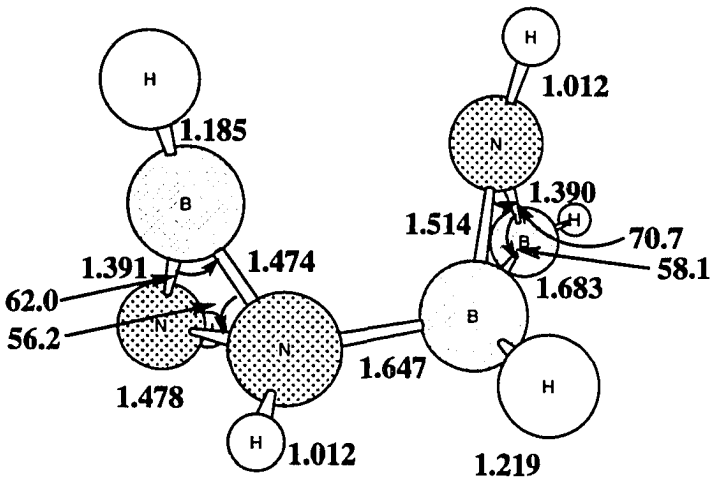

minimum

Relative Energies:

RHF/SBKJ(d)	**15.8 kcal/mol**
MP2/SBKJ(d)	**22.5**

Figure 2. continued.

5

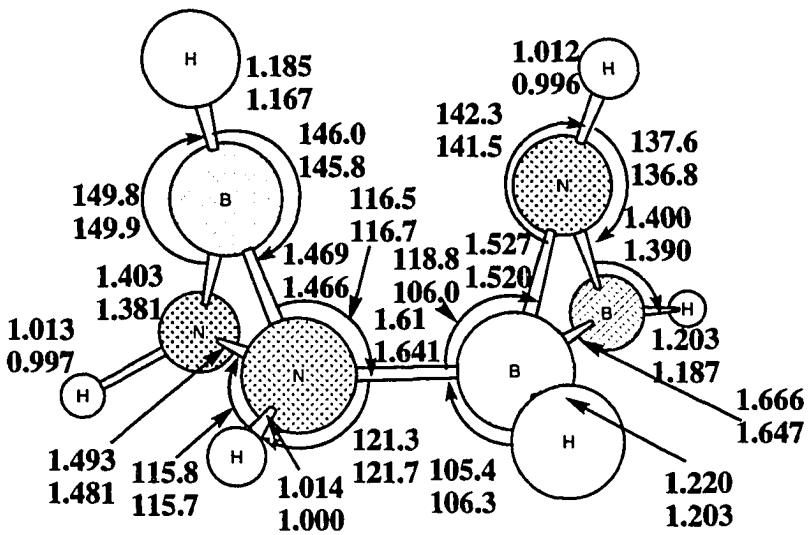

transition state

$i219.8\ cm^{-1}$ **RHF/SBK(d)**

$i217.9\ cm^{-1}$ **RHF/6-31G(d,p)**

Relative Energies:

RHF/SBKJ(d)	**26.4 kcal/mol**
MP2/SBKJ(d)	**35.3**
RHF/6-31G(d,p)//RHF/6-31G(d,p)	**23.6**

Figure 2. continued.

6

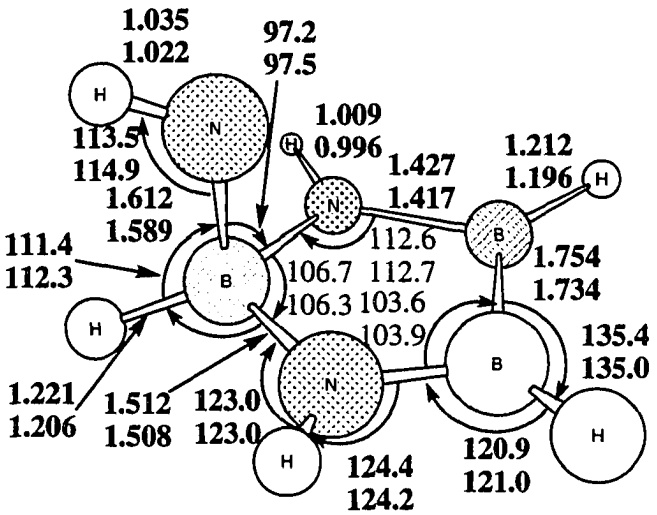

transition state

***i* 644.1 cm^{-1} RHF/SBK(d)**

***i* 685.2 cm^{-1} RHF/6-31G(d,p)**

Relative Energies:

RHF/SBKJ(d)	**8.4 kcal/mol**
MP2/SBKJ(d)	**32.1**
RHF/6-31G(d,p)//RHF/6-31G(d,p)	**9.1**

Figure 2. continued.

7

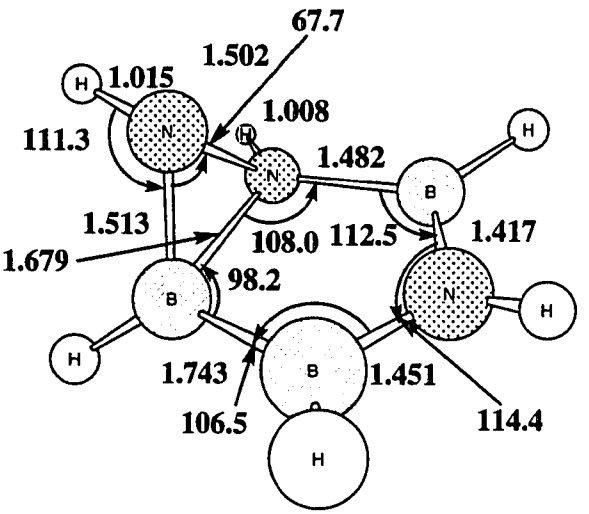

minimum

Relative Energies:

RHF/SBKJ(d)	**-53.7 kcal/mol**
MP2/SBKJ(d)	**-36.0**

Figure 2. continued.

8

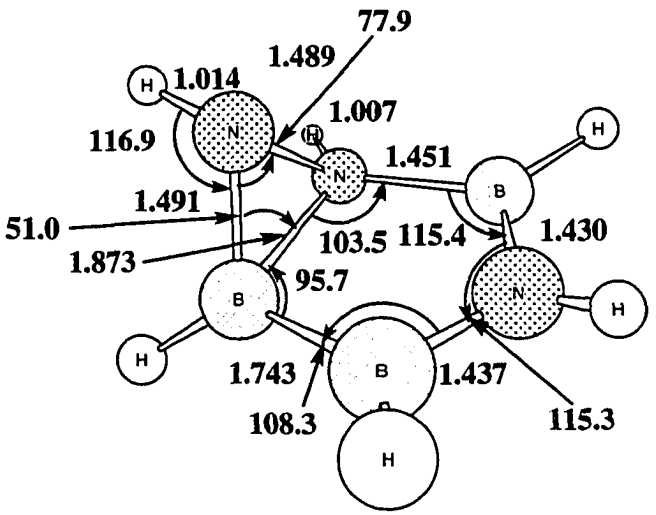

transition state

i 238.8 cm^{-1} **RHF/SBKJ(d)**

Relative Energies:

RHF/SBKJ(d)	**-53.7 kcal/mol**
MP2/SBKJ(d)	**-33.4**

Figure 2. continued.

9

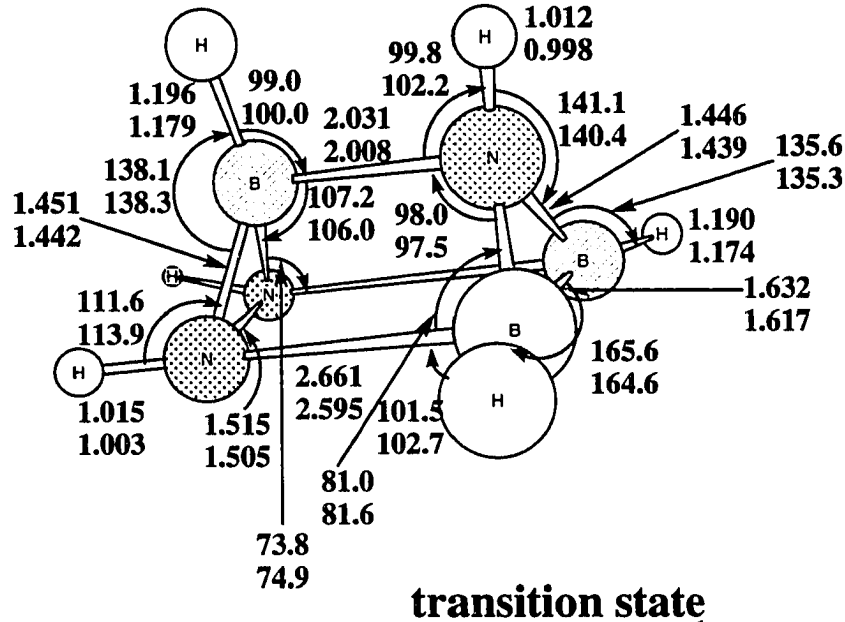

transition state

i **260.7 cm^{-1}** RHF/SBKJ(d)

2i **288.7 cm^{-1}** RHF/6-31G(d,p)

Relative Energies:

RHF/SBKJ(d)	**32.1 kcal/mol**
MP2/SBKJ(d)	**45.1**
RHF/6-31G(d,p)//RHF/6-31G(d,p)	**30.9**

Figure 2. continued.

10a

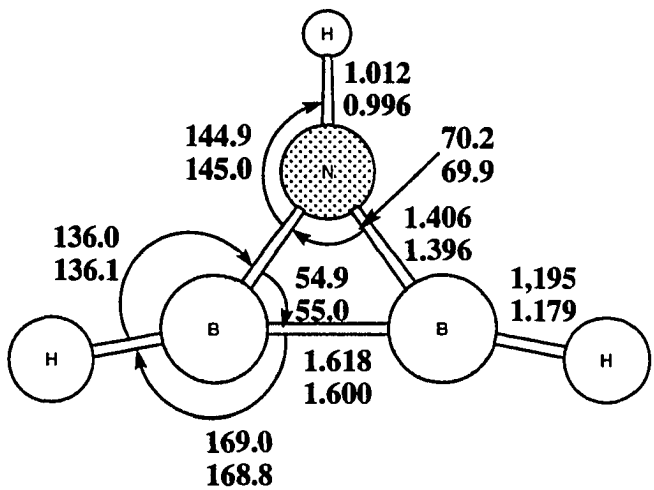

minimum

Relative Energies of 10a + 10b:

RHF/SBKJ(d)	**20.7 kcal/mol**
MP2/SBKJ(d)	**30.0**
RHF/6-31G(d,p)//RHF/6-31G(d,p)	**21.5**

Figure 2. continued.

10b

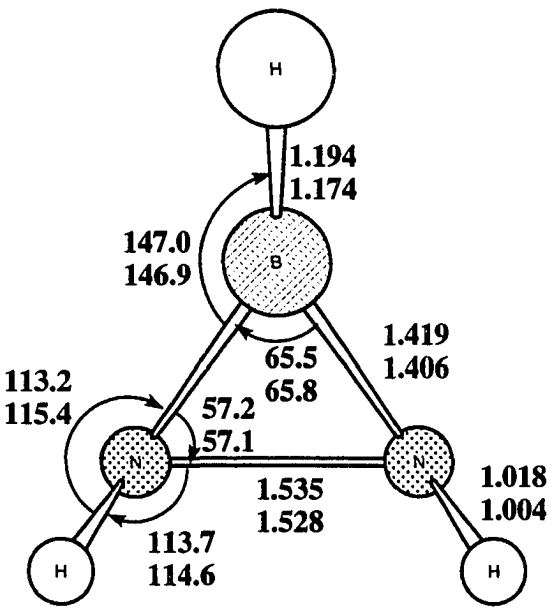

minimum

Vibrational Frequencies:

RHF/6-31G(d,p) vibrational frequencies (in cm^{-1})

597.7	712.8	819.8	883.2	1054.2
1121.2	1134.1	1443.4	1453.3	2877.7
3729.5	3746.0			

RHF/SBKJ(d) vibrational frequencies (in cm^{-1}) and intensities (in km/mol)

604.5(101.5)	687.8(80.8)	816.4(13.7)	856.1(10.5)	1048.3(115.7)
1081.6(70.6)	1134.8(8.3)	1427.5(102.4)	1432.6(1.8)	2856.8(126.8)
3686.8(0.6)	3703.6(11.3)			

Figure 2. continued.

11

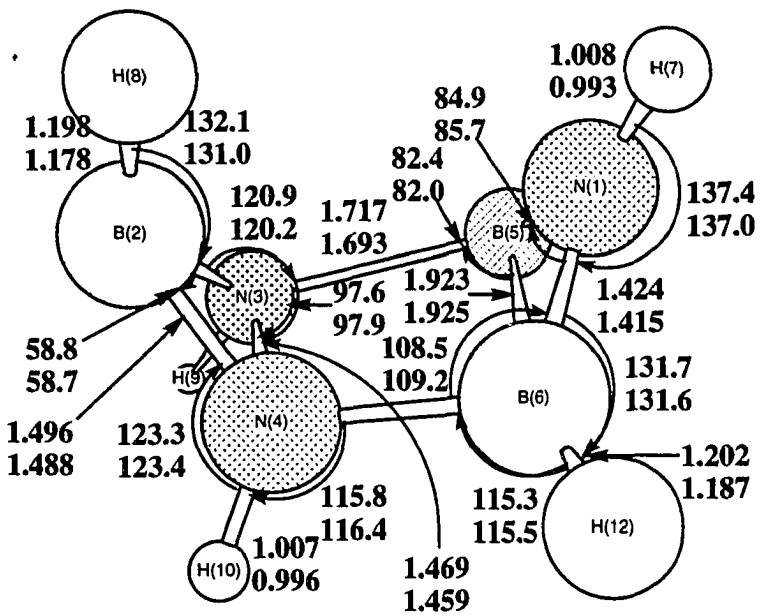

transition state:

***i* 788.6 cm^{-1} RHF/SBKJ(d)**

***i* 790.3 cm^{-1} RHF/6-31G(d,p)**

Relative Energies:

RHF/SBKJ(d)	**72.1 kcal/mol**
MP2/SBKJ(d)	**43.2**
RHF/6-31G(d,p)//RHF/6-31G(d,p)	**74.0**

Figure 2. continued.

12

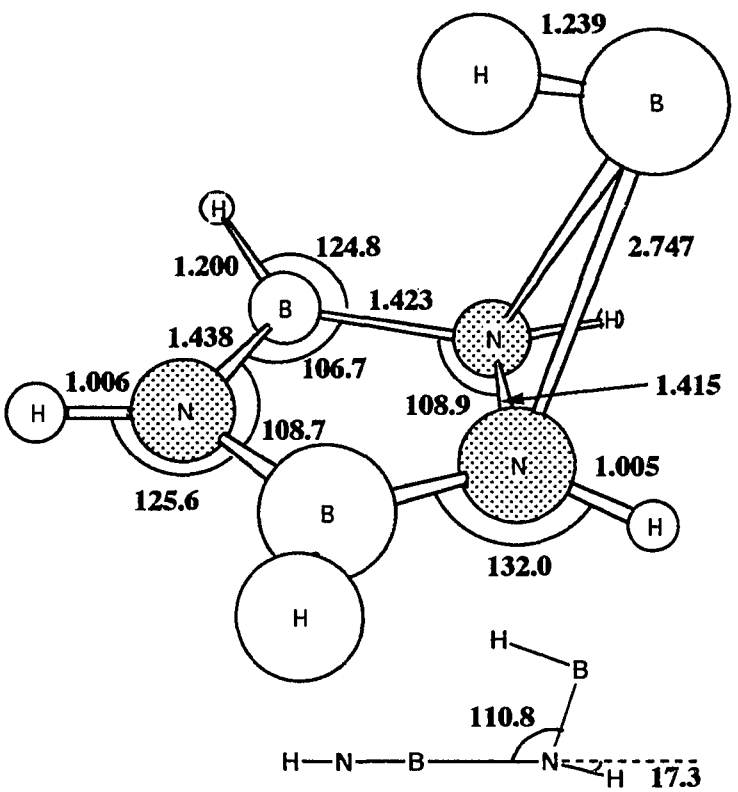

transition state:
351.2*i* cm^{-1} RHF/SBKJ(d)

Relative Energies:

RHF/SBKJ(d)	**8.2 kcal/mol**
MP2/SBKJ(d)	**-21.5**

Figure 2. continued.

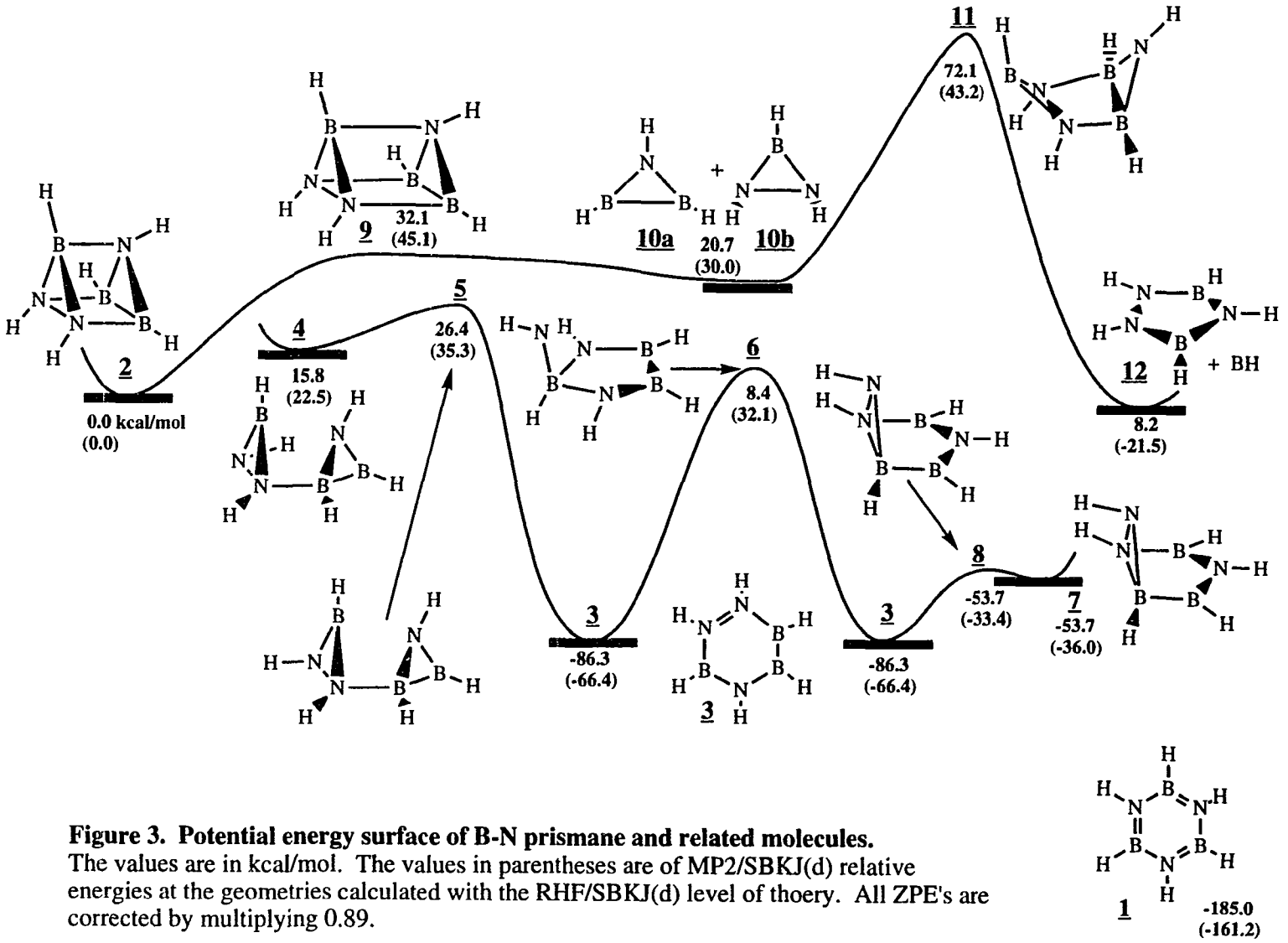

Figure 3. Potential energy surface of B-N prismane and related molecules.
The values are in kcal/mol. The values in parentheses are of MP2/SBKJ(d) relative energies at the geometries calculated with the RHF/SBKJ(d) level of thoery. All ZPE's are corrected by multiplying 0.89.

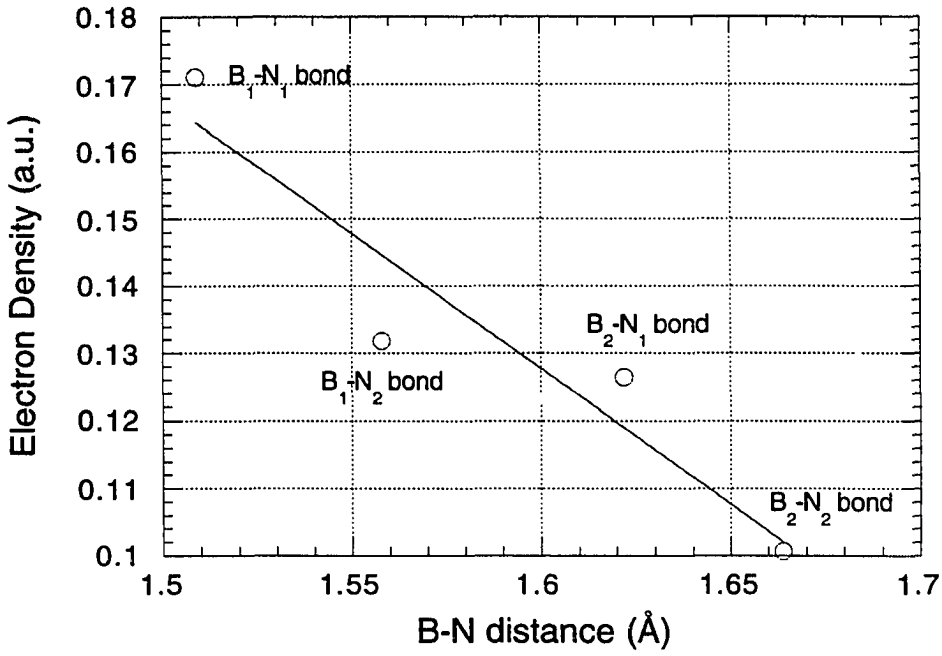

Figure 4. Electron density of B-N bonds at bond critical points. The values of electron density (a.u.) is plotted against B-N bond distances (Å). Electron density was calculated at the RHF/6-31G(d) level of theory. See Scheme 1 for numbering on B and N.

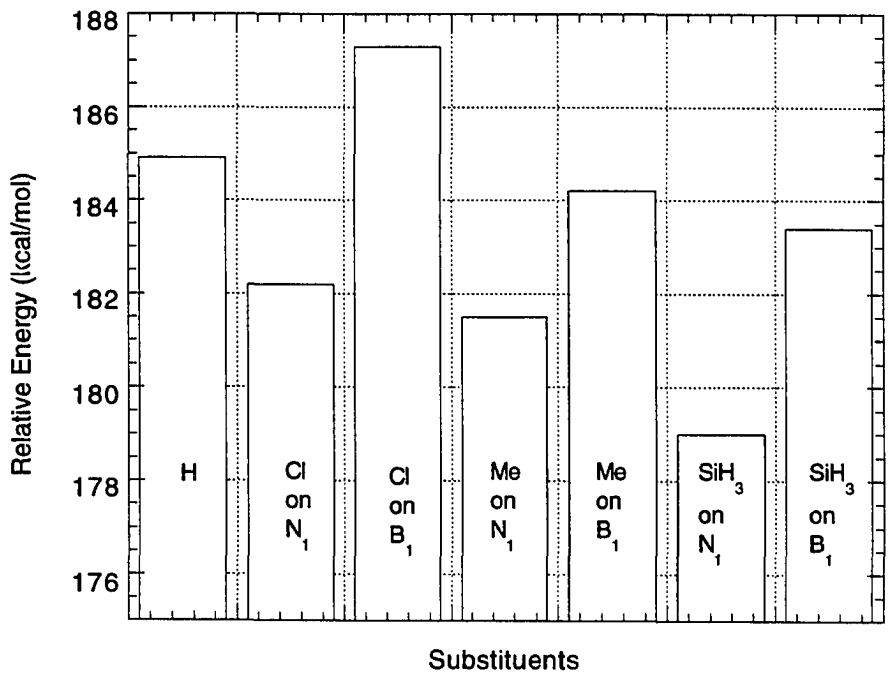

Figure 5. Substituent effects on relative energies between B-N prismane and borazine. The calculations are done at the RHF/SBKJ(d) level of theory. Each group is substituted on either N_1 or B_1 in place of a hydrogen.

GENERAL CONCLUSIONS

Possible high energy density materials were investigated. The potential energy surfaces of hypervalent NH_4^- and PH_4^- were investigated using additivity or correlation energies and basis set effects to estimate relative energies. The tetrahedral structures of NH_4^- and PH_4^- are predicted to be the high energy isomers, and they are minima on the potential energy surfaces. In order to elucidate possible dissociation paths of tetrahedral isomers, *ab initio* classical trajectory calculations were carried out. The dissociation barrier was estimated to be 32.5 kcal/mol for NH_4^- and 5.5 kcal/mol for PH_4^- in C_{3v} dissociation paths. Ionization potentials for tetrahedral structures were also calculated to be 0.39 and 0.32 eV for NH_4^- and PH_4^-, respectively. Since the dissociation of the tetrahedral NH_4^- ion appears to require considerably more energy than ionizaiton to the neutral, it is likely that the molecule will autoionize before it has a chance to dissociate. This is less likely to be the case for tetrahedral PH_4^-.

Inorganic benzenes $X_3Y_3H_6$ were investigated, with X and Y chosen from Zn, B, Al, Ga, C, Si, Ge, N, P, As, O, and S such that there are a total of six π electrons. If the ring contains C, N, or O, the isomer is a minimum on the potential energy surfaces. Others are either a saddle point or higher order saddle point. The ionic character increases in the order group IV-IV < group III-V < group IIB-VI, in line with chemical intuition and basic electronegativity arguments.

Inorganic prismanes $(XH\text{-}YH)_3$, where X = B, Al, Ga and Y = N, P and As, as well as X or Y = C, Si and Ge, as well as chair and boat conformers of inorganic benzenes were investigated for their stabilities and energetics. The nitrogen and carbon containing prismanes are stable on the potential energy surfaces, but they are very high in energy. The B-N system is 163 kcal/mol above borazine. On the other hand, the hexasila- and hexagermaprismane are the lowest energy prismane isomers found. This thermodynamic stability contributed to the synthesis of these prismanes. The total electron density analysis together with the localized orbital reveals that valence electrons are involved in bonding. The bonds are polarized where electronegativity difference exists for a given bond, and the donor and acceptor are readily identified.

Spin-orbit coupling was calculated using full valence MCSCF wavefunctions using the relativistic Breit-Pauli Hamiltonian to construct relativistic potential energy surfaces. The relativistic potential energy surfaces of XH_2 molecules, where X = C, Si, Ge, Sn or Pb, are

compared with the adiabatic non-relativistic potential energy surfaces. The noticeable difference in geometry were not found until fifth-period element is replaced for X. Similarly, the spin-orbit coupling affects the single-triplet splitting only by 1 kcal/mol for SnH_2, and 6 kcal/mol for PbH_2. The bond length at which the minimum energy crossing occurs is closer to that of the corresponding higher energy states (singlet for CH_2 and triplet for others). The energy separation between the spin-orbit coupled states is less than 1 kcal/mol for CH_2 and SiH_2, and 17 -24 kcal/mol for PbH_2. Transition probabilities for intersystem crossing are calculated using simple one-dimensional Landau-Zener model. The intersystem crossing occurs only for small kinetic regions in CH_2 and SiH_2. However, for SnH_2 and PbH_2 transition is readily accessible at any kinetic energy (zero to 2.0 eV studies) due to the strong spin-orbit coupling and larger mass. GeH_2 is an intermediate case where transition is accessible at a range of kinetic energy.

As an ongoing and future project, the potential energy surfaces of B-N prismane is currently being investigated. In Chapter 3, the prismane structure of $B_3N_3H_6$ was predicted to be 163 kcal/mol above borazine. It certainly qualifies for a candidate for high energy density material. Variety of stationary points on the $B_3N_3H_6$ potential energy surfaces is found at relatively low level of theory. We would like to extend the investigation with higher level of theory and to elucidate importance of spin-orbit coupling and vibronic coupling on dissociation/isomerization reactions.